









Jeon Jhon first author 1973-2004				
Back View Arrange By Action Share Edit Tags				
ame	^	Date Modified	Size	Kind
 Jeon 1991 PEO I deGennes lee.pdf		Sep 25, 2014, 9:28 AM	2.4 MB	PDF
 Jeon 1991 PEO II Proteins .pdf		Sep 25, 2014, 9:26 AM	1.7 MB	PDF
 Jeon 1992 Steric PEO Korean.pdf		Jul 14, 2006, 8:06 PM	1.2 MB	PDF
 Jeon 1993 AFM PEO Korean.pdf		Jul 14, 2006, 8:11 PM	1.5 MB	PDF
 Jeon 2004 CEDIA Model yang.pdf		Nov 3, 2004, 1:56 PM	646 KB	PDF
 Jhon 1973 Water Hydrogels .pdf		Jul 14, 2006, 8:22 PM	2 MB	PDF
 Jhon 1976 Hydrogels Bk Water ma hattori gregonis.pdf		Jul 14, 2006, 8:30 PM	1.5 MB	PDF
 Jhon 1976 Ions Membranes Korean lee kim.pdf		Jul 14, 2006, 8:45 PM	1.2 MB	PDF

Protein-Surface Interactions in the Presence of Polyethylene Oxide

I. Simplified Theory

S. I. JEON,¹ J. H. LEE, J. D. ANDRADE, AND P. G. DE GENNES*

*Departments of Bioengineering and Materials Science, Center for Biopolymers at Interfaces, College of Engineering, University of Utah, Salt Lake City, Utah 84112, and *College de France, Place Marcelin-Berthelot, 75231 Paris Cedex 05, France*

Received May 1, 1989; accepted August 21, 1990

The protein resistance character of polyethylene oxide (PEO) chains terminally attached to a hydrophobic solid substrate is theoretically studied. Steric repulsion, van der Waals attraction, and hydrophobic interaction free energies are considered. The results are dependent on the chain length and surface density of PEO. The protein approaches the PEO surface by diffusion and is affected by the van der Waals attraction between the PEO surface and protein through water. Further approach of the protein initiates the compression of PEO chains, which induces a steric repulsion effect; an additional van der Waals attraction becomes important between the substrate and protein through the water solvated PEO layer. The van der Waals component with the substrate decreases with increasing surface density and chain length of terminally attached PEO chains. Other synthetic polymers were also studied, indicating that the protein resistance character is related to the refractive index, with PEO having the lowest refractive index of the common water-soluble synthetic polymers. The osmotic and elastic constants of steric repulsion for terminally attached PEO were estimated as ~ 0.007 and 0.02 , respectively, from literature data for PEO adsorbed to mica. The steric repulsion free energy and the combined steric repulsion and hydrophobic interaction free energies were calculated as a function of surface density and chain length of PEO. The free energy calculations as a function of surface density and chain length of PEO reveal that a high surface density and long chain length of terminally attached PEO should exhibit optimal protein resistance, with the attainment of high surface density of PEO being more important than long chain length. These theoretical results should be helpful in the design and development of materials resistant to protein adsorption. © 1991 Academic Press, Inc.

INTRODUCTION

Protein adsorption generally occurs when artificial surfaces are exposed to blood or to other protein-containing solutions (1). There has been much effort in minimizing protein adsorption, which is important in areas of blood-contacting devices, chromatographic supports, contact lenses, immunoassays, etc. The most effective polymer for protein-resistant surfaces appears to be PEO, probably because of its unique solution properties and its

molecular conformation in aqueous solution (2-7). Direct force measurements (8-10) between two adsorbed PEO surfaces in a good aqueous solvent show that the repulsion forces develop at certain separation distances due to a steric repulsion phenomenon. The protein-resistant character of PEO is probably caused by a steric stabilization effect.

Recently, terminally attached polymer surfaces were prepared by using diblock and triblock copolymers. Such surfaces exhibit repulsion forces at longer separation distances than for adsorbed homopolymers, because of the longer chain lengths (11-13). PEO-containing block copolymers were synthesized and adsorbed to hydrophobic polyethylene (PE)

¹ On leave from the Department of Chemistry, Kangreung National University, Kangreung, Kangwondo 210-702, Korea.

substrates. The PEO surfaces which resulted (14–16) were used for protein adsorption experiments and showed that protein adsorption is decreased on PEO-treated surfaces.

The physics of terminally attached polymer surfaces has been studied theoretically by de Gennes (17–20), who explained that the repulsion forces between surfaces can be attributed to osmotic pressure and elastic restoring forces. Van der Waals attraction must also be considered in the case of relatively short PEO chains attached to a LDPE hydrophobic substrate. The steric repulsion effect competes with the van der Waals attraction term. Our aim is to study the interaction between a model PEO surface on a hydrophobic substrate with a hypothetical "protein" of infinite size (the more realistic case of a protein of finite size is given in the following paper) (42). Little protein adsorption is observed when the degree of polymerization of PEO approaches about 100 (1). The protein-resistant effect is expected to depend on PEO chain length and surface density, both of which affect the attached layer thickness, a hypothesis supported by various block copolymer measurements (14, 15).

We assume the "protein" has a hydrophobic patch which can be oriented toward the hydrophobic substrate, resulting in an attractive hydrophobic interaction (3). We have assumed that the hydrophobic "patch" is a hydrophobic surface on the protein and is facing the hydrophobic substrate. The hydrophobic interaction is added to the effect of steric repulsion and van der Waals attraction and considered as a function of surface density and chain length of PEO. We do not consider here the possibility of a hydrophobic interaction between the "protein" and the PEO layer; that is considered in the following paper (42).

MODELING

PEO is assumed to be a neutral homopolymer with linear and flexible chains terminally attached to a PE hydrophobic substrate in water, a good solvent. "Proteins" are treated as

homogeneous, infinite particles, and are thus considered as a plate (40-Å width) in water. The more realistic treatment utilizing relevant dimensions and shapes is treated in the next paper (42). The crucial parameters are the distance D between the terminally attached PEO chains, a measure of the surface density; and the degree of polymerization, N , a measure of the chain length. Our modeling picture is shown in Fig. 1. Only the "brush" case is considered (20), meaning that the distance D between the terminally attached PEO chains is less than the Flory radius, R_F , i.e., $a < D < R_F$ (here, a is monomer size).

METHOD

By X-ray and infrared analysis (21–23) crystalline PEO has a helical conformation which contains two turns in a seven-segment unit. The crystallographic unit cell contains four molecular chains and is monoclinic with $a = 8.05$ Å, $b = 13.04$ Å, $c = 19.48$ Å and $\beta = 125.4^\circ$. From these data, the monomer size of PEO, a , is determined as 2.78 Å and the surface density of crystalline PEO, $\sigma = a^2/D^2$, is 0.36; the average distance between terminally attached PEO chains, D , is 4.63 Å.

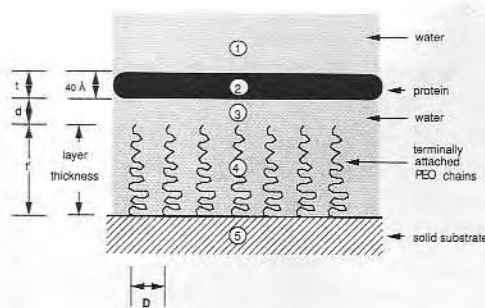


FIG. 1. Our model picture for terminally attached PEO chains to a solid substrate with a protein of infinite size and 40-Å width in water solvent. 1, 2, 3, 4, and 5 are the water, protein, water, terminally attached PEO chains in water, and solid substrate, respectively. d , t , and t' are the distance between PEO surface and protein, the width of the protein, and the layer thickness of terminally attached PEO chains. D is the distance between the terminally attached chains.

To calculate the steric repulsion free energy per unit surface area, we used the method of Patel *et al.* (24), which is based on the treatment by de Gennes (17–20). Two effects, osmotic and elastic, are considered and the contribution of each effect is taken as the proportionality constants k_1 and k_2 , respectively, which are different for each polymer-solvent system. The k_1 and k_2 values of PEO in water are not available in the literature. We have estimated the values by using the universal curve-fitting method of Patel *et al.* (24) and published data (8, 9) on directly measured first compression forces between PEO adsorbed on mica surfaces in 0.1 M aqueous KNO₃ solvent. (Although there are now preliminary experimental data on the forces between adsorbed layers of PEO graft copolymers (43), the information available is not sufficient to use in this theoretical treatment; therefore we have assumed that the values for the adsorbed PEO chains can also approximate the terminal attachment case.) The calculated results are $k_1 \sim 0.021$ and $k_2 \sim 0.23$ for PEO with 1.6×10^5 molecular mass [radius of gyration $R_g = 130$ Å (8, 9)], and $k_1 \sim 0.013$ and $k_2 \sim 0.09$ for PEO with 4.0×10^4 molecular mass ($R_g = 65$ Å (8, 9)). The measured repulsion force appeared at $3R_g$ distance from the PEO adsorbed mica surface (8, 9); the surface concentration was about 4 mg m^{-2} , irrespective of the two different molecular masses of PEO (8, 9). Thus the experimentally determined equilibrium layer thickness, L_0 , is about 390 Å for 1.6×10^5 molecular mass and about 195 Å for 4.0×10^4 molecular mass. The theoretical equilibrium layer thickness of terminally attached chains in a good solvent system (24) is $L_0 = (\frac{5}{7}k_1/k_2)^{1/3}aNs^{1/3}$. To calculate this theoretical value, it is necessary to know σ , which can be calculated from the PEO surface concentration. σ is 0.0011 and 0.0047 for 1.6×10^5 and 4.0×10^4 molecular masses of PEO, respectively. The theoretically calculated L_0 values using the above-obtained k_1 and k_2 values are about 420 and 198 Å, which are in relatively good agreement with the experimental results (8, 9). The k_1 and k_2 values in

the molecular mass range of interest to us, $\sim 5.0 \times 10^3$, is roughly estimated as $k_1 \sim 0.007$ and $k_2 \sim 0.02$. Inserting these values of k_1 and k_2 , we can calculate the steric repulsion free energy per unit surface area as a function of N and D , using the equation (24)

$$\frac{\Delta F_s}{kT} = \frac{k_1}{a^2} \left(\frac{7}{5} \frac{k_2}{k_1} \right)^{5/12} N \sigma^{11/6} \left\{ \left[\left(\frac{L_0}{L} \right)^{5/4} - 1 \right] + \frac{5}{7} \left[\left(\frac{L}{L_0} \right)^{7/4} - 1 \right] \right\} \quad [1]$$

Our modeling picture in Fig. 1 is composed of five different phases: (1) water, (2) protein, (3) water between PEO and protein, (4) terminally attached PEO chains in water solvent, and (5) hydrophobic solid substrate. Assuming the same absorption frequencies in all five media, the nonretarded van der Waals interaction free energy per unit surface area (\AA^2) between macroscopic bodies (25–29) is given as

$$\frac{\Delta F_a}{kT} = -\frac{1}{12\pi kT} \left[\frac{A(1)}{d^2} + \frac{A(2)}{(d+t)^2} + \frac{A(3)}{(d+t')^2} + \frac{A(4)}{(d+t+t')^2} \right] \quad [2]$$

and

$$\begin{aligned} A(1) &= \frac{3h\nu_e}{8\sqrt{2}} \frac{(n_2^2 - n_3^2)(n_4^2 - n_3^2)}{(n_2^2 + n_3^2)^{1/2}(n_4^2 + n_3^2)^{1/2}} \\ &\quad \times \frac{1}{[(n_2^2 + n_3^2)^{1/2} + (n_4^2 + n_3^2)^{1/2}]} \\ &\quad + \frac{3}{4} kT \frac{(\epsilon_2 - \epsilon_3)(\epsilon_4 - \epsilon_3)}{(\epsilon_2 + \epsilon_3)(\epsilon_4 + \epsilon_3)} \\ A(2) &= \frac{3h\nu_e}{8\sqrt{2}} \frac{(n_4^2 - n_3^2)(n_1^2 - n_2^2)}{(n_4^2 + n_3^2)^{1/2}(n_1^2 + n_2^2)^{1/2}} \\ &\quad \times \frac{1}{[(n_4^2 + n_3^2)^{1/2} + (n_1^2 + n_2^2)^{1/2}]} \\ &\quad + \frac{3}{4} kT \frac{(\epsilon_4 - \epsilon_3)(\epsilon_1 - \epsilon_2)}{(\epsilon_4 + \epsilon_3)(\epsilon_1 + \epsilon_2)} \end{aligned}$$

$$\begin{aligned}
A(3) &= \frac{3h\nu_e}{8\sqrt{2}} \frac{(n_2^2 - n_3^2)(n_5^2 - n_4^2)}{(n_2^2 + n_3^2)^{1/2}(n_5^2 + n_4^2)^{1/2}} \\
&\quad \times \frac{1}{[(n_2^2 + n_3^2)^{1/2} + (n_5^2 + n_4^2)^{1/2}]} \\
&\quad + \frac{3}{4} kT \frac{(\epsilon_2 - \epsilon_3)(\epsilon_5 - \epsilon_4)}{(\epsilon_2 + \epsilon_3)(\epsilon_5 + \epsilon_4)} \\
A(4) &= \frac{3h\nu_e}{8\sqrt{2}} \frac{(n_1^2 - n_2^2)(n_5^2 - n_4^2)}{(n_1^2 + n_2^2)^{1/2}(n_5^2 + n_4^2)^{1/2}} \\
&\quad \times \frac{1}{[(n_1^2 + n_2^2)^{1/2} + (n_5^2 + n_4^2)^{1/2}]} \\
&\quad + \frac{3}{4} kT \frac{(\epsilon_1 - \epsilon_2)(\epsilon_5 - \epsilon_4)}{(\epsilon_1 + \epsilon_2)(\epsilon_5 + \epsilon_4)} \quad [3]
\end{aligned}$$

where k is the Boltzmann constant; h is Planck's constant; ν_e is the main electronic absorption frequency ($3 \times 10^{15} \text{ sec}^{-1}$); $A(1)$, $A(2)$, $A(3)$, and $A(4)$ are the nonretarded Hamaker constants for the interaction between bodies 2 and 4 across a medium 3, bodies 1 and 4 across media 2 and 3, bodies 2 and 5 across media 3 and 4, and bodies 1 and 5 across media 2 and 4, respectively; d , t , and l' are the distance between PEO surface and protein, the width of protein (40 Å), and the layer thickness of terminally attached PEO chains, respectively; n_1 , n_2 , n_3 , n_4 , and n_5 are the refractive indices of phase 1 [$n_1 = 1.333$ (30)], phase 2 [$n_2 = 1.539$ (31)], phase 3 [$n_3 = 1.333$], phase 4 [$n_4 = \phi_{\text{PEO}}(n_{\text{PEO}} - n_{\text{H}_2\text{O}}) + n_{\text{H}_2\text{O}}$ (32), where ϕ_{PEO} is the dimensionless PEO volume fraction, n_{PEO} is the refractive index of PEO, 1.456, and $n_{\text{H}_2\text{O}}$ is the refractive index of water, 1.333], and phase 5 [$n_5 = 1.510$ (31)], respectively; ϵ_1 , ϵ_2 , ϵ_3 , ϵ_4 , and ϵ_5 are the static dielectric constants of phase 1 [$\epsilon_1 = 79.69$ (30)], phase 2 [$\epsilon_2 = 2.64$ (31)]; the inner part of the dry protein is primarily nonpolar and the static dielectric constant is assumed to be equal to the square of refractive index],³ phase 3 ($\epsilon_3 = 79.69$), phase 4 [ϵ_4 is determined by the same method of refractive

index, i.e., $\epsilon_4 = \phi_{\text{PEO}}(\epsilon_{\text{PEO}} - \epsilon_{\text{H}_2\text{O}}) + \epsilon_{\text{H}_2\text{O}}$, where ϵ_{PEO} is the dielectric constant of PEO, 3.50 (33, 34), and $\epsilon_{\text{H}_2\text{O}}$ is the dielectric constant of H₂O, 79.69], and phase 5 [$\epsilon_5 = 2.25$ (31)], respectively.

The existence of hydrophobic attractive forces between uncharged hydrophobic surfaces is generally recognized (35–40) and such forces are 10 to 100 times stronger than the van der Waals forces at separation distances between hydrophobic surfaces below 200 Å (39). This concept can be applied to our system, which can have a hydrophobic interaction between the hydrophobic solid substrate and an assumed hydrophobic surface on the protein. We used the hydrophobic interaction free energy function determined experimentally by Pashley *et al.* (36) for the dihexadecyldimethylammonium acetate monolayer:

$$\frac{\Delta F_h}{kT} = -0.1359e^{-s/14}(\text{\AA}^{-2}) \quad [4]$$

where s is the distance (Å) between the hydrophobic surfaces.

The individual and combined free energy calculations were performed using N values from 80 to 120 and D values from 5 to 9 Å (higher than the crystalline PEO value of 4.63) for the variation of distances between solid substrate and protein, and PEO surface and protein.

The protein is also considered to be influenced by water. We assume a certain average water content for the protein, which we call the "diluted" protein. The diluted protein is assumed to be an infinite plate. In this case, the refractive index and dielectric constant of diluted protein are different from those of the bulk protein. Only one diluted value, half volume fraction, is used for comparison.

RESULTS AND DISCUSSION

If one examines polystyrene (PS) adsorbed on mica in toluene, a different force diagram and adsorbed layer thickness are obtained than in the case of PEO (12, 13, 41), clearly demonstrating the different k_1 and k_2 values for

³ The case of hydrated protein is discussed later (Fig. 4d).

each system. The correct values of k_1 and k_2 for each different copolymer system and copolymer composition in solvent must be obtained from experimental force data. Our estimated k_1 and k_2 values are based on the adsorbed PEO homopolymer data because other appropriate data are not yet available. Terminally attached polymer surfaces generally have longer chain lengths than adsorbed homopolymer (11–13), so there is the possibility of a larger equilibrium layer thickness for terminally attached PEO. This possibility is neglected in our paper because of the difficulty of direct comparison. When force data for terminally attached PEO chains in water become available, different k_1 and k_2 values will be used to refine the calculations.

As the distance between terminally attached chains decreases, meaning the space between chains is more limited, then the equilibrium layer thickness, L_0 , increases. L_0 can be compared with the fully extended layer thickness (contour length), $L_c = aN$, $L_0/L_c = 0.43$ to 0.29 for $D = 5$ to 9 Å. Thus the chains are stretched to about 29 to 43% of their fully extended length. From the experimentally determined L_0 values, the ratio of layer thicknesses are as follows: $L_0/L_c \sim 0.04, 0.05$, and 0.12 for molecular masses of 3.1×10^5 , 1.6×10^5 , and 4.0×10^4 of adsorbed PEO homopolymer in toluene, respectively (10); $L_0/L_c \sim 0.03, 0.04$, and 0.08 for molecular masses of 3.1×10^5 , 1.6×10^5 , and 4.0×10^4 of adsorbed PEO homopolymer in 0.1 M KNO_3 aqueous solvent, respectively (8); $L_0/L_c \sim 0.20$ and 0.23 for the molecular mass of 1.31×10^5 of terminally attached PS via the PEO block and zwitterionic group in toluene, respectively (12, 13); $L_0/L_c \sim 0.15$ and 0.23 for molecular masses of 1.5×10^5 and 6.0×10^4 of terminally attached PS via the poly(vinyl-2-pyridine) block in toluene, respectively (39). PEO is more extended in toluene than in aqueous electrolyte solvent and the ratio of layer thickness is increased with the decrease of molecular mass of polymer. However, the comparison of the same polymer-solvent system in the adsorbed or ter-

minally attached cases is not possible because of the absence of experimental data.

In the following discussion of the figures, note the *magnitude* of the forces (the vertical axis) and the sign of the forces (positive is repulsive, negative is attractive). Figures 2 and 3 represent the steric exclusion forces (strongly repulsive), Figs. 4 and 5 represent the van der Waals interaction between the protein and the PEO layer (weakly attractive), Fig. 6 is the very weak attractive interaction between the protein and the underlying hydrophobic substrate, and Fig. 7 represents the steric plus attractive hydrophobic forces.

The steric free energies per unit surface area were calculated as a function of PEO layer thickness (Figs. 2 and 3). Figures 2a and b show the effect of the elastic and osmotic contributions of PEO to the steric free energy at constant surface density and chain length. If the osmotic and elastic contributions are doubled, the equilibrium layer thickness changes by factors of 1.26 and $1/1.26$, respectively. Thus precise values of k_1 and k_2 are not critical

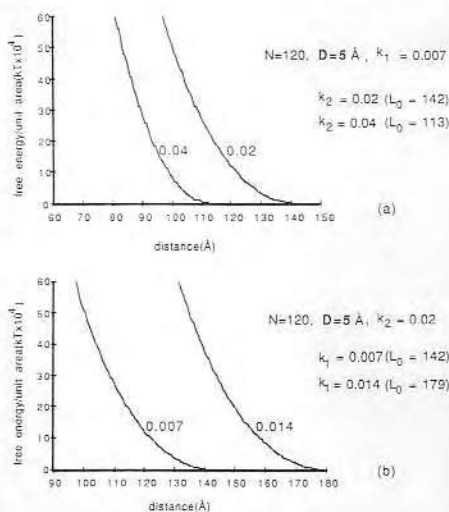


FIG. 2. (a) Steric repulsion free energy per unit surface area (\AA^2) (divided by kT)—terminally attached PEO layer thickness profiles for two different elastic coefficients at $N = 120$ and $D = 5$ Å. (b) Steric repulsion free energy per unit surface area (\AA^2) (divided by kT)—terminally attached PEO layer thickness profiles for two different osmotic coefficients at $N = 120$ and $D = 5$ Å.

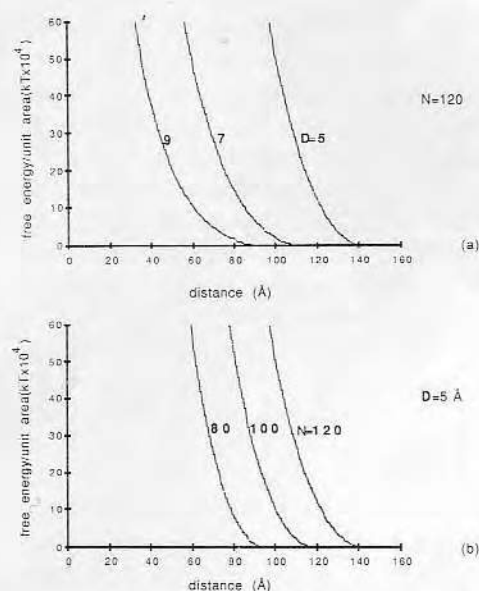


FIG. 3. (a) Steric repulsion free energy per unit surface area (\AA^2) (divided by kT)—terminally attached PEO layer thickness profiles for three different D values at $N = 120$ ($k_1 = 0.007$ and $k_2 = 0.02$). (b) Steric repulsion free energy per unit surface area (\AA^2) (divided by kT)—terminally attached PEO layer thickness profiles for three different N values at $D = 5$ Å ($k_1 = 0.007$ and $k_2 = 0.02$).

for these approximate calculations. The crowding of polymer chains in any fixed space results in an osmotic pressure. If the polymer has a higher osmotic contribution, it extends easily into the solvent space and has a longer equilibrium layer thickness. Polymers with higher elastic contributions can shrink to a small space, and have a shorter equilibrium layer thickness. To obtain terminally attached polymer chains with longer equilibrium layer thicknesses, which exhibit repulsion at longer separation distances, it is necessary to increase the osmotic contribution and to decrease the elastic contribution. The extent of osmotic and elastic contribution depends on the combination of polymer and solvent, and decreases with the molecular mass of polymer. The steric repulsion free energy develops as the chain is compressed and the tendency increases as the osmotic and elastic contributions increase (Fig. 2). The steric free energy dependence on the surface density and chain length is shown

in Fig. 3 for $k_1 = 0.007$ and $k_2 = 0.02$. As the surface density of PEO increases, the repulsion starts at longer layer thickness and the curve steepens, a more desirable condition to resist the approaching protein.

Assuming the protein is floating over the PEO surface as shown in Fig. 1, it first approaches the PEO surface by diffusion. Further approach results in compression of the PEO coil. The interaction between the PEO surface and protein is considered; a possible interaction between them across water is van der Waals interaction. The van der Waals free

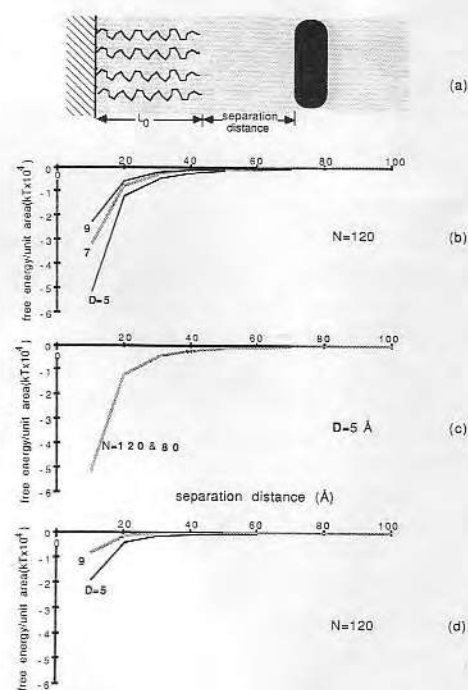


FIG. 4. (a) Model picture showing five different phases. L_0 is the equilibrium layer thickness of terminally attached PEO chains and is invariable at fixed N and D values. Separation distance is the distance between PEO surface and protein and is variable. (Protein is assumed to be infinite size.) (b) Van der Waals free energy per unit surface area (\AA^2) (divided by kT)—separation distance profiles for three different D values at $N = 120$. (c) Van der Waals free energy per unit surface area (\AA^2) (divided by kT)—separation distance profiles for two different N values at $D = 5$ Å. (d) Van der Waals free energy per unit surface area (\AA^2) (divided by kT)—separation distance profiles for two different D values at half volume fraction of protein and $N = 120$.

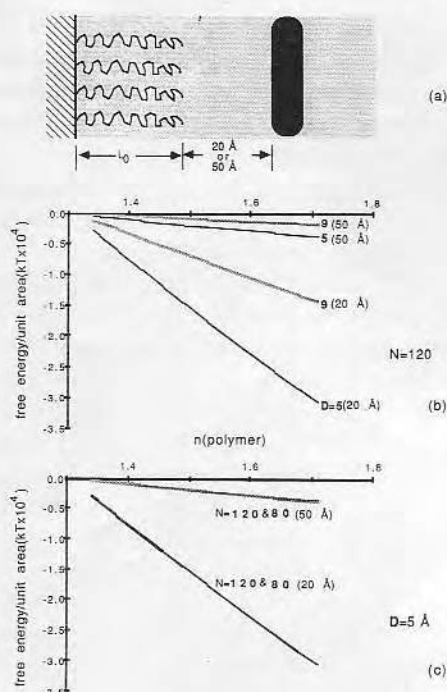


FIG. 5. (a) Model picture showing five different phases. Separation distances are selected as 20 and 50 Å. (Protein is assumed to be infinite size.) (b) Van der Waals free energy between protein and polymer chains per unit surface area (\AA^2) (divided by kT)—refractive indices of polymer profiles for two different D values at each separation distance and $N = 120$. (c) Van der Waals free energy per unit surface area (\AA^2) (divided by kT)—refractive indices of polymer profiles for two different N values at each separation distance and $D = 5$ Å.

energies between a PEO surface and protein in water are calculated as a function of the distance between them (Fig. 4). Our modeling picture is given in Fig. 4a. As the surface density increases, the PEO volume fraction of phase 4 of Fig. 1 increases, the refractive index increases, and the static dielectric constant decreases, resulting in an increase in van der Waals free energy (Fig. 4b). On the other hand, variation of degree of polymerization at constant surface density has no effect on the van der Waals free energy (Fig. 4c). Note that the magnitude of the attractive van der Waals force is small in comparison to the repulsive steric interactions (Figs. 2 and 3). The effect of dilution of protein (the volume fraction of

protein is 0.5) is also observed; it results in a decrease in refractive index and a large increase in the static dielectric constant of the protein, and represents a pronounced decrease in van der Waals attraction between the PEO surface and diluted protein (Fig. 4d). This also demonstrates that the exact value of the static dielectric constant used for the protein in Eq. [3] is not critical.

It is valuable to consider other terminally attached polymer systems in water and to compare them with PEO. The nature of polymer is considered at two separation distances (20 and 50 Å) (Fig. 5a). The composition of the terminally attached polymer chain affects the refractive index and static dielectric constant of the polymer layer. The dependence of van der Waals free energies on the refractive indices is calculated and shown in Figs. 5b and c. The refractive index of the relatively low molecular weight PEO which we are considering is 1.456 (31), which is the lowest of any common water-soluble synthetic polymer (31). Polymers with a refractive index below 1.456 are fluoropolymers. Although they would have a lower van der Waals free energy than PEO, they are not water soluble and thus are not considered here. Therefore PEO exhibits the weakest van der Waals attraction to protein among the common water-soluble synthetic polymers. We think that the protein resistance property of PEO is due in part to this fact. The protein resistance properties of PEO improve as the surface density of PEO chains increases.

We assume that the protein can approach the PEO surface by diffusion because of the lack of long-range repulsion forces. It is assumed that the protein is nonadsorptive to PEO and that the distance between the protein and the PEO surface is 3 Å, which is slightly longer than the monomer size of PEO, 2.78 Å. The continuous approach of the protein to the PEO surface, while maintaining this distance (3 Å), induces a continuous contraction of terminally attached PEO chains.

The van der Waals interaction between the underlying solid substrate and protein across

the contracted PEO layer must be considered, (Fig. 6a). The dependence of van der Waals attraction on surface density at constant chain length is shown in Figs. 6b and c, and can be compared with the van der Waals attraction in water in the absence of the PEO phase. The refractive index of the PEO-water region increases with increasing PEO content, and the static dielectric constant therefore decreases. This tendency is more pronounced as the PEO chain becomes compressed or as more chains

are attached to substrate, and the van der Waals attraction between substrate and protein is thus diminished, which is another component to the protein resistance. The effect of surface density on van der Waals attraction is pronounced at lower chain length and lower surface density. So longer chain lengths and higher surface densities are desirable for protein resistance from the point of view of protein interaction with the PE substrate, which is opposite to the results for the resistance of protein to the PEO surface (Fig. 4b). The effect of dilution of protein is also shown in Fig. 6d. As the protein is diluted, the van der Waals attraction is decreased and the change to van der Waals repulsion occurs at shorter separation distances, because of the higher dielectric constant of the protein region than of the terminally attached PEO region. *The magnitude of the van der Waals attraction between substrate and protein across PEO is negligible compared to the steric repulsion which is developed as the PEO chain is compressed.* However, the hydrophobic attraction between protein and underlying PE substrate is not negligible (not shown).

Ignoring the weak van der Waals interactions, the combined free energies of steric repulsion (Eq. [1]) and hydrophobic attraction (Eq. [4]) as a function of separation distances between substrate and protein, at constant PEO chain length, are shown in Figs. 7a, b, and c. PEO with the higher surface density exhibits the strongest repulsion due to the compression of PEO chains. As the chain length increases, then PEO surfaces with lower surface density begin to exhibit repulsion. The hydrophobic attraction between the substrate and protein is exaggerated, as the assumed hydrophobic surface on the protein in reality would not necessarily be directed toward the hydrophobic substrate and would not be infinite in extent. Hydrophobic areas or patches on globular proteins are generally small and limited in area. Also the hydrophobic interaction between substrate and protein across water may be decreased by the gradual re-

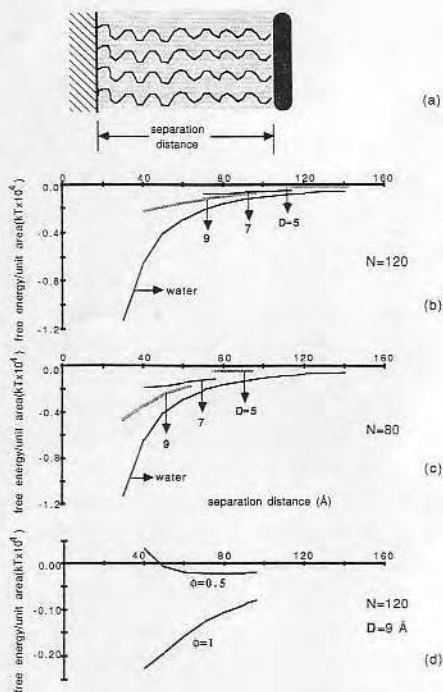


FIG. 6. (a) Model picture showing three different phases. Separation distance is the layer thickness of terminally attached PEO chains due to compression. (Protein is assumed to be infinite size.) (b) Van der Waals free energy between protein and HDPE substrate per unit surface area (\AA^2) (divided by kT)—separation distance profiles for three different D values and only water instead of PEO at $N = 120$. (c) Van der Waals free energy per unit surface area (\AA^2) (divided by kT)—separation distance profiles for three different D values and only water instead of PEO at $N = 80$. (d) Van der Waals free energy per unit surface area (\AA^2) (divided by kT)—separation distance profiles for bulk and half volume fraction of protein at $N = 120$ and $D = 9 \text{ \AA}$.

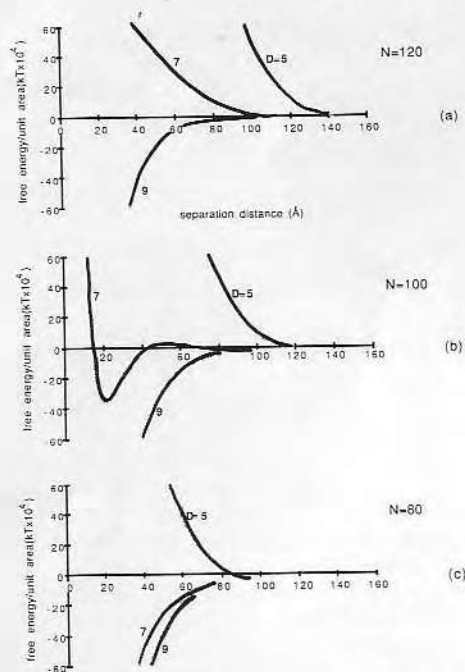


FIG. 7. (a) Combined steric repulsion and hydrophobic attraction free energy per unit surface area (Å^2) (divided by kT)—separation distance profiles for three different D values at $N = 120$. (b) Combined steric repulsion and hydrophobic attraction free energy per unit surface area (Å^2) (divided by kT)—separation distance profiles for three different D values at $N = 100$. (c) Combined steric repulsion and hydrophobic attraction free energy per unit surface area (Å^2) (divided by kT)—separation distance profiles for three different D values at $N = 80$.

placement of the water with the terminally attached PEO chains, and this decrease may be more pronounced as the surface density and chain length increase. The van der Waals and hydrophobic interactions exhibit strong attraction below about 100 Å (21, 26, 29). The choice of a slightly higher equilibrium layer thickness than 100 Å is sufficient and the variation of surface density and chain length must be considered under this condition. The variation of surface density rather than that of chain length has a great effect on the steric repulsion.

In this paper, we treated the "protein" as an infinite plate. Proteins of finite size are considered in the next paper (42).

CONCLUSION

This study is based on the assumption of PEO chains terminally attached to a hydrophobic substrate in water, interacting with a "protein" of infinite size. Steric repulsion, van der Waals attraction, and hydrophobic attraction are calculated as a function of surface density and chain length of PEO. The osmotic and elastic contributions of steric repulsion for our PEO system are roughly estimated using $k_1 \sim 0.007$ and $k_2 \sim 0.02$, deduced from experimental force data of PEO adsorbed to mica in water. The approach of protein to a PEO surface is considered. The good protein resistance properties of PEO are related to the fact that its refractive index is the lowest among the water-soluble synthetic polymers, resulting in a low van der Waals interaction with the protein. If the protein collides with the PEO surface, the terminally attached PEO chains are compressed and steric repulsion and van der Waals attraction between the solid substrate and protein across PEO must be considered. The van der Waals attraction is small in comparison with the steric repulsion. The hydrophobic interaction between the protein and the hydrophobic substrate is considered and competes with the steric repulsion.

High surface density and long chain length of PEO are desirable for protein resistance. The surface density has a greater effect than chain length on the steric repulsion.

Although a number of assumptions and estimations have had to be made to permit the calculations reported, the qualitative trends and conclusions should remain valid.

ACKNOWLEDGMENTS

S. I. Jeon acknowledges partial support from the Korea Science and Engineering Foundation (KOSEF) during his stay at the University of Utah. This work has been partially supported by a fellowship grant from Ciba-Geigy Pharmaceuticals (Horsham, England) to the Center for Biopolymers at Interfaces (CBI), University of Utah. We thank C. G. Golander, K. Caldwell, J. Kopecek, and K. Petrak for stimulating discussions. J. Andrade thanks Professor M. Jozefowicz, Université de Paris-Nord, for arranging for a month in Paris and for several visits to Pro-

fessor de Gennes at the College de France, during which this collaborative study was initiated. We thank one of the reviewers for bringing Ref. (43) to our attention.

REFERENCES

- Andrade, J. D., Nagaoka, S., Cooper, S., Okano, T., and Kim, S. W., *ASAIO J.* **10**, 75 (1987).
- Kjellander, R., and Florin, E., *J. Chem. Soc. Faraday Trans. 1* **77**, 2023 (1981).
- Andrade, J. D. (Ed.), "Surface and Interfacial Aspects of Biomedical Polymers," Ch. 1. Plenum, New York, 1985.
- Lee, J. H., Kopecek, J., and Andrade, J. D., *Proc. Polym. Mater. Sci. Eng. Div. ACS* **57**, 613 (1987).
- Lee, J. H., "Interactions of PEO-Containing Polymeric Surfactants with Hydrophobic Surfaces," Ph.D. thesis, University of Utah, 1988.
- Gregonis, D. E., Bucrger, D. E., Van Wagenen, R. A., Hunter, S. K., and Andrade, J. D., *Biomaterials* **84**, *Trans. Soc. Biomater.* **7**, 766 (1984).
- Gombotz, W. R., Hoffman, A. S., Harris, J. M., Hovancs, B., Wang, G. H., and Safran, A., IUPAC—Macromolecules Symposium, Seoul, Korea, June 1989.
- Klein, J., and Luckham, P., *Nature (London)* **300**, 429 (1982).
- Klein, J., and Luckham, P., *Macromolecules* **17**, 1041 (1984).
- Luckham, P., and Klein, J., *Macromolecules* **18**, 721 (1985).
- Tirrell, M., Patel, S., and Hadzioannou, G., *Proc. Natl. Acad. Sci. USA* **84**, 4725 (1987).
- Taunton, H. J., Toprakcioglu, C., and Klein, J., *Macromolecules* **21**, 3336 (1988).
- Taunton, H. J., Toprakcioglu, C., Fetters, L. J., and Klein, J., *Nature (London)* **332**, 712 (1988).
- Lee, J. H., Kopeckova, P., Zhang, J., Kopecek, J., and Andrade, J. D., *Polym. Mater. Sci. Eng. (ACS Prepr.)* **59**, 234 (1988).
- Lee, J. H., Kopecek, J., and Andrade, J. D., *J. Biomed. Mater. Res.* **23**, 351 (1989).
- Lee, J. H., Kopeckova, P., Kopecek, J., and Andrade, J. D., *New Polym. Mater.* **1**, 289 (1990).
- de Gennes, P. G., "Scaling Concepts in Polymer Physics." Cornell Univ. Press, Ithaca, NY, 1979.
- de Gennes, P. G., *Macromolecules* **14**, 1637 (1981).
- de Gennes, P. G., *Macromolecules* **15**, 492 (1982).
- de Gennes, P. G., *Ann. Chim.* **77**, 389 (1987).
- Tadokoro, H., Chatani, Y., Yoshihara, T., Tahara, S., and Murahashi, M., *Makromol. Chem.* **73**, 109 (1964).
- Takahashi, Y., and Tadokoro, H., *Macromolecules* **6**, 672 (1973).
- Bailey, F. E., Jr., and Koleske, J. Y., "Poly(Ethylene Oxide)." Academic Press, New York, 1976.
- Patel, S., Tirrell, M., and Hadzioannou, G., *Colloids Surf.* **31**, 157 (1988).
- Tabor, D., and Winterton, R. H. S., *Proc. R. Soc. Ser. A* **312**, 435 (1969).
- Israelachvili, J. N., and Tabor, D., *Proc. R. Soc. London Ser. A* **331**, 19 (1972).
- Israelachvili, J. N., *Proc. R. Soc. London Ser. A* **331**, 39 (1972).
- Derjaguin, B. V., Churaev, N. V., and Rabinovich, Ya.I., *Adv. Colloid Interface Sci.* **28**, 197 (1988).
- Israelachvili, J. N., "Intermolecular and Surface Forces." Academic Press, New York, 1985.
- Weast, R. C. (Ed.), "CRC Handbook of Chemistry and Physics," 53rd ed. CRC Press, Boca Raton, FL, 1972.
- Brandrup, J., and Immergut, E. H. (Eds.), "Polymer Handbook," 2nd ed. Wiley-Interscience, New York, 1975.
- Klein, J., *J. Chem. Soc. Faraday Trans. 1* **79**, 99 (1983).
- Porter, C. H., and Boyd, R. H., *Macromolecules* **4**, 589 (1971).
- Se, K., Adachi, K., and Kotaka, T., *Polym. J.* **13**, 1009 (1981).
- Israelachvili, J. N., and Pashley, R. M., *J. Colloid Interface Sci.* **98**, 500 (1984).
- Pashley, R. M., McGuiggan, P. M., and Ninham, B. W., *Science* **229**, 1088 (1985).
- Perez, E., and Proust, J. E., *J. Phys. Lett.* **46**, 79 (1985).
- Claesson, P. M., Kjellander, R., Stenius, P., and Christenson, H. K., *J. Chem. Soc. Faraday Trans. 1* **82**, 2735 (1986).
- Rabinovich, Ya.I., and Derjaguin, B. V., *Colloids Surf.* **30**, 243 (1988).
- Claesson, P. M., and Christenson, H. K., *J. Phys. Chem.* **92**, 1650 (1988).
- Hadzioannou, G., Patel, S., Granick, S., and Tirrell, M., *J. Amer. Chem. Soc.* **108**, 2869 (1986).
- Jeon, S. I., and Andrade, J. D., *J. Colloid Interface Sci.* **142**, 159 (1991).
- De L. Costello, B. A., Luckham, P. F., and Tadros, Th. F., *Colloids Surf.* **34**, 301 (1988/1989).

Protein-Surface Interactions in the Presence of Polyethylene Oxide

II. Effect of Protein Size

S. I. JEON¹ AND J. D. ANDRADE

Departments of Bioengineering and Materials Science, Center for Biopolymers at Interfaces, College of Engineering, University of Utah, Salt Lake City, Utah 84112

Received October 16, 1989; accepted August 21, 1990

Polyethylene oxide (PEO) surfaces exhibit low protein adsorption. PEO surface-protein interactions are examined theoretically as a function of surface density and chain length of PEO and variation in the size of the protein (assumed to be a sphere). Recent studies suggest that the PEO surface may have a small hydrophobic character. We study the effect of surface density of PEO and protein size and deduce the PEO surface density conditions for optimal protein resistance. For small proteins ($R \sim 20$ Å), D should be small (~ 10 Å), while for large proteins ($R \sim 60$ – 80 Å), D should be larger (~ 15 Å), where R is the protein radius and D is the average distance between end-attached PEO chains. These results evolve from the trade-offs between steric repulsion and the assumed weak hydrophobic interaction between the PEO layer and the protein. The longest chain length of PEO at optimum surface density appears best for protein resistance. As a number of assumptions and estimates are involved in the model, the results can be taken only as qualitative trends at this time. The trends should be helpful in the design and evaluation of surfaces resistant to protein adsorption. © 1991 Academic Press, Inc.

INTRODUCTION

Polyethylene oxide (PEO) surfaces are becoming recognized as exhibiting strongly reduced protein adsorption (1–5). The protein-resistant character of PEO is generally recognized as a steric stabilization effect (6–9). Besides this steric exclusion character, we must consider the van der Waals attraction between PEO and protein, although the van der Waals attraction force is generally much smaller than the steric repulsion force (9). Recent studies (10–13) suggest that PEO surfaces have a hydrophobic character (11), which may induce a weak hydrophobic interaction between PEO and protein when an assumed hydrophobic patch on the protein is oriented to PEO. Here we assume a hydro-

phobic character to PEO and include this assumed hydrophobic interaction in the analysis.

All of the forces (steric, van der Waals, and hydrophobic) are considered as functions of the size of the protein (protein is assumed to be a sphere) and surface density and chain length of PEO.

MODELING

We use a model similar to that in our previous paper (9) except that the protein has a finite spherical shape. Our modeling picture is shown in Fig. 1. We assume that the PEO surface can be represented as a flat plate for simplicity, even when the spherical protein approaches and affects the PEO surface. The variables are protein size (radius of spherical protein, R) and the surface density and chain length of PEO, the distance D between the terminally attached PEO chains, and the degree of polymerization, N , respectively. Only the "brush" case is considered (6), meaning that

¹ On leave from the Department of Chemistry, Kangreung National University, Kangreung, Kangwondo 210-702, Korea.

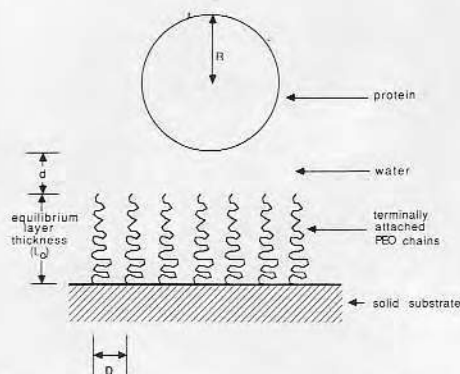


FIG. 1. Our model picture for terminally attached PEO chains to a solid substrate with a finite size of spherical protein in water solvent. R , d , and D are the radius of spherical protein, the distance between the flat PEO surface and a protein, and the distance between the terminally attached PEO chains, respectively.

the distance D is less than the Flory radius, $R_F = aN^{3/5}$.

METHOD

The nonretarded van der Waals interaction free energies (divided by kT) between the flat PEO surface and spherical protein across water media, and between the solid substrate and spherical protein across the terminally attached PEO media, are given as (14)

$$\frac{E_A}{kT} = -\frac{A}{6kT} \left(\frac{R}{d} + \frac{R}{d+2R} + \ln \frac{d}{d+2R} \right) \quad [1]$$

$$A = \frac{3h\nu_e}{8\sqrt{2}} \frac{(n_1^2 - n_3^2)(n_2^2 - n_3^2)}{(n_1^2 + n_3^2)^{1/2}(n_2^2 + n_3^2)^{1/2}} \times \frac{1}{[(n_1^2 + n_3^2)^{1/2} + (n_2^2 + n_3^2)^{1/2}]} + \frac{3}{4} kT \frac{(\epsilon_1 - \epsilon_3)(\epsilon_2 - \epsilon_3)}{(\epsilon_1 + \epsilon_3)(\epsilon_2 + \epsilon_3)} \quad [2]$$

where A is the Hamaker constant between bodies 1 and 2 across a medium 3 (water or PEO in water); R is the radius of spherical protein; d is the distance between the flat PEO

surface and spherical protein; h is Planck's constant; ν_e is the main electronic absorption frequency ($3 \times 10^{15} \text{ sec}^{-1}$); n_1 , n_2 , and n_3 are the refractive indices (15, 16) of phases 1, 2, and 3, respectively, which are determined by the same method as in our previous paper (9); and ϵ_1 , ϵ_2 , and ϵ_3 are the static dielectric constants (15, 16) of phases 1, 2, and 3, respectively, which are also determined by the same method as in our previous paper (9).

The steric repulsion free energy of terminally attached PEO chains under the effect of spherical protein is calculated as the steric repulsion free energy per unit surface area, which is treated as in our previous paper (9), multiplied by πR^2 for simplicity, where R is the radius of the spherical protein. The k_1 and k_2 values used for PEO are 0.007 and 0.02, respectively, which were developed in our previous paper (9).

The existence of hydrophobic attractive forces are generally recognized, and such forces may be 10 to 100 times stronger than the van der Waals forces (17–21). The hydrophobic character of PEO in water has been discussed (10–13); the nearly linear increases in protein adsorption on PEO surfaces with temperature have been discussed in terms of the increasing hydrophobic interaction between PEO and protein (13), perhaps due to an increasing hydrophobicity of PEO with temperature, i.e., $H \propto t/t_0$, where H is the relative hydrophobicity of PEO, t is the system temperature, and t_0 is the reference temperature ($^\circ\text{C}$). The thickness of adsorbed PEO appears to increase linearly with temperature (11), $L/L_0 \propto t/t_0$, where L is the thickness of PEO and L_0 is the thickness at the reference temperature. We estimate a relationship between hydrophobicity and thickness of PEO from the linear relationship between the experimental data and temperature (11, 13), i.e., $H \sim 1.98L/L_0$. The scaling theory relation between D and L for a brush model is $L \propto D^{-2/3}$. A decrease in D induces an increase in volume fraction of PEO (6), $\phi_{\text{PEO}} \propto D^{-4/3}$, where ϕ_{PEO} is the volume fraction of PEO. Thus we can relate an increase

in volume fraction of PEO to the increased hydrophobicity of PEO from the above concepts; $H \sim 1.98[\phi_{\text{PEO}}/(\phi_{\text{PEO}})_0]^{1/2}$, where $(\phi_{\text{PEO}})_0$ is the reference volume fraction of PEO ("reference" will be defined in the next section). As the hydrophobicity of PEO is increased, the hydrophobic interaction between the PEO surface and protein is also increased. The hydrophobic interaction free energy (E_H) (divided by kT) was determined by Pashley *et al.* (18) for the case of dihexadecyldimethylammonium acetate (DHDA) monolayers. For the case of a sphere of radius R near a flat surface (17),

$$\frac{E_H}{kT} = -1.903 R e^{-d/14} \quad [3]$$

where d is the distance between a sphere and flat surface. The hydrophobic interaction between the PEO surface and an assumed uniform hydrophobic surface on the protein is treated as 1, 2%, etc., of the hydrophobic interaction (given by Eq. [3]) between DHDA monolayer surfaces. In this manner we can very roughly incorporate the effect of possible hydrophobic interactions between PEO and protein in the overall analysis.

The D value derived from an adsorption experiment (11) (for PEO with molecular mass 1900) is 17 Å, which we choose as the experimental value. Each different degree of hydrophobic interaction between the PEO surface and hydrophobic patch on the protein is combined with the steric repulsion at various layer thicknesses of PEO for different D and N values. These calculations were also performed as a function of protein size. "Optimum" D and N values for each different protein size were thus obtained.

RESULTS AND DISCUSSION

The van der Waals attraction free energy (divided by kT) between the flat PEO surface and a spherical protein is obtained as a function of the radius (R) of protein (Fig. 2). Figure 2a shows the effect of distance (d) between

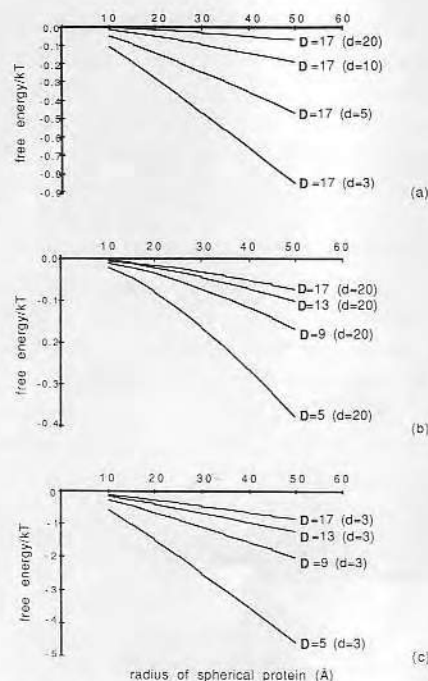


FIG. 2. (a) Van der Waals attraction free energy (divided by kT)–radius of spherical protein profiles for four different d values at constant surface density ($D = 17$ Å). (b) Van der Waals attraction free energy (divided by kT)–radius of spherical protein profiles for four different surface density values at constant distance between the PEO surface and a protein ($d = 20$ Å). (c) Van der Waals attraction free energy (divided by kT)–radius of spherical protein profiles for four different surface density values at constant $d = 3$ Å.

the PEO surface and protein at constant experimentally obtainable surface density ($D = 17$ Å). As the spherical protein approaches the PEO surface, the effect of the size of the protein becomes greater. Similar behavior results at constant distance, d , with the variation of surface density (Figs. 2b and c). As the surface density increases, the effect of protein size increases and the tendency is greater at smaller d values. We choose $d = 3$ Å as the least distance between the PEO surface and a protein under the condition of no adsorption between them [$d = 3$ Å is almost same as the PEO monomer size (2.78 Å)]. If the attraction is greater than the repulsion at this distance, at-

traction is assumed, and the reverse situation is assumed for the reverse case (repulsion).

To examine the effect of van der Waals attraction toward steric repulsion, these two free energies are combined as a function of PEO layer thickness at $d = 3 \text{ \AA}$ and shown in Fig. 3 at $N = 120$ and $D = 17 \text{ \AA}$ for $R = 20$ and 40 \AA , respectively. In this figure, the van der Waals attraction between the solid substrate and a protein across the terminally attached PEO medium is also added, but it does not play a significant role. The addition of any van der Waals attraction to the steric repulsion energy changes the curve only slightly, with no significant change in attraction or repulsion. Therefore, van der Waals attraction between the PEO surface and protein is neglected in our further considerations.

As mentioned above, the hydrophobic interaction between hydrophobic species is much stronger than the van der Waals attraction. If we assume that the PEO surface and the hydrophobic patch on the protein have the

same hydrophobicity as DHDAA, and the spherical protein approaches with its hydrophobic surface oriented toward the PEO surface, the hydrophobic interaction free energy (divided by kT) between the flat PEO surface and spherical protein is calculated by Eq. [3]. The results are shown in Fig. 4 for four different d values as a function of the spherical protein size. The same trend is obtained as for the van der Waals attraction case, and only $d = 3 \text{ \AA}$ is chosen for our further consideration.

We can obtain the basic hydrophobic interaction free energy (divided by kT) at $d = 3 \text{ \AA}$ for each different R value of protein. We assume the PEO-protein interaction to be some small percentage of the DHDAA-protein interaction and compare with the steric repulsion free energy at different surface density and chain length as a function of PEO layer thickness. Because the variation of surface density affects the volume fraction of PEO and thus its possible hydrophobicity, the experimentally obtainable surface density, $D = 17 \text{ \AA}$, is chosen as a reference at equilibrium chain length [in this case, the volume fraction of PEO at equilibrium chain length, $(\phi_{\text{PEO}})_0 = 0.14$]. If the protein continues its approach to the PEO surface without adsorption, the thickness of the PEO layer decreases, the volume fraction of PEO increases, the hydrophobicity of PEO increases, and the hydrophobic interaction between the flat PEO surface and a spherical protein increases. One, two, and three percent hydrophobicity is considered and the hydrophobic interaction free energies are calculated for these three assumed hydrophobicity values of PEO. The combined steric repulsion and hydrophobic interaction free energies (divided by kT) are given in Figs. 4b, c, and d for two different protein sizes, assuming 1, 2, and 3% hydrophobicity of DHDAA for PEO ($N = 120$, $D = 17 \text{ \AA}$), respectively, as a function of the PEO layer thickness. For comparison, the pure steric repulsion free energy (divided by kT) is given in Fig. 4a.

As the hydrophobicity of PEO increases, the attraction increases and no overall repulsion

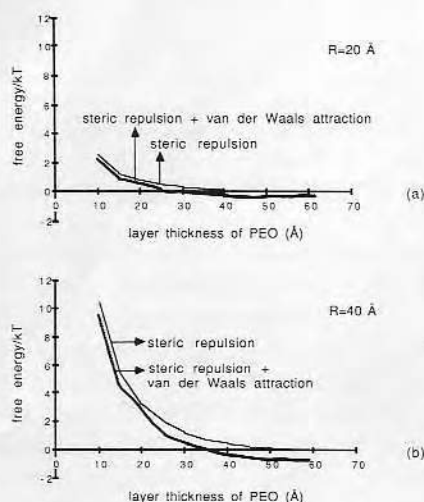


FIG. 3. (a) Steric repulsion and combined steric repulsion and van der Waals attraction free energies (divided by kT)-PEO layer thickness profiles for $R = 20 \text{ \AA}$ at $N = 120$ and $D = 17 \text{ \AA}$. (b) Steric repulsion and combined steric repulsion and van der Waals attraction free energies (divided by kT)-PEO layer thickness profiles for $R = 40 \text{ \AA}$ at $N = 120$ and $D = 17 \text{ \AA}$.

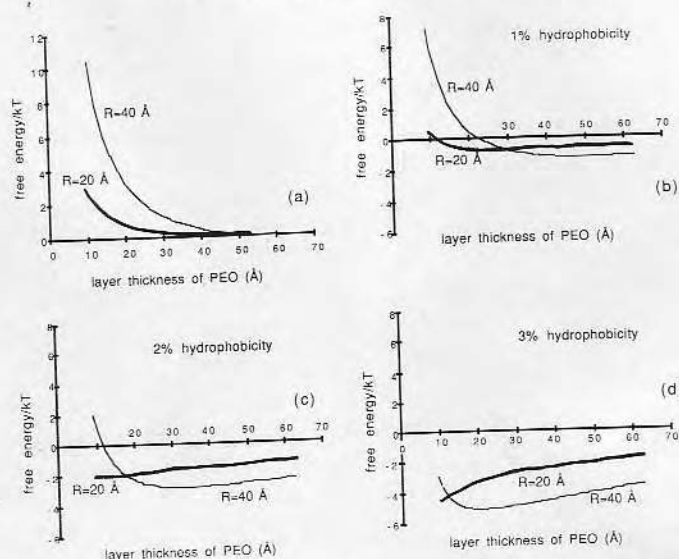


FIG. 4. (a) Steric repulsion free energy (divided by kT)–PEO layer thickness profiles for two different R values at $N = 120$ and $D = 17$ Å. (b) Combined steric repulsion and hydrophobic interaction free energy (divided by kT)–PEO layer thickness profiles for two different R values at $N = 120$ and $D = 17$ Å under the assumption of 1% hydrophobicity of PEO. (c) Combined steric repulsion and hydrophobic interaction free energy (divided by kT)–PEO layer thickness profiles for two different R values at $N = 120$ and $D = 17$ Å under the assumption of 2% hydrophobicity of PEO. (d) Combined steric repulsion and hydrophobic interaction free energy (divided by kT)–PEO layer thickness profiles for two different R values at $N = 120$ and $D = 17$ Å under the assumption of 3% hydrophobicity of PEO.

occurs, regardless of the size of protein. For larger proteins, the attraction between the PEO surface and protein occurs predominantly in an early stage of approach, as the hydrophobicity of PEO increases. The experimentally obtainable PEO surface with $D = 17$ Å has a property of protein resistance (11). We feel that the assumption that the hydrophobicity of PEO is 1% of that of a DHDA monolayer is more probable than the higher assumed hydrophobicity figures. The 1% hydrophobicity assumption is considered for the remainder of the paper.

To observe the effect of surface density on the repulsion and attraction pattern between the PEO surface and a protein is interesting. The variation of surface density at constant chain length reflects the equilibrium layer thickness of PEO and induces different values of layer thickness of PEO as the protein approaches. The calculated free energy plots as

a function of layer thickness of PEO (not shown here) show that the effect of surface density is very complex. The layer thickness of PEO is a function of volume fraction of PEO, and the plot of free energy as a function of volume fraction of PEO (instead of layer thickness) shows the variation of surface density, which is very simple and meaningful. The combined free energies as a function of volume fraction of PEO at constant chain length ($N = 120$) for various D values are given in Fig. 5 for $R = 20, 40, 60$, and 80 Å, respectively. The PEO with low surface density (high D value) starts the curve at low volume fraction of PEO (ϕ_{PEO}) and the repulsion against attraction increases as the chain has been compressed (as the protein approaches without adsorption). As the protein continues to approach without adsorption, the protein-resistant property develops at any volume fraction of PEO, as steric repulsion develops more rap-

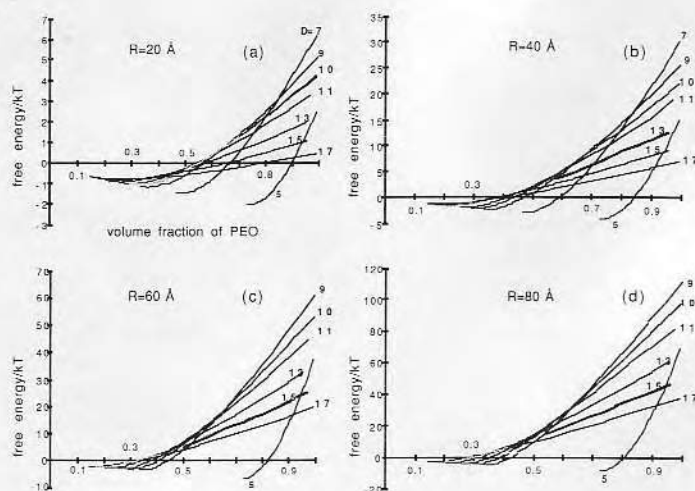


FIG. 5. (a) Combined steric repulsion and hydrophobic interaction free energy (divided by kT)–volume fraction of PEO profiles for various D values at constant radius of spherical protein ($R = 20$ Å) and $N = 120$. (b) Combined steric repulsion and hydrophobic interaction free energy (divided by kT)–volume fraction of PEO profiles for various D values at constant $R = 40$ Å and $N = 120$. (c) Combined steric repulsion and hydrophobic interaction free energy (divided by kT)–volume fraction of PEO profiles for various D values at constant $R = 60$ Å and $N = 120$. (d) Combined steric repulsion and hydrophobic interaction free energy (divided by kT)–volume fraction of PEO profiles for various D values at constant $R = 80$ Å and $N = 120$.

idly than hydrophobic attraction. The predominance of repulsion over attraction at lower volume fractions of PEO is better for protein resistance. The existence of repulsion at lower volume fraction of PEO means that the repulsion occurs as soon as the protein approaches the PEO surface. We can obtain the optimum surface density, which starts the repulsion at lowest volume fraction of PEO, for each different R value. But the difference between the surface densities is small. Thus the approximate optimum surface density for different R values becomes $D = 9$ – 11 Å for $R = 20$ Å, 11 – 15 Å for 40 Å, and 13 – 17 Å for 60 and 80 Å (Figs. 5a, b, c, and d, respectively). From this result, a relatively high surface density of PEO is best to resist small proteins; a lower surface density of PEO is better for larger ones; and the highest surface density (for example, $D = 5$ or 7 Å) may not be effective for protein resistance.

To investigate the effect of chain length of PEO on protein resistance, the combined free

energies as a function of volume fraction of PEO at constant surface density ($D = 10$ Å) and constant size of protein ($R = 20$ Å) for three different N values are calculated and given in Fig. 6. For these three different N values, the attraction has the same magnitude because of the same surface density. For PEO with longer chain length, the repulsion starts

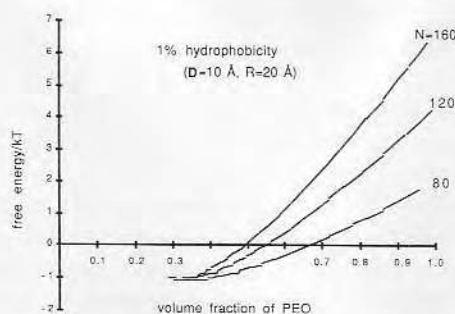


FIG. 6. Combined steric repulsion and hydrophobic interaction free energy (divided by kT)–volume fraction of PEO profiles for three different N values at constant $R = 20$ Å and $D = 10$ Å.

at the lower volume fraction of PEO after the compression of PEO begins. From Fig. 6, we know that the magnitude of repulsion is the greatest for the longest chain length of PEO. *PEO with the longest chain length (highest N value), at the optimum surface density, is best for protein resistance.* In the attachment of longer-chain PEO molecules to substrate, the decrease in surface density occurs naturally (22–24); i.e., the smaller chain length results in higher surface density of attached PEO, although it is difficult to have a very high surface density from the end attachment of a high-molecular-weight PEO. The optimum condition for protein resistance is to produce PEO surfaces with the longest chain length while maintaining the above-mentioned D values for each different size of protein.

CONCLUSION

This study is based on the assumption of PEO chains, terminally attached to a solid substrate in water, interacting with a finite spherical protein. Steric repulsion is compared with van der Waals attraction, showing that the van der Waals attraction has little effect. We then considered hydrophobic interaction between the flat PEO surface and spherical protein under the *assumption* that PEO has a low hydrophobicity and that the protein has a hydrophobic surface. The more realistic case of a small, hydrophobic "patch" on the protein remains to be studied.

As the PEO chains are compressed, the surface density of PEO is increased gradually; thus the "hydrophobicity" of the PEO layer increases. This concept is applied to seek an optimum surface density for each different size of protein. The study of the effect of chain length of PEO on protein resistance suggests that the longest chain length of PEO is best, assuming constant surface density. The variation in chain length of PEO induces a variation in PEO surface density. So the optimum condition of PEO for protein resistance is to obtain the PEO surface with longer chain

length, maintaining the "optimal" D values for each different protein size range.

It is hoped and expected that these predictions may be experimentally tested in the near future. For the time being, those investigators applying PEO surfaces to minimize protein adsorption or to enhance biocompatibility should be aware that their results may be sensitive to the details of their PEO surfaces, that is, surface density and chain length, and to the detailed protein composition and nature of the solution.

ACKNOWLEDGMENTS

S. I. Jeon acknowledges partial support from the Korea Science and Engineering Foundation (KOSEF). This work has been partially supported by a grant from Ciba-Geigy Pharmaceuticals (Horsham, England) to the Center for Biopolymers at Interfaces (CBI), University of Utah. We thank C. G. Golander, K. Caldwell, J. Kopecek, and K. Petrak for stimulating discussions. We thank Professor P. G. de Gennes for stimulating our interest in scaling approaches to interfacial phenomena.

REFERENCES

1. Gregonis, D. E., Buerger, D. E., Van Wagenen, R. A., Hunter, S. K., and Andrade, J. D., *Biomaterials* **84**, *Trans. Soc. Biomater.* **7**, 766 (1984).
2. Andrade, J. D. (Ed.), "Surface and Interfacial Aspects of Biomedical Polymers," Ch. 1. Plenum, New York, 1985.
3. Andrade, J. D., Nagaoka, S., Cooper, S., Okano, T., and Kim, S. W., *ASAIO J.* **10**, 75 (1987).
4. Lee, J. H., "Interactions of PEO-Containing Polymeric Surfactants with Hydrophobic Surfaces," Ph.D. thesis, University of Utah, 1988.
5. Gombotz, W. R., Hoffman, A. S., Harris, J. M., Hovanes, B., Wang, G. H., and Safran, A., "IUPAC—Macromolecules Symposium, Seoul, Korea, June 1989."
6. de Gennes, P. G., *Ann. Chim.* **77**, 389 (1987).
7. Taunton, H. J., Toprakcioglu, C., Fetters, L. J., and Klein, J., *Nature (London)* **332**, 712 (1988).
8. Patel, S., Tirrell, M., and Hadziioannou, G., *Colloids Surf.* **31**, 157 (1988).
9. Jeon, S. I., Lee, J. H., Andrade, J. D., and de Gennes, P. G., *J. Colloid Interface Sci.* **142**, (1991).
10. Claesson, P. M., Kjellander, R., Stenius, P., and Christenson, H. K., *J. Chem. Soc. Faraday Trans. 1* **82**, 2735 (1986).

11. Claesson, P. M., and Golander, C. G., *J. Colloid Interface Sci.* **117**, 366 (1987).
12. Florin, E., Kjellander, R., and Eriksson, J. C., *J. Chem. Soc. Faraday Trans. 1* **80**, 2889 (1984).
13. Golander, C. G., Kiss, E., Eriksson, J. C., and Stenius, P., "Proceedings, 5th Colloid Chemistry Conference, Balatonfured, Hungary, Oct. 1988."
14. Mahanty, J., and Ninham, B. W., "Dispersion Forces." Academic Press, London, 1976.
15. Brandrup, J., and Immergut, E. H. (Eds.), "Polymer Handbook," 2nd ed. Wiley-Interscience, New York, 1975.
16. Weast, R. C., "CRC Handbook of Chemistry and Physics," 53rd ed. CRC Press, Boca Raton, FL, 1972.
17. Israelachvili, J. N., and Pashley, R. M., *J. Colloid Interface Sci.* **98**, 500 (1984).
18. Pashley, R. M., McGuiggan, P. M., and Ninham, B. W., *Science* **229**, 1088 (1985).
19. Perez, E., and Proust, J. E., *J. Phys. Lett.* **46**, 79 (1985).
20. Rabinovich, Ya.I., and Derjaguin, B. V., *Colloids Surf.* **30**, 243 (1988).
21. Claesson, P. M., and Christenson, H. K., *J. Phys. Chem.* **92**, 1650 (1988).
22. Klein, J., and Luckham, P. F., *Nature (London)* **300**, 429 (1982).
23. Luckham, P. F., and Klein, J., *Macromolecules* **18**, 721 (1985).
24. Taunton, H. J., Toprakcioglu, C., Fetters, L. J., and Klein, J., *Macromolecules* **23**, 571 (1990).

The Steric Repulsion Properties of Polyethylene Oxide

Sang Il Jeon* and Joseph D. Andrade†

*Department of Chemistry, Kangnung National University, Kangnung 210-702

†Departments of Bioengineering and Materials Science, University of Utah, Salt Lake City, Utah 84112, U.S.A.

Received October 29, 1991

Polyethylene oxide (PEO) surfaces are recognized as having an effective steric stabilization character. A theoretical scaling analysis involves the osmotic and elastic coefficients of the polymer as a function of molecular weight, in a good solvent. The calculated results show that PEO in water may exhibit the greatest flexibility among water soluble polymers, probably due to its lowest elastic contribution.

Introduction

Polymers adsorbed on solid surfaces immersed in a liquid medium are considerably protected against aggregation, a phenomenon termed steric stabilization. There exist long-range repulsion forces between two surfaces bearing such adsorbed layers, and these repulsive forces overcome the attractive van der Waals forces acting between the bare surfaces.

Polyethylene oxide (PEO) adsorbed surfaces are recognized as effective in minimizing protein adsorption¹⁻⁵, probably due to a steric stabilization effect^{6,7}. Direct force measurements⁸⁻¹⁰ between two adsorbed PEO surfaces onto mica in a good aqueous 0.1 M KNO₃ solvent by the Israelachvili force method¹¹ show that the repulsion forces develop at certain separation distances due to the steric repulsion phenomenon.

A scaling model of chains adsorbed onto a surface in a good solvent was proposed by Alexander¹² and further extended by de Gennes¹³ to give a form for the steric repulsion force profile. The force is analyzed in terms of a repulsive

osmotic term, which comes from the increased polymer concentration in the intersurface gap as the surfaces approach, and an elastic term in which the reduction in free energy, on compression of the over-extended chains, is taken into account. The Alexander-de Gennes model has been developed into a theory of the forces between two such adsorbed layers by Patel *et al.*¹⁴. Their result is that the force *vs* separation distance between two adsorbed surfaces can be expressed as a universal dimensionless function which contains two unknown proportionality constants resulting from the osmotic and elastic contributions.

In this paper, the more effective character of PEO for protein-resistant surfaces was studied by comparison of the osmotic and elastic coefficients of PEO of several molecular weights in good aqueous electrolyte and toluene solvents. The osmotic and elastic coefficients of PEO in aqueous electrolyte and toluene solvents were estimated by the universal curve-fitting method of Patel *et al.*¹⁴ adsorbed on mica surfaces in 0.1 M aqueous KNO₃^{8,9,15,16} and toluene solvents^{10,16,17}, using a least-squares curve fitting method. The data for polystyrene (PS) adsorbed on mica surface in toluene^{7,18} is also

Table 1. The Calculated Osmotic and Elastic Coefficients of PEO and PS in Aqueous 0.1 M KNO₃ and Toluene Solvents with the Variation of Molecular Weight of Polymer

	PEO in aq. KNO ₃		PEO in toluene			PS in toluene		
M_w	3.1×10^5	4.0×10^4	3.1×10^5	1.6×10^5	4.0×10^4	3.75×10^5	1.81×10^5	1.41×10^5
Γ (mg · m ⁻²)	4.0	4.0	2.0	1.5	1.0	3.0	1.6	3.0
L_0 (exp) (Å)	400	225	750	550	280	1100	750	650
k_1	0.004	0.002	0.12	0.23	0.18	0.64	11.44	1.50
k_2	0.12	0.025	1.08	0.68	0.24	0.07	0.75	0.16
L_0 (Å)	397	218	705	640	270	1170	690	616

considered for comparison.

Method

The universal dimensionless function relating the dimensionless energy (ϵ) and dimensionless separation distance (∂) in a good solvent was obtained by Patel *et al.*¹⁴ as follows:

$$\epsilon = 4\pi k_1 x^{5/4} \{[(x\partial)^{-5/4} - 1] + (5/7)[(x\partial)^{7/4} - 1]\} \quad (1)$$

where,

$$x^3 = (7/5)(k_2/k_1), \quad \partial = D/(2aN\sigma^{1/3}),$$

and

$$\epsilon = (F/R)(a^2/k_B T)(1/N\sigma^{11/6})$$

In these formulas, two unknown proportionality coefficients, k_1 and k_2 , are referred to as the osmotic and elastic contributions to the force, respectively, D is the separation distance between the two adsorbed surfaces, a is the size of a segment of the polymer chain (2.78 Å for PEO and 2.22 Å for PS from crystallographic data¹⁹⁻²¹), N is the number of segments in the nonadsorbing part of the chain, $k_B T$ is the thermal energy, F/R is the force between crossed cylinders having radius R , which is 2π times the energy per unit area of interaction between parallel plates²², and σ is a dimensionless surface density of chains emanating from the surface, $\sigma = a^2/\delta^2$, where δ is the average spacing between chains on the surface.

The surface density (σ) can be calculated from the data of adsorbed amounts by assuming hexagonal packing of spheres of polymer¹⁵. D and F/R are given by the published experimentally determined force *vs* separation distance plots, which are reduced to the dimensionless distance (∂) and dimensionless energy (ϵ) based on σ . The coefficients k_1 and x are then calculated from Eq. (1) by using the least-squares curve fitting method, giving the final k_1 and k_2 values for PEO and PS of several molecular weights in good aqueous electrolyte and toluene solvents.

Force *vs* separation profiles^{7-10,15-18} represent the onset of repulsions as a function of separation distance, which is the basis of the experimentally determined effective layer thickness of the adsorbed chains, L_0 (exp), as measured by half the range for onset of repulsive interactions. The theoretically effective single layer thickness of the adsorbed chains, L_0 , is given by consideration of the osmotic and elastic contributions, $L_0 = [(5/7) \cdot (k_1/k_2)]^{1/3} \cdot Na\sigma^{1/3}$, which is also compared with the L_0 (exp).

Results and Discussion

The calculated results from the published data^{7-10,15-18} are given in Table 1. To some extent, a consistency of experimental and theoretical layer thickness values of adsorbed chains (L_0 (exp) and L_0) tells that the theory is about correct and suitable to study the steric repulsion properties of PEO in water. The remaining data except L_0 are inconsistent and are not easily comparable with each other, which may be largely due to the lack of certainties of experimentally determined adsorbed amounts (the adsorbed amounts affect the degree of osmotic and elastic contributions to the force). The adsorbed amounts in the literature are rough values, which is verified by the experimental fact^{8,9,15,16} that all direct force measurements between two adsorbed polymer surfaces show different force values, even for measurements at the same molecular weight and solvent conditions, i.e., different measurements for the same sample produce the different results (in part due to difference in the adsorbed amounts of polymer on the surface).

The repulsive osmotic coefficient is increased due to increased polymer concentration in the intersurface gap as the surfaces approach. The osmotic effect will dominate at very high compressions^{7,15} and is expressed in Eq. (1). If Table 1 is looked at as a rough estimate, the osmotic coefficients (k_1) are nearly similar for each different polymer-solvent system in spite of the difference of molecular weight, which means that the osmotic pressure is about the same for the same polymer-solvent systems. The comparison of k_1 values for each different polymer-solvent system (about >1 for PS-toluene, 0.1-0.5 for PEO-toluene, and 0.002-0.01 for PEO-aqueous KNO₃) show that toluene is a good solvent for PS and PEO and the aqueous 0.1 M KNO₃ solution is a solvent (not good) for PEO. Toluene is a better solvent for PS than PEO, which is also supported by the experimental fact that the PEO block is adsorbed onto the mica and PS does not, for PS-PEO diblock copolymers in toluene¹⁷. To have approximately the same value of k_1 for different molecular weight PEO-water systems, it is necessary to control the adsorbed amounts. It is also a prior condition that the adsorbed amounts generally increase with adsorption of longer chains¹⁰. The same procedures are also applied for PEO-toluene and PS-toluene systems. The results are shown in Table 2. Comparing the L_0 values, PEO is less stretched in aqueous 0.1 M KNO₃ solvent than in toluene, which could be due in part to a greater decrease in k_1 in aqueous solvent. The lower value of k_1 of PEO in aqueous electrolyte than in orga-

Table 2. The Revised Osmotic and Elastic Coefficients of PEO and PS in Good Solvents with the Correction of the Adsorbance

	PEO in aq. KNO ₃		PEO in toluene			PS in toluene		
M_w	3.1×10^5	4.0×10^4	3.1×10^5	1.6×10^5	4.0×10^4	3.75×10^5	1.8×10^5	1.41×10^5
Γ (mg · m ⁻²)	4.0	3.2	1.6	1.6	0.9	2.1	3.9	3.0
k_1	0.004	0.004	0.2	0.2	0.2	1.5	1.5	1.5
k_2	0.12	0.03	1.43	0.51	0.23	0.12	0.25	0.16
L_0/L_c (%)	3.95	8.6	3.6	6.3	10.7	14.6	17.9	20.5

nic solvent is also supported by the polymer-solvent interaction parameter, χ (0.39 and 0.48 for PEO-toluene²³ and PEO-0.1 M KNO₃²⁴, respectively). Values of χ up to 0.5 are found for systems showing complete miscibility, while for $\chi > 0.5$ the systems are characterized by only limited miscibility, with higher values of χ corresponding to decreasing extent of interaction of the two components⁴. In our previous study²⁵, the osmotic contribution has the more effect on the chain extension than the elastic contribution. The variation of the k_1 value has the more effect on the change of the layer thickness of the chain in a good solvent.

The effects of k_1 and k_2 values on the steric force are opposite; the increase of osmotic contribution (k_1) gives rise to an increase of the spacing between chains in solvent, stretching them. On the other hand the elastic contribution (k_2) is a stiffness factor; its increase makes the chain more stiff and less flexible, and harder to stretch. PEO in water has lower k_1 and k_2 values than in other solvent systems. The lower the k_1 value, the less stretch (i.e., it is less effective for steric repulsion) of the chain. On the other hand, the lower the k_2 value, the more flexible the chain. The k_2 value of PEO in aqueous solvent is lower than in any other investigated polymer-solvent systems.

PEO is very flexible and movable. Long flexible PEO chains on the surface have been called "molecular cilia" by Nagaoka and coworkers³. Thus the prominent steric repulsion properties of PEO in water are mainly contributed by this flexibility, which is probably caused by the large decrease in k_2 in spite of the decrease of k_1 . On the other hand, the remarkable stretching of the PS chain in toluene is mainly attributed to the large increase in the osmotic contribution in spite of the increase of the elastic contribution. Table 2 shows that change of molecular weight has great influence on the degree of the elastic contribution to the force and also on the layer thickness (L_0) (the osmotic contribution is assumed to be constant for the same polymer-solvent system, even if the molecular weight of polymer is varied). L_0 can be compared with the fully extended layer thickness (contour length)²⁶, $L_c = aN$. L_0/L_c values are shown in last row of Table 2. The chains are stretched to about 3 to 20% of their fully extended length according to their molecular weight. Considering the effect of solvent on PEO, for a given mass of polymer the L_0/L_c values are similar for each PEO-solvent systems in spite of the larger decrease in k_1 value in aqueous electrolyte, which could be due to a decrease in k_2 value and the difference in the conformation of the PEO in organic solvents and in water. PEO in organic solvents exists as a random coil, whereas in water its conformation is helical^{14,27,28}. As the molecular weight of the polymer

is decreased, the ratio, L_0/L_c , is increased, mainly due to the larger decrease of the elastic contribution. The chain is actually more flexible and stretched, as the chain is shortened. Thus the longest chain of PEO in water without any flexibility may not be effective for steric repulsion, which is supported experimentally³ and theoretically^{24,29} by some investigators. A suitable length of PEO with higher flexibility (higher L_0/L_c value) is appropriate for steric repulsion, i.e., protein-resistance.

Conclusion

We examined the main factors in the prominent steric repulsion properties of PEO adsorbed surfaces in water, considering the osmotic and elastic contributions to the steric repulsion force. As the elastic contribution of the polymer chain in a good solvent is lowered, the stiffness is lowered, and the flexibility is increased. PEO in water has the highest flexibility, probably caused by having the lowest elastic contribution. The prominent steric repulsion properties of PEO adsorbed surfaces in water may be mainly due to the greater contribution of an elastic factor than an osmotic one. Comparing the osmotic contributions of various polymer-solvent systems, water may not be a very good solvent for PEO, and toluene is a good solvent for both PEO and PS, but it is a better one for PS. The layer thickness of the chains is mainly controlled by the osmotic factor, so longer chains are observed in PS-toluene than in any other polymer-solvent system because of higher osmotic contribution to the steric repulsion force. As the molecular weight of the polymer is lowered, the chain is more stretched to its fully extended state and is more flexible. Thus a moderate length of PEO with higher flexibility should be more suitable for steric repulsion.

Acknowledgement. This work was supported by the research fund from the Kangnung National University, 1991.

References

1. D. E. Gregonis, D. E. Buerger, R. A. Van Wagenen, S. K. Hunter, and J. D. Andrade, *Biomaterials* **84**, *Trans. Soc. Biomater.*, **7**, 766 (1984).
2. J. D. Andrade (Ed.), "Surface and Interfacial Aspects of Biomedical Polymers", Ch. 1, Plenum Press, New York, 1985.
3. J. D. Andrade, S. Nagaoka, S. Cooper, T. Okano, and S. W. Kim, *ASAIO J.*, **10**, 75 (1987).
4. J. H. Lee, "Interactions of PEO-Containing Polymeric Surfactants with Hydrophobic Surfaces", Ph. D. Thesis,

- University of Utah, 1988.
5. W. R. Gombotz, A. S. Hoffman, J. M. Harris, B. Hovanes, G. H. Wang, and A. Safran, "IUPAC Macromolecules Symposium", Seoul, Korea, June, 1989.
6. P. G. de Gennes, *Ann. Chim.*, **77**, 389 (1987).
7. H. J. Taunton, C. Toprakcioglu, L. J. Fetters, and J. Klein, *Nature (London)*, **332**, 712 (1988).
8. J. Klein and P. Luckham, *Nature (London)*, **300**, 429 (1982).
9. J. Klein and P. Luckham, *Macromolecules*, **17**, 1041 (1984).
10. P. Luckham and J. Klein, *Macromolecules*, **18**, 721 (1985).
11. J. N. Israelachvili and G. J. Adams, *J. Chem. Soc., Faraday Trans. 1*, **79**, 975 (1978).
12. S. J. Alexander, *J. Phys. (Les Ulis, Fr.)*, **38**, 983 (1977).
13. P. G. de Gennes, *Acad. Sci. Paris*, **300**, 839 (1985).
14. S. Patel, M. Tirrell, and G. Hadziioannou, *Colloids Surf.*, **31**, 157 (1988).
15. P. F. Luckham and J. Klein, *J. Chem. Soc. Faraday Trans.*, **86**, 1363 (1990).
16. J. Klein and P. F. Luckham, *Macromolecules*, **19**, 2007 (1986).
17. H. J. Taunton, C. Toprakcioglu, and J. Klein, *Macromolecules*, **21**, 3333 (1988).
18. H. J. Taunton, C. Toprakcioglu, L. J. Fetters, and J. Klein, *ACS: Div. of Polym. Chem. (Polym. Preprints)*, **30**, 368 (1989).
19. H. Tadokoro, Y. Chatani, T. Yoshihara, S. Tahara, and M. Murahashi, *Makromol. Chem.*, **73**, 109 (1964).
20. Y. Takahashi and H. Tadokoro, *Macromolecules*, **6**, 672 (1973).
21. J. Brandrup and E. H. Immergut (Eds.), "Polymer Handbook", 3rd ed., Wiley-Interscience, New York, 1989.
22. J. N. Israelachvili, "Intermolecular and Surface Forces", Academic Press, New York, 1985.
23. F. J. Ansorena, M. J. Fernandez-Berridi, M. J. Barandiaran, G. M. Guzman, and J. J. Iruin, *Polym. Bull.*, **4**, 25 (1981).
24. B. Vincent, P. F. Luckham, and F. A. Waite, *J. Colloid Interface Sci.*, **73**, 508 (1980).
25. S. I. Jeon, J. H. Lee, J. D. Andrade, and P. G. de Gennes, *J. Colloid Interface Sci.*, **142**, 149 (1991).
26. G. Hadziioannou, S. Patel, S. Granick, and M. Tirrell, *J. Am. Chem. Soc.*, **108**, 2869 (1986).
27. S. H. Maron and F. E. Filisko, *J. Macromol. Sci.*, **B6**, 57 (1972).
28. S. H. Maron and F. E. Filisko, *J. Macromol. Sci.*, **B6**, 79 (1972).
29. S. I. Jeon and J. D. Andrade, *J. Colloid Interface Sci.*, **142**, 159 (1991).

Analysis of Steric Repulsion Forces in Atomic Force Microscope with Polyethylene Oxide in Aqueous Media

Sang Il Jeon* and Joseph D. Andrade†

Department of Chemistry, Kangnung National University, Kangnung 210-702

*†Departments of Bioengineering and Materials Science, University of Utah,
Salt Lake City, Utah 84112, U.S.A., Received October 27, 1992*

We present a theoretical analysis for the use of long-range intermolecular steric repulsion forces for imaging by atomic force microscope (AFM). Polyethylene oxide (PEO) is assumed to be terminally attaching to a spherical AFM tip in aqueous media. Only two long-range intermolecular forces (van der Waals attraction and steric repulsion) are considered. All calculated forces are near 10^{-11} N, which should not produce deformation of the soft protein surface. Calculations are presented as a function of surface density and chain length of terminally attached PEO, and other variables. Longer chain length and maximal surface density of terminally attached PEO to a smaller sized spherical AFM tip (modified AFM system) is appropriate to obtain optimum images of proteins on the surface.

Introduction

The atomic force microscope (AFM) can be used to obtain atomic scale images of observable surfaces¹⁻³. The imaging contrast originates from intermolecular forces between the tip and the surface. The sample need not be a conductor to be imaged. The surfaces to be imaged can also be in an aqueous environment^{3,4}, which enables one to realistically image biological systems and monitor biological processes in real time. Most AFM research is performed in an air media^{1,2,5,6} using short-range intermolecular forces^{7,8}. Long-range intermolecular forces can reduce the risk of damage of the soft protein surface. Long-range intermolecular forces that have been utilized with the AFM are van der Waals force⁹ in air and van der Waals and electrostatic forces¹⁰ in aqueous media.

Polymers attached on solid surfaces immersed in a liquid medium are protected against aggregation by steric stabilization^{11,12}. There exist long-range steric repulsion forces between two surfaces bearing such adsorbed polymer layers. These repulsive forces often exceed the long-range van der Waals and electrostatic forces acting between the bare surfaces⁹. Polyethylene oxide (PEO) surfaces are becoming recognized as exhibiting strongly reduced protein adsorption¹⁴⁻²⁰. The protein-resistant character of PEO is generally recognized as a steric stabilization effect. The origin of these repulsive forces is attributed to two components²¹⁻²³; the osmotic and elastic components. The osmotic component arises from

the local increase in chain segment concentration upon compression resulting in the development of an osmotic pressure. The elastic component arises from the chain segments that have a tendency to extend themselves upon compression.

PEO can be attached to AFM tips of different sizes. The attached PEO can vary in molecular weight (chain length) and in number of chains per unit surface area (surface density), the 2 major molecular factors in steric repulsion^{19,20}. In this paper we present a qualitative theoretical analysis of the steric repulsion forces of PEO attached to a spherical AFM tip interacting with a soft protein sample surface as a function of the surface density and chain length of PEO with the variation of the sizes of tip and sample surface.

Modeling

The shape of the tip is pyramidal and terminates in a point; the apex of the pyramid is approximated as a sphere²⁴. PEO is assumed to be a neutral homopolymer with linear and flexible chains terminally attached to a spherical AFM tip (Figure 1(a)). The surface is assumed to be a hypothetical cylindrical protein adsorbed on mica. Although there can be various cylindrical shapes on the surface, only one unique cylindrical surface is considered (Figures 1(a)). It has a shape of circle from a top view. The surface is treated as one circle because that the assumed cylindrical surface is positioned under the PEO attached AFM tip and we consider

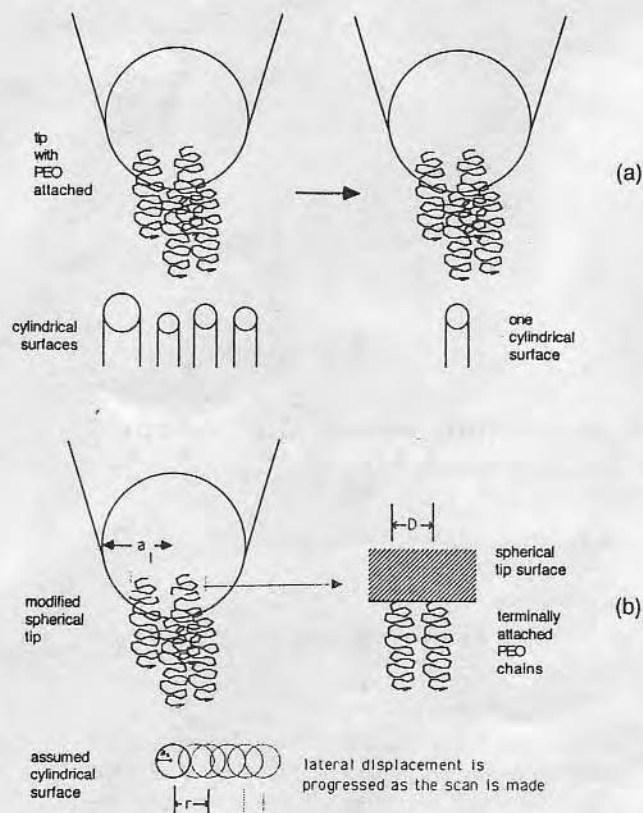


Figure 1. (a) Our model geometry, consisting of a spherical tip with terminally attached PEO chains and sample surface of cylindrical shapes. (b) One circular surface is moved laterally while the modified tip is fixed (scanning). The intermolecular forces between them are calculated as a function of the degree of lateral displacement of the circular surface, $r/2a_2$, where r is the distance from the original circular center to the displaced circular center and a_2 is the radius of sample surface of assumed circular shape. a_1 and D is the radius of assumed spherical tip and the distance between the terminally attached PEO chains, respectively.

only the long-range intermolecular forces between them (Figure 1(b)). The attached PEO chains exhibit steric repulsion force upon compression^{19,20}.

The crucial parameters are the distance D between the terminally attached PEO chains to the AFM tip, a measure of the surface chain density, the degree of polymerization, N , a measure of the chain length, the radius of circular surface, a_2 , a measure of the size of adsorbed protein on mica, and the radius of spherical tip, a_1 , a measure of the AFM tip size (Figure 1(b)). Only the "brush" case is considered¹¹.

Method

Considered long-range intermolecular forces in aqueous media for our modified AFM system are van der Waals and steric repulsion (electrostatic forces are ignored because of the attached neutral PEO chains^{19,20}). The non-retarded van der Waals force between the large spherical AFM tip and one small circle surface across the terminally attached PEO media is given as⁹:

$$F(\text{VDW}) = -\pi a_2^2 \cdot \frac{A}{6\pi L^3} \quad (1)$$

where A is the Hamaker constant^{19,20} between the AFM tip and protein adsorbed circle surface across a medium (PEO in water); a_2 is the radius of circular protein (πa_2^2 is the area); L is the separation distance between the spherical AFM tip and circular protein surface. The long-range repulsive steric force of the PEO-modified tip under the effect of circular protein is calculated as the steric repulsion force per unit surface area^{13,19} multiplied by πa_2^2 :

$$F(S) = \pi a_2^2 \cdot kT \frac{k_1}{a^2} \left(\frac{7}{5} \frac{k_2}{k_1} \right)^{5/12} N \sigma^{1/6} \left(\frac{5}{4} \frac{1}{L_0} \right) \left[\left(\frac{L_0}{L} \right)^{9/4} - \left(\frac{L}{L_0} \right) \right] \quad (2)$$

where k is the Boltzmann constant; T is the absolute temperature; a is the monomer size of PEO (2.78 Å)^{25,26}; N is the degree of polymerization; σ is the surface density of PEO ($\sigma = a^2/D^2$); L_0 is the theoretical equilibrium layer thickness of terminally attached chains in a good solvent system, $L_0 = (5/7 \cdot k_1/k_2)^{1/3} a N \sigma^{1/3}$; and the k_1 and k_2 are the osmotic and elastic contribution of PEO chains and given as 0.004 and 0.03, respectively, which are discussed in our previous paper²⁷.

We assume a minimum detectable force of 10^{-11} N^{24,28}, thus minimizing sample damage. To obtain the AFM detectable real long-range force, the attractive van der Waals force is added to the steric repulsion force. The individual and combined force ($F = F(\text{VDW}) + F(S)$) calculations were performed using N values from 50 to 150 and D values from 5 to 11 Å for the variation of separation distances between the spherical tip and one circular protein surface.

AFM scanning involves the lateral movement of the sample with respect to the tip^{4,5,29}. If the separation distance between two centers increases, the interaction force between them is decreased (Figure 1(b)) (constant "height" method)^{4,5,29}. The rate of the decrease of the force during a scan can affect the cantilever deflection, and the "resolution" of the image of one circular surface.

Results and Discussion

The larger steric repulsion forces are reduced by the attractive van der Waals forces. The combined force must be considered in the following text (the force means the combined force if without any remark). The combined force is also compared with the attractive van der Waals force (resulting from our bare AFM tip without any attached polymer chains). The increase of the forces above 10^{-11} N can damage the protein surface^{24,28}. Maintaining the forces at about 10^{-11} N is important in AFM measurements without the damage of sample.

Separation distances between the tip and one circular surface, maintaining a force of 10^{-11} N, are calculated as a function of the circular surface area for different surface density and chain length of terminally attached PEO (Figure 2). To have the merit of using the steric repulsion forces of the modified AFM system compared with the unmodified ones, the separation distances with maintaining the combined force at 10^{-11} N must be longer than those with the van der Waals force of 10^{-11} N (the tip must closely approach to the surface

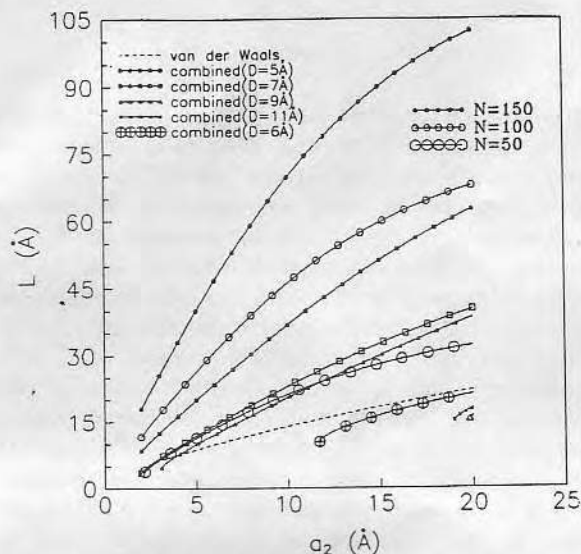


Figure 2. The separation distance, L , plotted against various sizes of circular surfaces for 2 different D values (5 and 6 Å) at $N=50$, 3 different D values (5, 7, and 9 Å) at $N=100$, and 4 different D values (5, 7, 9, and 11 Å) at $N=150$, maintaining a constant combined force of 10^{-11} N. The separation distances with maintaining a constant absolute value of van der Waals force of 10^{-11} N are also inserted for comparison.

of sample to detect the van der Waals force of 10^{-11} N, and then the tip can damage the surface²⁶). It can be achieved by the increase of surface density and chain length of PEO attached to the AFM tip. The distance between the terminally attached PEO chains, D , above 5 Å must be considered because the surface density of crystalline PEO is 0.36^{19,20,25,26}. The distances, D , longer than 6 Å for $N=50$, 9 Å for $N=100$, and 11 Å for $N=150$ produce a combined force lower than the absolute value of van der Waals force in our studied range of circular surface size, meaning the loss of steric repulsion concept under the assumption of only two long-range forces (steric and van der Waals). The distance between the terminally attached chains must be shorter (higher density) than the above critical values to have the combined force detectable at 10^{-11} N. The separation distances between the modified AFM tip and the sample surface increase with increase of observable protein surface size and the extent is greater at longer chain length of PEO. Maintaining forces of 10^{-11} N at longer separation distances can be obtained by higher surface density and longer chain length of PEO. This is desirable for AFM measurements because operation of AFM at shorter separation distances between the AFM tip and the circular surface can induce abrupt attraction of the tip to the substrate (the tip adheres strongly to the substrate end can be withdrawn only with difficulty), and can deform and distort the adsorbed protein surface^{28,30,31}. The higher surface density of attached PEO is very difficult to obtain experimentally^{12,32,33}. Longer chains with experimentally obtainable higher surface density of PEO must be attached to the AFM tip to get the larger steric repulsion forces at longer separation distances.

As the scan is made, the larger spherical tip with PEO is fixed and the smaller circular surface is moved laterally

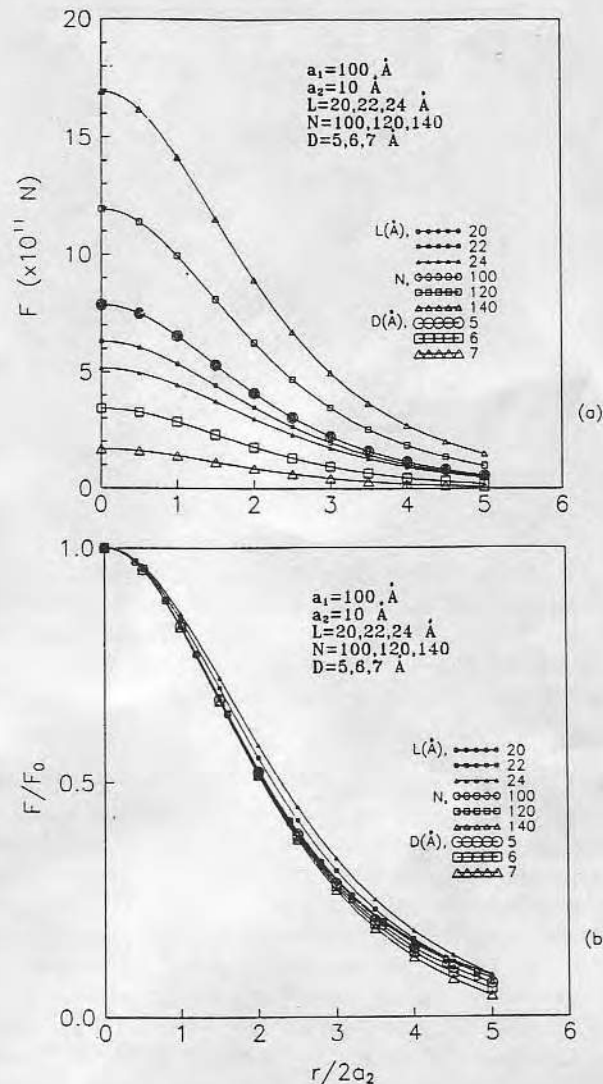


Figure 3. (a) The combined force F , and (b), its relative value, F/F_0 , plotted against the lateral displacement of one circle, $r/2a_2$, for 3 different separation distances ($L=20, 22$, and 24 Å) at $N=100$ and $D=5$ Å, 3 different chain lengths ($N=100, 120$, and 140) at $L=20$ Å and $D=5$ Å, and 3 different surface density ($D=5, 6$, and 7 Å) at $L=20$ Å and $N=100$ as the scan is made. a_1 and a_2 are fixed at 100 Å and 10 Å, respectively. F , the force between tip and one circular surface at any lateral movement of the surface (during scanning) divided by, F_0 , the starting force between tip and assumed center circular surface just under the tip (before scanning), i.e., F/F_0 , gives the relative value of the combined force.

under it, exhibiting gradually declining long-range intermolecular forces between them (Figure 1(b)). The combined long-range intermolecular forces are calculated as a function of the lateral movement of the circular surface from the tip, represented as $r/2a_2$, where r is the distance from the original circular center to the displaced circular center and a_2 is the radius of assumed single circular surface. First, we examine the effect of variation of the separation distance between the constant sizes of tip and circular surface, and the degree of polymerization and the surface density of attached PEO, to the combined intermolecular force (Figure

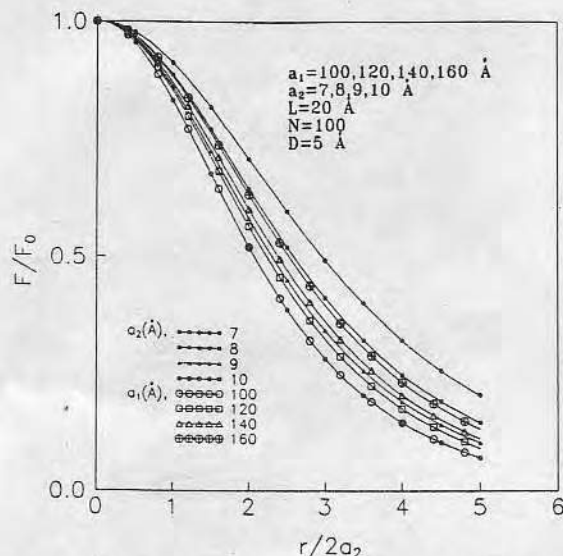


Figure 4. The relative value, F/F_0 , plotted against $r/2a_2$ for 4 different sizes of assumed circular surface ($a_2=7, 8, 9$, and 10 Å) at $a_1=100$ Å and 4 different sizes of assumed spherical tip ($a_1=100, 120, 140$, and 160 Å) at $a_2=10$ Å. L, N , and D are fixed at 20 Å, 100 , and 5 Å, respectively.

3(a)). The force is gradually decreased as the scan is made for all of our examined cases. To compare the extent of decreasing force for the lateral movement of the circular surface, the calculated force is expressed as a relative value, which affects the degree of cantilever deflection and gives a rough estimate of the "resolution" of surface image (Figure 3(b)). The difference of slopes is slight. The interested one is that the increase of chain length and surface density of PEO induces a larger increase of the force (Figure 3(a)), but the relative force has no profound difference (Figure 3(b)). Thus "resolution" is not affected, but the force is easier to detect by AFM. If the un-modified AFM cannot detect the smaller intermolecular force at some longer separation distance because of instrumental limitations, one must increase the detectable force by decrease of separation distance. The AFM can detect the larger force, but the closer approach of two surfaces (tip and sample surface) can induce attraction between them; perhaps deforming the surface^{28,30,31}. All of these problems are alleviated with the modified AFM, obtained by increasing chain length and surface density of the attached PEO, allowing longer separation distances to be used.

A larger circular surface decreases the intermolecular force more steeply and can give a finer circle image (Figure 4), which may be a naturally occurring consequence. AFM tip size has also to be decreased at a fixed chain length and surface density of PEO to obtain a finer surface image i.e., the smaller the tip size, the better the "resolution" (Figure 4).

Modified AFM tips to permit detectable force at relatively longer separation distances and with minimal sample surface deformation require the following conditions: longer chain length and maximal surface density of terminally attached PEO to the smallest possible AFM tip. The surface density is more important than chain length in maximizing the steric

repulsion^{19,20}.

Conclusion

This study is based on the assumption of PEO chains terminally attached to a spherical AFM tip in aqueous media, interacting with one finite circular "protein" surface (i.e., modified AFM system). Only two long-range intermolecular forces between the two surfaces are assumed: van der Waals attraction and steric repulsion. To obtain an estimate of the total force detected by the AFM, the two individual forces are combined. The combined forces are calculated as a function of surface density and chain length of PEO, as well as other variables, and compared with the absolute values of the van der Waals force to obtain the use of long-range steric repulsion force. To get the AFM detectable combined force of 10^{-11} N at relatively longer separation distance, an increase in surface density and chain length of PEO is necessary. The best conditions for $N=50$, $N=100$, and $N=150$ require the chains on the surface to be less than 6, 9, and 11 Å apart, respectively. The intermolecular forces between the spherical AFM tip and one circular protein surface decrease with an increase in separation distance. The longer separation distances, while maintaining forces of 10^{-11} N (which minimally deform the "protein" surface and are more desirable for AFM), can be obtained by higher surface density and longer chain length of PEO. The variation of surface density and chain length of PEO affects the magnitude of the steric repulsion force, but does not significantly affect the "resolution". "Resolution" is improved by the decrease of tip size.

Acknowledgement. This paper was supported (in part) by NON DIRECTED RESEARCH FUND, Korea Research Foundation, 1991 and one of the authors (SIJ) also thanks to the Natural Science Research Institute at Kangnung National University.

References

1. G. Binning, C. F. Quate, and Ch. Gerber, *Phys. Rev. Lett.*, **56**, 930 (1986).
2. P. K. Hansma, V. B. Elings, O. Marti, and C. E. Bracker, *Science*, **242**, 209 (1988).
3. J. N. Lin, B. Drake, A. S. Lea, P. K. Hansma, and J. D. Andrade, *Langmuir*, **6**, 509 (1990).
4. B. Drake, C. B. Prater, A. L. Weisenhorn, S. A. C. Gould, T. R. Albrecht, C. F. Quate, D. S. Cannelli, H. G. Hansma, and P. K. Hansma, *Science*, **243**, 1586 (1989).
5. G. Friedbacher, P. K. Hansma, E. Ramli, and G. D. Stucky, *Science*, **253**, 1261 (1991).
6. J. H. Hoh, R. Lal, S. A. John, J.-P. Revel, and M. F. Arnsdorf, *Science*, **253**, 1405 (1991).
7. O. M. Leung and M. C. Goh, *Science*, **255**, 64 (1992).
8. A. S. Lea, A. Pungor, V. Hlady, J. D. Andrade, J. N. Heron, and E. W. Voss, Jr., *Langmuir*, **8**, 68 (1992).
9. J. N. Israelachvili, "Intermolecular and Surface Forces", Academic Press, London, 1985.
10. W. A. Ducker, T. J. Senden, and R. M. Pashley, *Nature*, **353**, 239 (1991).
11. P. G. de Gennes, *Ann. Chim.*, **77**, 389 (1987).
12. H. J. Taunton, C. Toprakcioglu, L. J. Fetters, and J. Klein,

- Nature*, **332**, 712 (1988).
13. S. Patel, M. Tirrell, and G. Hadziioannou, *Colloids and Surfaces*, **31**, 157 (1988).
14. D. E. Gregonis, D. E. Buerger, R. A. Van Wagenen, S. K. Hunter, and J. D. Andrade, *Biomaterials* **84**, *Trans. Soc. Biomaterials*, **7**, 766 (1984).
15. J. D. Andrade ed., "Surface and Interfacial Aspects of Biomedical Polymers", Ch. 1, Plenum Press, NY, 1985.
16. J. D. Andrade, S. Nagaoka, S. Cooper, T. Okano, and S. W. Kim, *ASAIO J.*, **10**, 75 (1987).
17. J. H. Lee, "Interactions of PEO-containing Polymeric Surfactants with Hydrophobic Surfaces", Ph. D. Thesis, University of Utah, 1988.
18. W. R. Gombotz, A. S. Hoffman, J. M. Harris, B. Hovanes, G. H. Wang, and A. Safran, IUPAC-Macromolecules Symposium, Seoul, Korea, June 1989.
19. S. I. Jeon, J. H. Lee, J. D. Andrade, and P. G. de Gennes, *J. Colloid Interface Sci.*, **142**, 149 (1991).
20. S. I. Jeon and J. D. Andrade, *J. Colloid Interface Sci.*, **142**, 159 (1991).
21. P. G. de Gennes, "Scaling Concepts in Polymer Physics", Cornell University Press, Ithaca, 1979.
22. P. G. de Gennes, *Macromolecules*, **14**, 1637 (1981).
23. P. G. de Gennes, *Macromolecules*, **15**, 492 (1982).
24. B. N. J. Persson, *Chem. Phys. Letters*, **141**, 366 (1987).
25. H. Tadokoro, Y. Chatani, T. Yoshihara, S. Tahara, and M. Murahashi, *Macromol. Chem.*, **73**, 109 (1964).
26. Y. Takahashi and H. Tadokoro, *Macromolecules*, **6**, 672 (1973).
27. S. I. Jeon and J. D. Andrade, *Bull. Korean Chem. Soc.*, **13**, 245 (1992).
28. U. Hartmann, to be published.
29. S. I. Jeon and J. D. Andrade, to be published.
30. H. G. Hansma, J. Vesenska, C. Siegerist, G. Kelderman, H. Morrett, R. L. Sinsheimer, V. Elings, C. Bustamante, and P. K. Hansma, *Science*, **256**, 1180 (1992).
31. C. Bustamante and J. Vesenska, *Polymer Preprints (ACS)*, **31**, 743 (1992).
32. J. Klein and P. F. Luckham, *Nature*, **300**, 429 (1982).
33. P. F. Luckham and J. Klein, *Macromolecules*, **18**, 721 (1985).

Modeling of homogeneous cloned enzyme donor immunoassay

Sang Il Jeon¹, Xiaoyun Yang, Joseph D. Andrade*

Department of Bioengineering, University of Utah, Salt Lake City, UT 84112-9202, USA

Received 3 April 2004

Available online 5 August 2004

Abstract

One of the most widely used analytical techniques for sensitive detection of biologically and clinically significant analytes is the immunoassay. In recent years direct immunoproboscules allowing label-free detection of the interaction between the antibody and the target analyte have proved their capabilities as fast, simple, and nevertheless highly sensitive methods. Cloned enzyme donor immunoassay (CEDIA) homogeneous assay is based on the bacterial enzyme β -galactosidase, which has been genetically engineered into two inactive fragments, enzyme donor and enzyme acceptor. Reassociation of the fragments in the assay forms active enzyme, which acts on substrate to generate a colored product. A comprehensive kinetic model of CEDIA is developed to aid in understanding this method and to facilitate development of a truly homogeneous version, potentially applicable to a dipstick-type multianalyte point of care analytical device (ChemChip). Although the standard assay involves a two-step process, we also chose to model a single-combined process, which would be simpler to apply in a ChemChip device. From the modeling simulation, we obtain the time courses of the amounts of product and active enzyme, from which the dynamic ranges can be obtained as 10^{-6} – 10^{-7} and 10^{-5} – 10^{-7} M analyte concentration for two-step and single-combined processes under the conditions of the assumed parameters, respectively. A simple one-step immunoassay has the merit of reducing time and cost and has an improved dynamic range.

© 2004 Elsevier Inc. All rights reserved.

Keywords: CEDIA immunoassay; Modeling; Analyte; Enzyme acceptor; Analyte-conjugated enzyme donor; Primary antibody; Secondary antibody; Association and dissociation rate constant; Affinity constant; Dynamic range

Immunoassay has become one of the most widely used analytical techniques for sensitive detection of analytes, such as hormones, drugs, tumor markers, specific proteins, viral antigens, etc. Point of care testing applications have also been developed. Improvements in both antibodies and detection systems have resulted in increased sensitivity of immunoassays. For many years radioactive isotopes were used as labels. However, concerns with regard to safety and disposal resulted in the move toward nonradioactive

labels [1]. Fluorescent, luminescent, and enzyme labels are now frequently used in commercially available assays. Of these labels the most commonly used reporter molecule is the enzyme, because it introduces signal amplification through turnover of an appropriate substrate to detectable products [2]. In recent years direct immunoproboscules allowing label-free detection of the interaction between the antibody and the target analyte have proved their capabilities as fast, simple, and highly sensitive methods. A major breakthrough in immunoassay technology was the introduction of the homogeneous immunoassay, which did not require a physical separation of the bound and unbound fractions, much simplifying the assay and allowing it to be potentially applicable to a simple, quantitative “dipstick” format.

* Corresponding authors. Fax: +1-801-585-5361.

E-mail address: joeandrade@uofu.net (J.D. Andrade).

¹ On leave from the Department of Chemistry, Kangnung National University, Kangnung 210-702, Republic of Korea.

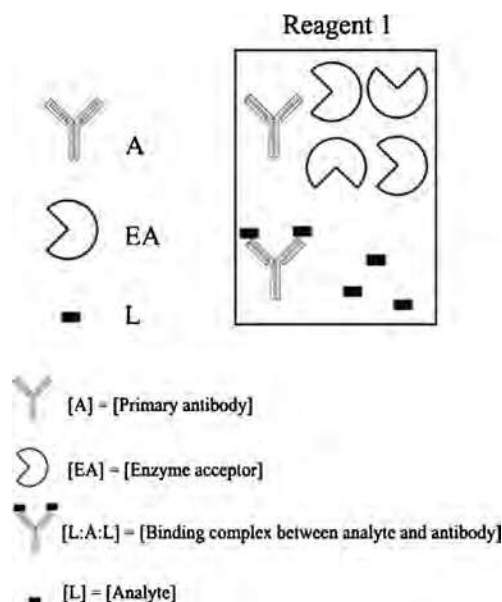


Fig. 1. Schematic representation of step 1 of CEDIA kit experiment [7].

Cloned enzyme donor immunoassay (CEDIA)² homogeneous assay (Figs. 1–3) allows highly sensitive detection of low-molecular-mass analytes without separation steps. It is based on the bacterial enzyme β -galactosidase, which has been genetically engineered into two inactive fragments, enzyme donor (ED) and enzyme acceptor (EA) [3–5]. Complementation of ED and EA forms an active enzyme. The covalent attachment of analyte or ligand to ED does not affect the ability of EA and ED to form active enzyme. Analyte present in a sample competes for binding to the limited number of antibody sites, making ED–ligand conjugate available for enzyme formation. Thus, the amount of enzyme formed is directly proportional to the analyte concentration in the sample.

We have chosen to develop a comprehensive kinetic model of CEDIA [3,4] to aid our understanding of this method and to facilitate development of a truly homogeneous version potentially applicable to a dipstick-type multianalyte point of care analytical device (ChemChip) [6]. This model simulates all the parameters used in the

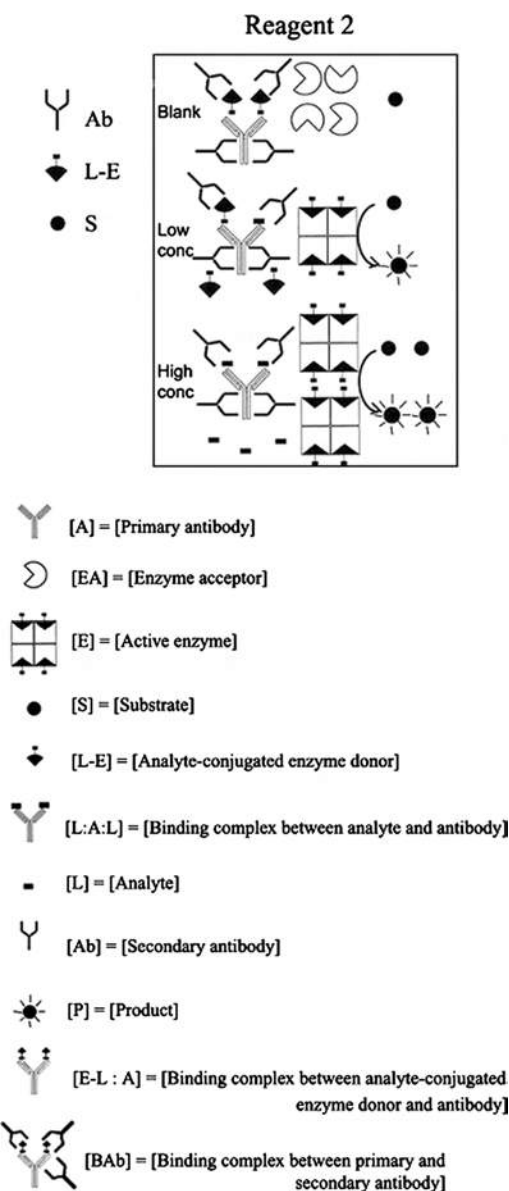


Fig. 2. Schematic representation of step 2 of CEDIA kit experiment [7].

experiment, modeling the association and dissociation rate constants for each reaction taking place in the CEDIA. The model allows for optimizing conditions in the real experiment, helping determine the detection limit of analyte in the sample, and in estimating dynamic range of the assay. It is understood that the commercial kit likely includes a variety of additives and/or excipients which are not considered in the model to follow.

Modeling

Modeling is based on the Microgenics valproic acid (VPA) CEDIA kit experiment [7] (www.microgenics.com). This commercial CEDIA kit is designed to perform the procedure in two steps.

² Abbreviations used: A, primary antibody or antibody; Ab, secondary antibody; CEDIA, cloned enzyme donor immunoassay; E, active enzyme; EA, enzyme acceptor; L-E, analyte-conjugated enzyme donor; E-L:A, binding complex between analyte-conjugated enzyme donor and antibody; ES, enzyme-substrate complex; L, analyte, ligand, or antigen; L:A, binding complex between one antibody and one analyte; L:A:L, binding complex between one antibody and two analytes; E-L:A:L, binding complex between antibody, analyte, and analyte-conjugated enzyme donor; E-L:A:L-E, binding complex between antibody and two analyte-conjugated enzyme donors; BAb, binding complex between primary and secondary antibodies; P, product; R1, reagent 1; R2, reagent 2; S, substrate; VPA, valproic acid; ED, enzyme donor.

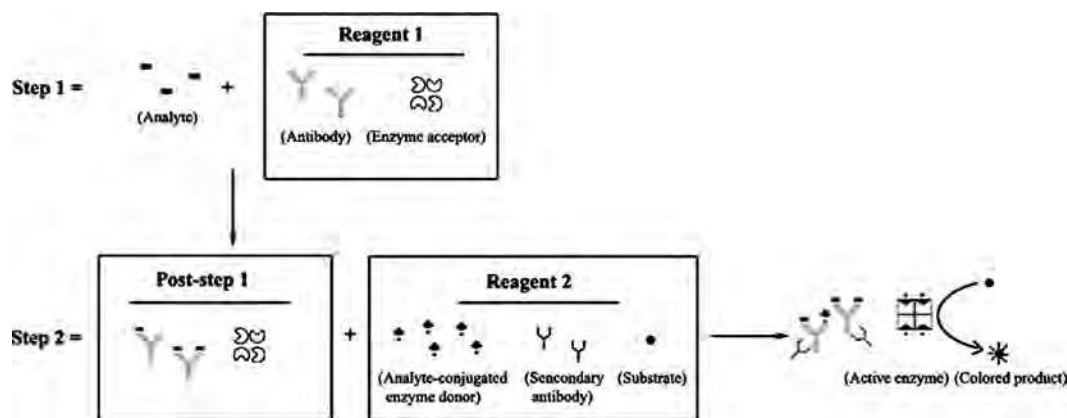


Fig. 3. Simple description of two-step CEDIA homogeneous immunoassay.

Step 1. Sample with analyte (valproic acid) is incubated with reagent 1 (Fig. 1), containing anti-analyte (anti-VPA) mouse monoclonal antibody (mAb) and an enzyme acceptor. L, A, and EA in Fig. 1 represent analyte, anti-analyte antibody, and enzyme acceptor, respectively.

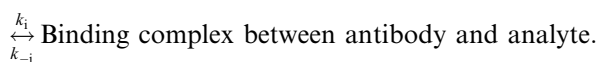
Step 2. After incubation of sample with reagent 1 in step 1, reagent 2 (upper part of Fig. 2) is added. Reagent 2 is a liquid mixture containing VPA-conjugated enzyme donor, secondary antibody (goat anti-mouse IgG secondary antibody), and substrate for β -galactosidase, which is also pictured in Fig. 2. L-E, Ab, and S in Fig. 2 represent the VPA-conjugated enzyme donor, secondary antibody, and substrate for β -galactosidase, respectively.

After addition of reagent 2, colored product of catalysis by β -galactosidase is monitored as a function of time via absorbance (standard spectrophotometric assay). Fig. 3 briefly describes the generalization of the two-step CEDIA procedure.

Methods

The Scatchard model is the most widely used mathematical approach to the quantitative description of the multiple equilibriums taking place when an antibody binds reversibly to an analyte molecule [4]. The Scatchard model focuses on the individual binding sites of the antibody and applies the law of mass action for each site, defining the affinity constant (association constant) K_i and assuming that the affinity of each particular site for the ligand is not influenced by the extent of occupancy of the other sites (independent and noninteracting binding sites). The reaction between antibody and analyte may be simplistically described:

Antibody + Analyte



Here, k_i is the association rate constant and k_{-i} is the dissociation rate constant. The ratio of the two rate con-

stants gives the equilibrium constant K_i , which represents the final ratio of bound to unbound analyte and antibody. It is also known as the affinity constant,

$$K_i = \frac{k_i}{k_{-i}} = \frac{[\text{binding complex between antibody and analyte}]}{[\text{antibody}][\text{analyte}]}$$

Step 1

Step 1 involves antibody (A) reversibly binding to a ligand molecule (L, antigen or analyte; depicted as ■ in (Fig. 1). The antibodies are assumed to have two equivalent binding sites, i.e., they are divalent. The reactions are



and



All of the parameters (symbols) and rate constants of step 1 are given in Table 1.

The rates of reaction are represented as four differential equations with four unknown parameters: L, A, L : A, and L : A : L.

Table 1
Rate constants and parameters in Step 1 of CEDIA

Rate constants	
K_1 : affinity constant for reaction (1)	k_1 : association rate constant for reaction (1)
	k_{-1} : dissociation rate constant for reaction (1)
K_2 : affinity constant for reaction (2)	k_2 : association rate constant for reaction (2)
	k_{-2} : dissociation rate constant for reaction (2)

Parameters (symbols); L (■): analyte in reactions (1) and (2); A (Y): antibody for the analyte in reaction (1); L : A (Y): binding complex between one antibody and one analyte in reactions (1) and (2); L : A : L (Y): binding complex between one antibody and two analytes in reaction (2).

$$\frac{d[L]}{dt} = k_{-1}[L : A] - k_1[L][A] + k_{-2}[L : A : L] - k_2[L : A][L]. \quad (3)$$

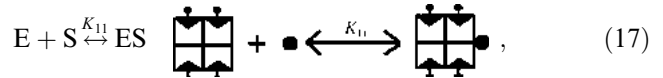
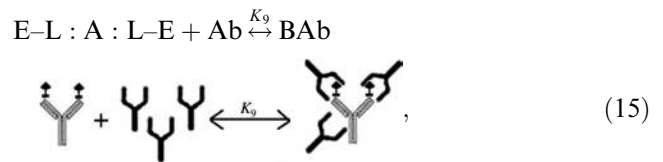
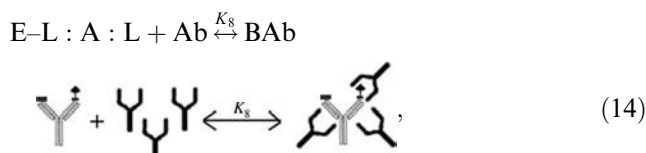
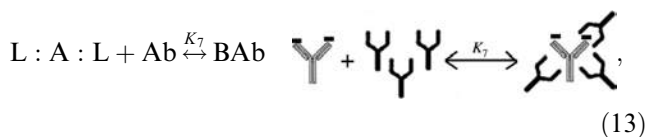
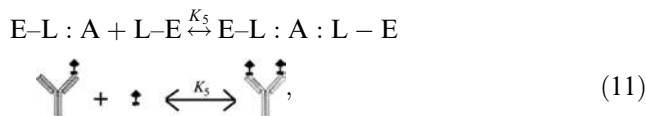
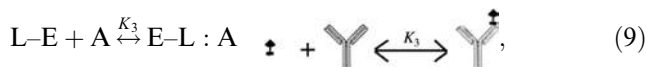
$$\frac{d[A]}{dt} = k_{-1}[L : A] - k_1[L][A]. \quad (4)$$

$$\frac{d[L : A]}{dt} = k_1[L][A] - k_{-1}[L : A] + k_{-2}[L : A : L] - k_2[L : A][L]. \quad (5)$$

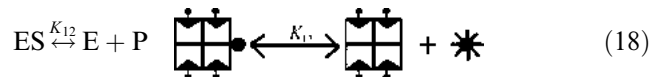
$$\frac{d[L : A : L]}{dt} = k_2[L : A][L] - k_{-2}[L : A : L]. \quad (6)$$

Step 2

In the standard CEDIA kit [7], first the analyte and antibody are mixed and incubated for a fixed time (step 1), and second the analyte-conjugated enzyme donor (L-E), the second antibody (Ab), and the substrate (S) are added (step 2) (Fig. 2). All of the reacting species participating in the reactions are involved in step 2. The possible interaction and reaction schemes of step 2 are:



and



All of the parameters (symbols) and rate constants used in reactions (7)–(18) are summarized in Table 2.

The rates of reaction are represented as 15 differential equations with 15 unknown parameters:

$$\begin{aligned} \frac{d[L : A]}{dt} &= k_1[L][A] - k_{-1}[L : A] + k_{-2}[L : A : L] \\ &\quad - k_2[L : A][L] + k_{-6}[E-L : A : L] \\ &\quad - k_6[L : A][L-E], \end{aligned} \quad (19)$$

$$\begin{aligned} \frac{d[E-L : A]}{dt} &= k_3[L-E][A] - k_{-3}[E-L : A] \\ &\quad + k_{-4}[E-L : A : L] - k_4[E-L : A][L] \\ &\quad + k_{-5}[E-L : A : L-E] - k_5[E-L : A][L-E], \end{aligned} \quad (20)$$

$$\begin{aligned} \frac{d[L]}{dt} &= k_{-1}[L : A] - k_1[L][A] + k_{-2}[L : A : L] \\ &\quad - k_2[L : A][L] + k_{-4}[E-L : A : L] \\ &\quad - k_4[E-L : A][L], \end{aligned} \quad (21)$$

$$\begin{aligned} \frac{d[L-E]}{dt} &= k_{-3}[E-L : A] - k_3[L-E][A] \\ &\quad + k_{-5}[E-L : A : L-E] - k_5[E-L : A][L-E] \\ &\quad + k_{-6}[E-L : A : L] - k_6[L : A][L-E] \\ &\quad - k_{-10}[E] - k_{10}[L-E][EA], \end{aligned} \quad (22)$$

$$\begin{aligned} \frac{d[A]}{dt} &= k_{-1}[L : A] - k_1[L][A] - k_{-3}[E-L : A] \\ &\quad - k_3[L-E][A], \end{aligned} \quad (23)$$

$$\begin{aligned} \frac{d[L : A : L]}{dt} &= k_2[L : A][L] + k_{-2}[L : A : L] + k_{-7}[BAb] \\ &\quad - k_7[L : A : L][Ab], \end{aligned} \quad (24)$$

Table 2

Rate constants and parameters in step 2 of CEDIA

Rate constants	
K_1 : affinity constant for reaction (7)	k_1 : association rate constant for reaction (7)
K_2 : affinity constant for reaction (8)	k_{-1} : dissociation rate constant for reaction (7)
K_3 : affinity constant for reaction (9)	k_2 : association rate constant for reaction (8)
K_4 : affinity constant for reaction (10)	k_{-2} : dissociation rate constant for reaction (8)
K_5 : affinity constant for reaction (11)	k_3 : association rate constant for reaction (9)
K_6 : affinity constant for reaction (12)	k_{-3} : dissociation rate constant for reaction (9)
K_7 : affinity constant for reaction (13)	k_4 : association rate constant for reaction (10)
K_8 : affinity constant for reaction (14)	k_{-4} : dissociation rate constant for reaction (10)
K_9 : affinity constant for reaction (15)	k_5 : association rate constant for reaction (11)
K_{10} : affinity constant for reaction (16)	k_{-5} : dissociation rate constant for reaction (11)
K_{11} : affinity constant for reaction (17)	k_6 : association rate constant for reaction (12)
K_{12} : association rate constant for reaction (18)	k_{-6} : dissociation rate constant for reaction (12)
	k_7 : association rate constant for reaction (13)
	k_{-7} : dissociation rate constant for reaction (13)
	k_8 : association rate constant for reaction (14)
	k_{-8} : dissociation rate constant for reaction (14)
	k_9 : association rate constant for reaction (15)
	k_{-9} : dissociation rate constant for reaction (15)
	k_{10} : association rate constant for reaction (16)
	k_{-10} : dissociation rate constant for reaction (16)
	k_{11} : association rate constant for reaction (17)
	k_{-11} : dissociation rate constant for reaction (17)

Parameters (symbols). L (■): analyte in reactions (7), (8) and (10); A (Y): antibody for the analyte in reactions (7) and (9); L : A (Y): binding complex between one antibody and one analyte in reactions (7), (8) and (12); L : A : L (Y): binding complex between one antibody and two analytes in reactions (8) and (13); L-E (■): analyte-conjugated enzyme donor in reactions (9), (11), (12), and (16); E-L : A (Y): binding complex between analyte-conjugated enzyme donor and antibody in reactions (9)–(11); EA (Σ): enzyme acceptor in reaction (16); E (■): active enzyme in reaction (16); Ab (Y): secondary antibody in reactions (13)–(15); Bab (Y₁Y₂): binding complex between primary and secondary antibody in reactions (13)–(15); S (●): substrate in reaction (17); ES (■): enzyme–substrate complex in reaction (17); P (■): product in reaction (18); E-L : A : L (Y): binding complex between one antibody and one analyte and analyte-conjugated enzyme donor in reactions (10), (12) and (14); E-L : A : L-E (Y): binding complex between one antibody and two analyte-conjugated enzymes in reactions (11) and (15).

$$\begin{aligned} \frac{d[E-L : A : L]}{dt} = & k_4[E-L : A][L] - k_{-4}[E-L : A : L] \\ & + k_6[L : A][L-E] - k_{-6}[E-L : A : L] \\ & + k_{-8}[BAb] - k_8[E-L : A : L][Ab], \end{aligned} \quad (25)$$

$$\begin{aligned} \frac{d[E-L : A : L-E]}{dt} = & k_5[E-L : A][L-E] \\ & - k_{-5}[E-L : A : L-E] + k_{-9}[BAb] \\ & + k_9[E-L : A : L-E][Ab], \end{aligned} \quad (26)$$

$$\frac{d[EA]}{dt} = k_{-10}[E] - k_{10}[L-E][EA], \quad (27)$$

$$\begin{aligned} \frac{d[E]}{dt} = & k_{10}[L-E][EA] - k_{-10}[E] + k_{-11}[ES] \\ & - k_{11}[E][S] + k_{12}[ES], \end{aligned} \quad (28)$$

$$\begin{aligned} \frac{d[Ab]}{dt} = & k_{-7}[BAb] - k_7[L : A : L][Ab] + k_{-8}[BAb] \\ & - k_8[E-L : A : L][Ab] + k_{-9}[BAb] \\ & - k_9[E-L : A : L-E][Ab], \end{aligned} \quad (29)$$

$$\begin{aligned} \frac{d[BAb]}{dt} = & k_7[L : A : L][Ab] - k_{-7}[BAb] \\ & + k_8[L-E : A : L][Ab] - k_{-8}[BAb] \\ & + k_9[E-L : A : L-E][Ab] - k_{-9}[BAb], \end{aligned} \quad (30)$$

$$\frac{d[S]}{dt} = k_{-11}[ES] - k_{11}[E][S], \quad (31)$$

$$\frac{d[ES]}{dt} = k_{11}[E][S] - k_{-11}[ES] - k_{12}[ES], \quad (32)$$

and

$$\frac{d[P]}{dt} = k_{12}[ES]. \quad (33)$$

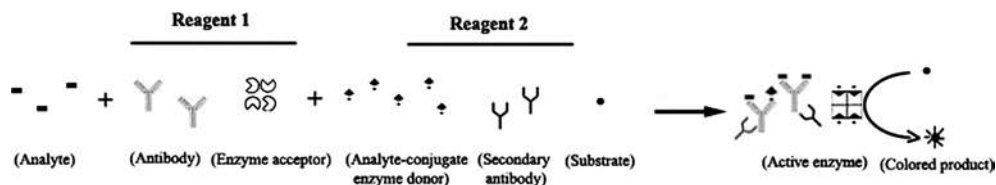


Fig. 4. Simple description of a one-step truly homogeneous process.

Combined step

Although the standard assay involves a two-step process, we also chose to model a single-combined-step process, which should be simpler to apply in a ChemChip device [6]. All reacting species are assumed to be simultaneously mixed in the same vessel at the same time; this concept is simply pictured in Fig. 4.

Procedures

The differential equations were numerically integrated using MatLab software, specifying the initial concentrations of each component and estimates of the rate constants. The time course of the materials for various concentrations were obtained.

Study of the kinetics of the CEDIA system allows the derivation of equations which predict the concentrations of reactants and products at any time, even if the system has not yet reached equilibrium. The assumptions of the model are: (1) all of the analytes and antibodies are in the same homogeneous conditions, (2) second-order reversible kinetics are considered for the interaction between analytes and antibodies, (3) analytes are considered monovalent with regard to each antibody, (4) the affinity of each particular site for the analytes is not influenced by the extent of occupancy of other sites (binding should be uniform with no positive or negative allosteric effects), and (5) no nonspecific binding occurs. Although it is impossible for all of these assumptions to be completely met in practice, the law of mass action does provide a useful framework on which to base a theoretical appreciation of the kinetic principles.

Results and discussion

Step 1

The affinity constant consists of association and dissociation rate constants. The knowledge of these rate constants is very important to perform the modeling. The advent of biosensor technology has generated considerable interest in its use to characterize high-affinity interactions between antigens and antibodies [8–12]. Many studies have employed the Biacore instrument

(Pharmacia Biosensor, Uppsala, Sweden), in which one reactant flows through a microchannel over the biosensor surface on which the secondary reactant is immobilized to form an affinity matrix, which is detected by surface plasma resonance. The IAsys instrument (Affinity Sensors, Cambridge, UK) has also been employed to study the affinity matrix between a reactant on the biosensor surface forming the base of a stirred cuvette and a flowing secondary reactant; the refractive index change associated with matrix formation is monitored by resonant mirror technology. These investigations have employed expressions developed for the analysis of the association and dissociation kinetics derived from the time course of the biosensor response. Many values of rate constants are generated with these methods and analyzed by pseudo first-order kinetics, based on the assumption of 1:1 stoichiometry and constant concentration of one of the reactants [8–12]. The diffusion-controlled association rate constant is assumed to be 10^6 or $10^7 \text{ M}^{-1} \text{ s}^{-1}$ [13]. But, the analyzed values of k_i from experiments are about $10^5 \text{ M}^{-1} \text{ s}^{-1}$; some authors explain this lower value as being due to the stagnant layer [13]. On the other hand, the dissociation rate constants depend on the binding strengths between reactants (in this case, the antigen and antibody). This affinity constant of the order of 10^7 order is a typical value for ordinary antigen–antibody systems determined by biosensor technology [14]. We assume this value for the high-affinity case [15]. We adopted the association and dissociation rate constant as $10^5 \text{ M}^{-1} \text{ s}^{-1}$ and 10^{-2} s^{-1} for our calculations. Table 3 shows the values of rate constants and parameters used in step 1 of the CEDIA.

The concentration changes of each component with time were calculated by integration of the differential equations under the conditions noted in Table 3. Time 0 is when the antibody is mixed with the ligand, analyte. A plateau is reached at equilibrium. Three cases, depending on the concentration of analyte at a fixed antibody concentration (10^{-7} M), are considered for the first step. The values chosen are appropriate to the CEDIA kit experiment [7]. The zero concentration case, i.e., only antibody is present in the reaction vessel, is shown in Fig. 5A. There is no reaction. Next is the case of low analyte concentration; the analyte and antibody react to form a complex. The complex is formed in a small amount in the presence of low analyte concentration, shown in Fig. 5B. If more analyte is added to react with

Table 3

Rate constants and parameters used to derive Fig. 5

Rate constants	Parameters
$k_1 = 10^5 \text{ M}^{-1} \text{ s}^{-1}$ and $k_{-1} = 10^{-2} \text{ s}^{-1}$ ($K_1 = 1.0 \times 10^7$)	$[L] = 0, 10^{-8}, \text{ and } 10^{-6} \text{ M}$
$k_2 = 10^5 \text{ M}^{-1} \text{ s}^{-1}$ and $k_{-2} = 10^{-2} \text{ s}^{-1}$ ($K_2 = 1.0 \times 10^7$)	$[A] = 10^{-7} \text{ M}$

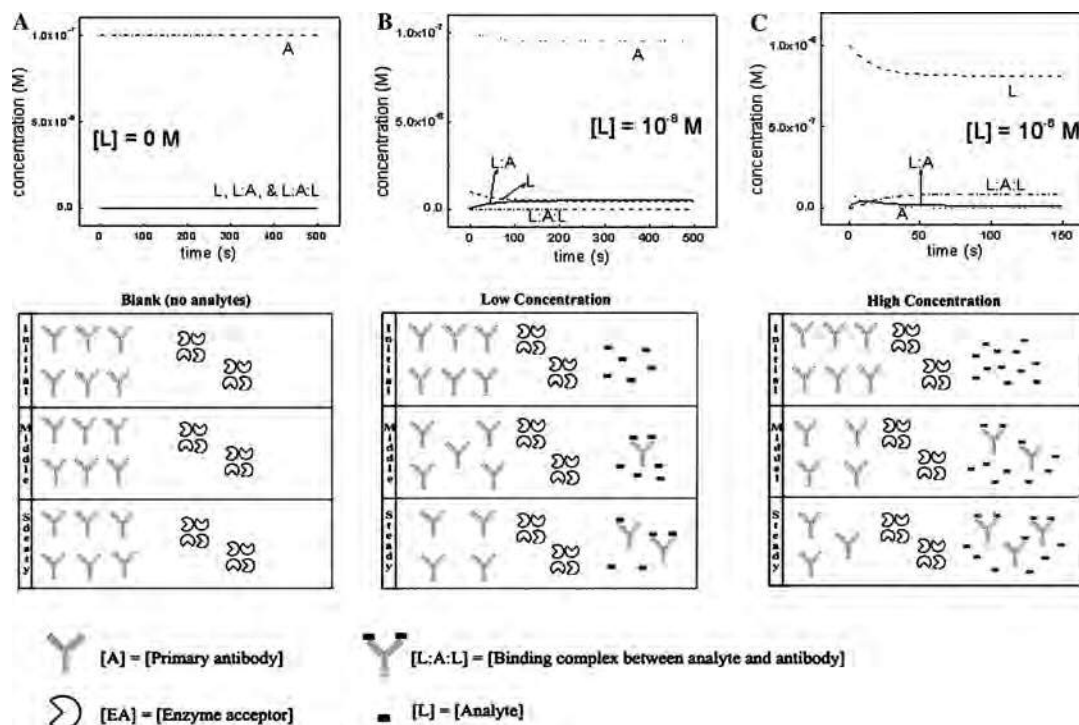


Fig. 5. Time courses of the binding reaction assuming divalent antibody for three analyte concentrations: (A) $[L] = 0 \text{ M}$ (blank), (B) $[L] = 10^{-8} \text{ M}$ (low concentration), and (C) $[L] = 10^{-6} \text{ M}$ (high concentration). Antibody concentration is fixed as 10^{-7} M , and k_i and k_{-i} are chosen as $10^5 \text{ M}^{-1} \text{ s}^{-1}$ and 10^{-2} s^{-1} . The calculated molar concentrations of each species (depicted in figure) are shown on the y axes.

antibody, the amount of free antibody is decreased, as the binding complex is produced in considerable amounts; this case is shown in Fig. 5C.

While the amounts of binding complex between one antibody and two analytes ($L:A:L$) can be greatly increased with time at the higher concentrations of analyte, no variation of it is observed in the lower concentration case. The consumption of antibody or the production of binding complex between analyte and antibody affects the assay. More binding complex means more free analyte-conjugated enzyme donor, which can produce more active enzyme.

Step 2

The analyte-conjugated enzyme donor, $L-E$ (♣), is added to the mixture of the first step of the CEDIA kit method; antibody binds to the analyte and analyte-conjugated enzyme donor as $L:A:L$ (Y), $E-L:A:L$ (Y), and $E-L:A:L-E$ (Y). Here, we have a sequential immunoassay where one of the two competing com-

ponents (i.e., the analyte and analyte-conjugated enzyme donor) reaches the antibody first to initiate the interaction that culminates in the equilibrium state (reactions 7,9). When the analyte-conjugated enzyme donor and antibody are present together in the sample, the analyte-conjugated enzyme donor is capable of binding, in a competitive fashion, either to antibody or to the enzyme acceptor (reactions 9,16). The active enzyme is involved in the conversion of substrate into product (signal); the active enzyme is produced by the binding of free analyte-conjugated enzyme donor and enzyme acceptor (reaction 16)). As the amount of analyte is increased, it binds to antibody, leaving more free analyte-conjugated enzyme to combine with the enzyme acceptor and produce more active enzyme. The secondary antibody, Ab, function is to bind to the primary antibody (reactions 13)–(15)) and improve the sensitivity of the analysis by inhibiting complementation [4]. The coupling of antibody to the ligand (analyte)-conjugated enzyme donor (reaction 9)) slows the rate of complementation of enzyme acceptor (EA) (S) and analyte-conjugated enzyme donor ($L-E$) (♣) (reaction 16)).

Such coupling, however, does not completely prevent complementation. If the secondary antibody (Ab) (Y) is coupled to the primary antibody–ligand–conjugated enzyme donor, it enhances steric interference of the primary antibody and may completely prevent complementation by that enzyme–donor population which is bound. The reactions (17) and (18) constitute the catalyzed enzyme reaction.

From the interaction of analyte and antibody of step 1, we can calculate $[L]$, $[A]$, $[L : A]$, and $[L : A : L]$ at the equilibrium condition. With these values and the added concentration of analyte–conjugated enzyme donor, enzyme acceptor, substrate, and secondary antibody as an initial condition, the concentrations of each constituent with time can be calculated by solution of the differential equations. The enzyme acceptor is originally inserted in step 1, but it remains in an unbound form and participates in an interaction of step 2. The values of the affinity constants and the accompanied rate constants of reactions (7) through (18) (Table 4) are based on the considerations for ordinary antigen–antibody systems; a 10^7 affinity constant is used for all antibody–antigen systems (reactions (7)–(15)). The rate constants of formation of active enzyme from the binding of free analyte–conjugated enzyme donor and enzyme acceptor (reaction (16)) are estimated from the folding and association of β -galactosidase [16], neglecting the detailed dimer–tetramer reaction mechanism. The rate constants of catalyzed enzyme reactions (reactions (17) and (18)) are also roughly estimated from information of ordinary Michaelis–Menten treatment for several enzymes [17].

The initial concentrations of each species are $[A] = 1.0 \times 10^{-7} \text{ M}$, $[L-E] = 1.0 \times 10^{-8} \text{ M}$, $[EA] = 1.0 \times 10^{-6} \text{ M}$, $[Ab] = 1.0 \times 10^{-5} \text{ M}$, and $[S] = 1.0 \times 10^{-4} \text{ M}$ for each analyte concentration. Table 4 summarizes the rate constants and parameters in step 2 of the CEDIA. The results obtained (only the concentrations of active enzyme and the final product are depicted) are given in Fig. 6, using the values suggested by Table 4. Fig. 6 has three pictures cor-

responding to the amounts of analytes. The shape of the time curves are similar, but their magnitudes are different. E and P produced are dependent on the added amounts of analytes, and the equilibration time becomes longer for higher amounts of analytes (Fig. 6C), which can be seen from the time course of E. If we add more analyte to the reagents, more time is needed to achieve equilibrium. The light signal increases steeply until the experimental condition reaches equilibrium (Fig. 6C).

The final product P is directly related to the light absorbance signal (accumulated amounts of product), which corresponds to the experimental signal. The calculated time courses at several analyte concentrations ($[L] = 0, 10^{-8}, 10^{-7}, 10^{-6}$, and 10^{-5} M) are shown in Fig. 7A as a function of analyte concentration. The amount of P increases with time. Reactions (17) and (18) are enzyme-catalyzed reactions and the final colored product (P) is entirely dependent on the amounts of active enzyme (E).

Many immunoassays employ chemiluminescence as the measured signal [4]. We are interested in modifying CEDIA to utilize chemiluminescence output. Chemiluminescence intensity is directly proportional to the enzyme activity (photons do not accumulate, as do chromophores in conventional CEDIA systems). Therefore, it is important to know the calculated amount of active enzyme and its variation with the change of concentrations of any other species. To illustrate this phenomenon, the time courses of the active enzyme concentrations at several analyte concentrations are given in Fig. 7B. The active enzyme concentration reaches equilibrium within 200 s at lower analyte concentrations and continues to increase at higher analyte concentrations. Fig. 7 is a kind of immunoassay dose–response curve. The response curve shows two groups, i.e., lower concentrations of analytes and higher concentrations of analytes. The discrimination of responses for the change of analyte concentrations in ranges of low concentration of analyte is slight; i.e., it is very difficult to discriminate the responses with the change of analyte concentration

Table 4
Rate constants and parameters used to derive Figs. 6 and 7

Rate constants	Parameters
$k_1 = 10^5 \text{ M}^{-1} \text{ s}^{-1}$ and $k_{-1} = 10^{-2} \text{ s}^{-1}$ ($K_1 = 1.0 \times 10^7$)	Step 1
$k_2 = 10^5 \text{ M}^{-1} \text{ s}^{-1}$ and $k_{-2} = 10^{-2} \text{ s}^{-1}$ ($K_2 = 1.0 \times 10^7$)	$[L] = 0$ and $[A] = 10^{-7} \text{ M}$
$k_3 = 10^5 \text{ M}^{-1} \text{ s}^{-1}$ and $k_{-3} = 10^{-2} \text{ s}^{-1}$ ($K_3 = 1.0 \times 10^7$)	$\rightarrow [L] = 0, [A] = 10^{-7}, [L : A] = 0$, and $[L : A : L] = 0 \text{ M}$
$k_4 = 10^5 \text{ M}^{-1} \text{ s}^{-1}$ and $k_{-4} = 10^{-2} \text{ s}^{-1}$ ($K_4 = 1.0 \times 10^7$)	$[L] = 10^{-8}$ and $[A] = 10^{-7} \text{ M}$
$k_5 = 10^5 \text{ M}^{-1} \text{ s}^{-1}$ and $k_{-5} = 10^{-2} \text{ s}^{-1}$ ($K_5 = 1.0 \times 10^7$)	$\rightarrow [L] = 5.10 \times 10^{-9}, [A] = 9.51 \times 10^{-8}, [L : A] = 4.85 \times 10^{-9}$, and $[L : A : L] = 2.43 \times 10^{-11} \text{ M}$
$k_6 = 10^5 \text{ M}^{-1} \text{ s}^{-1}$ and $k_{-6} = 10^{-2} \text{ s}^{-1}$ ($K_6 = 1.0 \times 10^7$)	$[L] = 10^{-6}$ and $[A] = 10^{-7} \text{ M}$
$k_7 = 10^5 \text{ M}^{-1} \text{ s}^{-1}$ and $k_{-7} = 10^{-2} \text{ s}^{-1}$ ($K_7 = 1.0 \times 10^7$)	$\rightarrow [L] = 8.62 \times 10^{-7}, [A] = 5.86 \times 10^{-9}, [L : A] = 5.06 \times 10^{-8}$, and $[L : A : L] = 4.35 \times 10^{-8} \text{ M}$
$k_8 = 10^5 \text{ M}^{-1} \text{ s}^{-1}$ and $k_{-8} = 10^{-2} \text{ s}^{-1}$ ($K_8 = 1.0 \times 10^7$)	Step 2
$k_9 = 10^5 \text{ M}^{-1} \text{ s}^{-1}$ and $k_{-9} = 10^{-2} \text{ s}^{-1}$ ($K_9 = 1.0 \times 10^7$)	$[L-E] = 1.0 \times 10^{-8} \text{ M}$
$k_{10} = 10^3 \text{ M}^{-1} \text{ s}^{-1}$ and $k_{-10} = 10^{-2} \text{ s}^{-1}$ ($K_{10} = 1.0 \times 10^5$) [13]	$[EA] = 1.0 \times 10^{-6} \text{ M}$
$k_{11} = 10^3 \text{ M}^{-1} \text{ s}^{-1}$ and $k_{-11} = 1 \text{ s}^{-1}$ ($K_{11} = 1.0 \times 10^3$) [14]	$[Ab] = 1.0 \times 10^{-5} \text{ M}$
$k_{12} = 0.1 \text{ M}^{-1} \text{ s}^{-1}$ [14]	$[S] = 1.0 \times 10^{-4} \text{ M}$

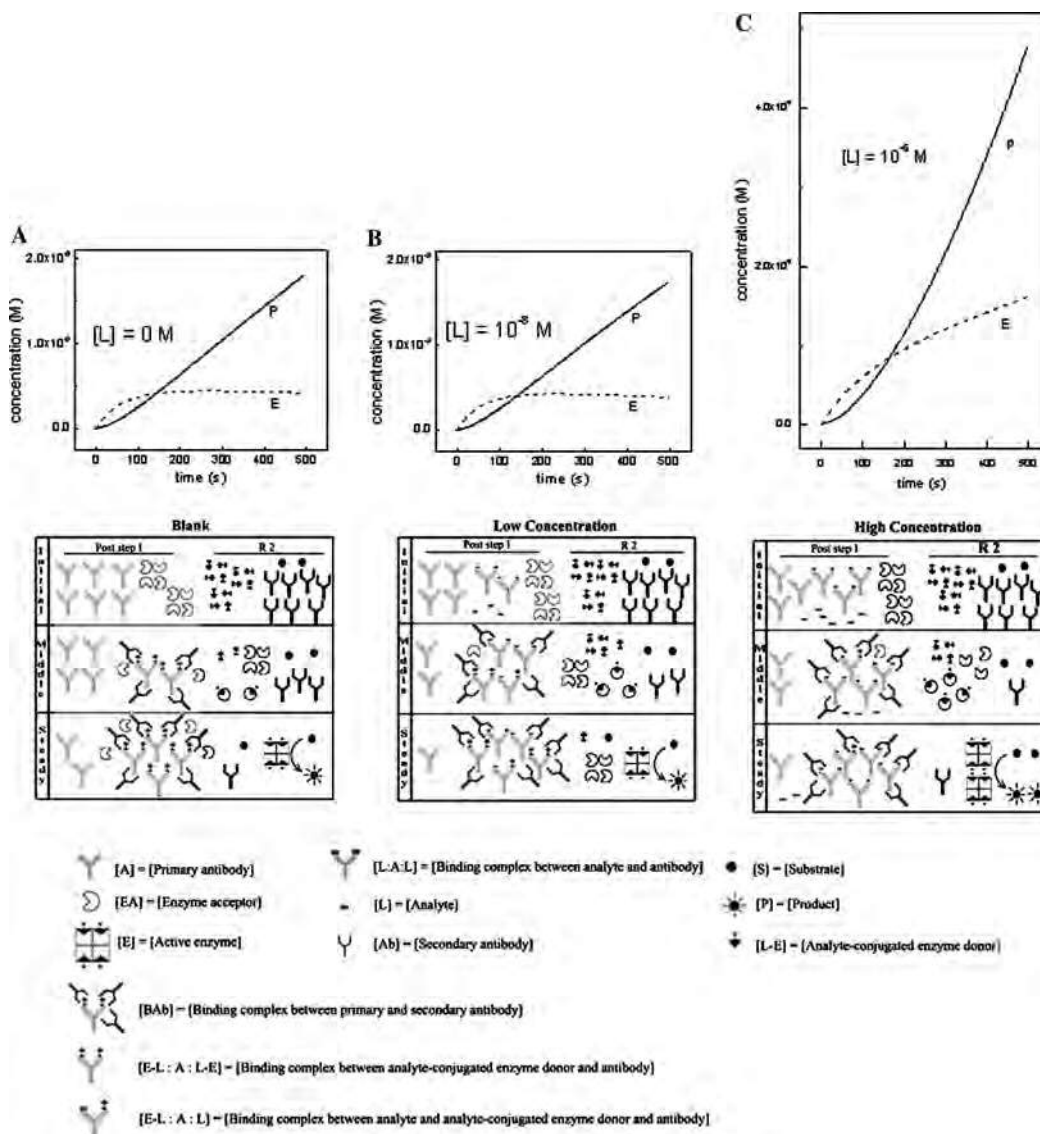


Fig. 6. Time courses of production of E (reaction (16)) and P (reaction (18)) assuming divalent antibody for three analyte concentrations: (A) $[L] = 0 \text{ M}$ (blank), (B) $[L] = 10^{-8} \text{ M}$ (low concentration), and (C) $[L] = 10^{-6} \text{ M}$ (high concentration). The calculated molar concentrations of final product, P (reaction (18)), and active enzyme, E (reaction (16)), are shown on the y axes. The initial concentrations of L, A, L : A, and L : A : L for three cases are obtained from the calculations of step 1 and are given in Table 4. The concentrations of the other species and the rate constants used are given in Table 4.

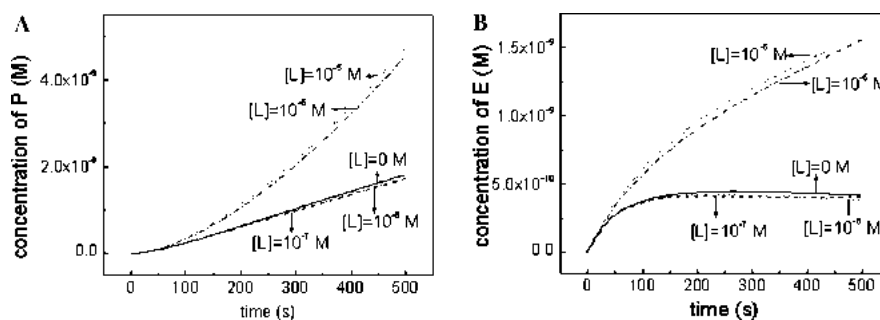


Fig. 7. Time courses of the production of P (reaction (18), (A)) and E (reaction (16), (B)) assuming divalent antibody for several analyte concentrations. The calculated molar concentrations of final product P (reaction (18)) and active enzyme E (reaction (16)) are shown on the y axes. The initial concentrations of L, A, L : A, and L : A : L for five different analyte concentrations are obtained from the calculations of step 1. The concentrations of the other species and the rate constants used are given in Table 4.

at any reaction time, so it has necessarily lower sensitivity. The responses in high concentration ranges of analytes (10^{-5} and 10^{-6} M) can be differentiated slightly. The reason for the difference of discrimination at low and high analyte concentrations is that we have 12 equations describing step 2 of the CEDIA. L and L-E compete for A. As the concentration of L increases, more L : A will be produced and the concentration of A will be necessarily reduced (reaction (7)). If the concentration of A is reduced, the amount of L-E will be reduced slightly (reaction (9)) and this effects the final concentration of active enzyme (reaction (16)); i.e., the concentration of active enzyme increases with the increase in L. But the reaction (12) will complicate the above reactions. More amounts of L : A produced with L will bind to L-E (reaction (12)), so the concentration of L-E decreases profoundly with the increase in L. In the case of very low analyte concentrations such as $L = 0$, 10^{-8} , and 10^{-7} M under the conditions of our assumed parameters, the model cannot be simulated as accurately as the high analyte concentrations. The dynamic range is the range in concentrations which can be distinguished and is not necessarily linear. Appropriate calibration is always used [18,19]. Concentration between 10^{-6} and 10^{-7} M (Fig. 7) can be readily detected—this range is indeed linear. In this case, the dynamic range might be estimated as 10^{-6} – 10^{-7} M. If one requires an extended dynamic range, it can be 10^{-5} – 10^{-7} M, although the coverage over this wider range is not completely linear.

The binding affinities between antibody and antigen were assumed to be the same. Secondary antibody is added to improve the sensitivity of CEDIA analysis by binding to the primary antibody [7], forming a complex. The binding affinities between them may be different from the binding between antigen and antibody. If we assume stronger binding affinities between primary and secondary antibodies, the calculation results representing responses are further improved (although the values are slightly lowered), which is shown in Fig. 8 assuming

the affinity constant for reactions (13)–(15) to be 1.0×10^8 . Only the association rate constant is 10 times increased ($k_7 = k_8 = k_9 = 1.0 \times 10^6 \text{ M}^{-1} \text{ s}^{-1}$), resulting in a 10 times increase in affinity constant. One can see the dynamic range of 10^{-5} – 10^{-8} M from Fig. 8. If the assumed parameters and rate constants are further revised, the responses may be further improved.

We assumed that the antibody has a divalent character and can bind up to two analytes. In the above calculations, the same rate constant values between analyte and antibody are used, regardless of the kind of analytes. The affinity constants of 10^7 (association rate constant of 10^5 and dissociation rate constant of 10^{-2}) are used for the reactions between any kinds of analyte (L and L-E) and antibody (A). Assuming the affinity constant of 10^8 (association rate constant of 10^6 and dissociation rate constant of 10^{-2}) between primary and secondary antibodies will expand the dynamic range. Thus the choice and nature of Ab is obviously critical to the analysis and the analytical behavior.

Combined step

In a one-step CEDIA, all of the reactants (L, A, L-E, S, Ab, and EA) are mixed simultaneously in the same vessel; the primary incubation step between analyte and antibody is omitted, reducing the time and cost (Fig. 4). Such a one-step assay would be simpler and easier to apply in our developing multianalyte ChemChip device [6]. The calculated results are similar to that of the two-step CEDIA method and are shown in Fig. 9. The results in the ranges of higher concentrations of analyte give better discrimination of responses than the two-step method. The distinction of the responses in the lower range is also not clear. The calculated rates of product formation vs analyte concentration show that the range of 10^{-5} – 10^{-7} M analyte concentration is simply linear from the view of calibration. A dynamic range of 10^{-5} – 10^{-7} M analyte concentration is clearly shown, which means that a one-step assay actually re-

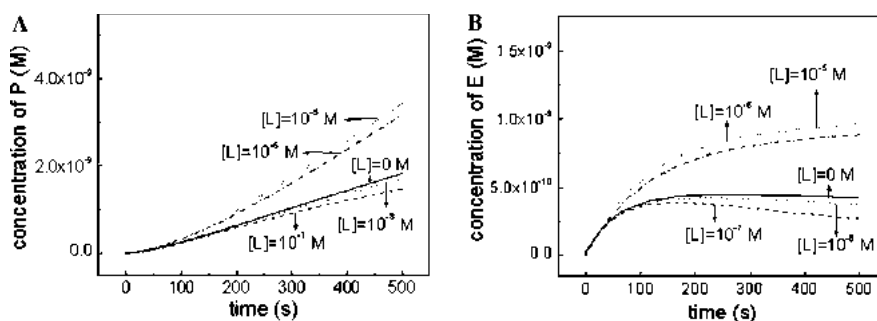


Fig. 8. Time courses of the production of P (reaction (18), (A)) and E (reaction (16), (B)) assuming divalent antibody for several analyte concentrations and stronger binding affinities between primary and secondary antibodies ($K_7 = K_8 = K_9 = 1.0 \times 10^8$ for reactions (13)–(15)). The calculated molar concentrations of final product P (reaction (18)) and active enzyme E (reaction (16)) are shown on the y axes. The initial concentrations of L, A, L : A, and L : A : L for five different analyte concentrations are obtained from the calculations of step 1. The concentrations of the other species and the rate constants used are given in Table 4 except for the reactions (13)–(15).

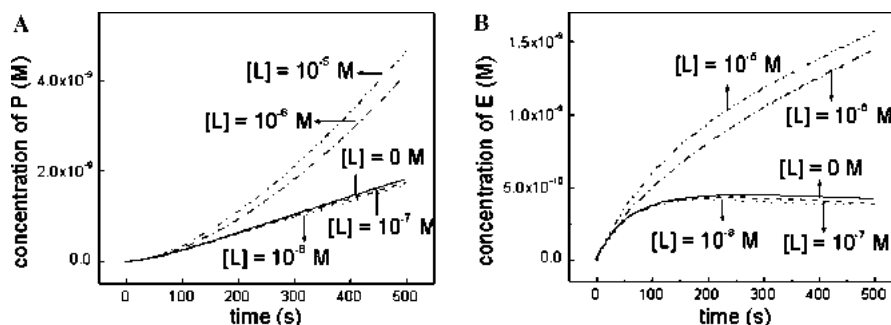


Fig. 9. Time courses of the production of P (reaction (18), (A)) and E (reaction (16), (B)) assuming divalent antibody for several analyte concentrations. The two steps normally used are treated as only one step. The concentrations of the species and the rate constants used are given in Table 5.

Table 5

Rate constants and parameters used to derive Fig. 9

Rate constants	Parameters
$k_1 = 10^5 \text{ M}^{-1} \text{ s}^{-1}$ and $k_{-1} = 10^{-2} \text{ s}^{-1}$ ($K_1 = 1.0 \times 10^7$)	[L] = 0 M
$k_2 = 10^4 \text{ M}^{-1} \text{ s}^{-1}$ and $k_{-2} = 10^{-2} \text{ s}^{-1}$ ($K_2 = 1.0 \times 10^7$)	[L] = 10^{-8} M
$k_3 = 10^5 \text{ M}^{-1} \text{ s}^{-1}$ and $k_{-3} = 10^{-2} \text{ s}^{-1}$ ($K_3 = 1.0 \times 10^7$)	[L] = 10^{-7} M
$k_4 = 10^4 \text{ M}^{-1} \text{ s}^{-1}$ and $k_{-4} = 10^{-2} \text{ s}^{-1}$ ($K_4 = 1.0 \times 10^7$)	[L] = 10^{-6} M
$k_5 = 10^4 \text{ M}^{-1} \text{ s}^{-1}$ and $k_{-5} = 10^{-2} \text{ s}^{-1}$ ($K_5 = 1.0 \times 10^7$)	[L] = 10^{-5} M
$k_6 = 10^4 \text{ M}^{-1} \text{ s}^{-1}$ and $k_{-6} = 10^{-2} \text{ s}^{-1}$ ($K_6 = 1.0 \times 10^7$)	and
$k_7 = 10^5 \text{ M}^{-1} \text{ s}^{-1}$ and $k_{-7} = 10^{-2} \text{ s}^{-1}$ ($K_7 = 1.0 \times 10^7$)	[A] = 1.0×10^{-7} M
$k_8 = 10^5 \text{ M}^{-1} \text{ s}^{-1}$ and $k_{-8} = 10^{-2} \text{ s}^{-1}$ ($K_8 = 1.0 \times 10^7$)	[L-E] = 1.0×10^{-8} M
$k_9 = 10^5 \text{ M}^{-1} \text{ s}^{-1}$ and $k_{-9} = 10^{-2} \text{ s}^{-1}$ ($K_9 = 1.0 \times 10^7$)	[EA] = 1.0×10^{-6} M
$k_{10} = 10^3 \text{ M}^{-1} \text{ s}^{-1}$ and $k_{-10} = 10^{-2} \text{ s}^{-1}$ ($K_{10} = 1.0 \times 10^5$) [13]	[Ab] = 1.0×10^{-5} M
$k_{11} = 10^3 \text{ M}^{-1} \text{ s}^{-1}$ and $k_{-11} = 1 \text{ s}^{-1}$ ($K_{11} = 1.0 \times 10^3$) [14]	[S] = 1.0×10^{-4} M
$k_{12} = 0.1 \text{ M}^{-1} \text{ s}^{-1}$ [14]	

sults in a wider measurable dynamic range than the two-step assay. The calculated rate of product formation vs analyte concentration shows that the range of 10^{-5} – 10^{-7} M is simply linear from the view of calibration. Table 5 lists the rate constants and parameters used to obtain Fig. 9. This situation must be more fully considered and tested.

Chemiluminescent assay methods are simple, inexpensive, and generally more sensitive than standard spectrophotometric assays [19] and can be applied to a one-step CEDIA, with greater simplicity and reduced time and cost [20]. To accomplish a luminescent read-out for our ChemChip purposes, it is necessary to replace the substrate, currently present in the Reagent 2 of Fig. 2, with a chemiluminescent substrate. This application is now underway in our laboratory. Chemiluminescent assay uses a chemiluminescent substrate, all the other reactants in the CEDIA are unchanged. So the results should be same as the color substrate modeled in the paper.

Conclusion

We obtained time course curves of the major reactants and products using a model of CEDIA by integration of the relevant differential kinetic equations. We

conclude the following: (1) the obtained time course curve of the production of P (Fig. 7A) can be compared with the light absorption signal of the CEDIA kit experiment [15]. The E time course curve (Fig. 7B) is being tested with a modified chemiluminescent assay method [15]. (2) Using assumed parameters, the analyte concentration response curve can be obtained. In a two-step case, a dynamic range of 10^{-6} – 10^{-7} M is obtained. If we assume stronger binding affinities between primary and secondary antibodies, the dynamic range can be expanded (10^{-5} – 10^{-8} M). (3) Simulation of a one-step CEDIA produces Fig. 9, a dynamic range of 10^{-5} – 10^{-7} M analyte concentration. (4) From this theoretical consideration, a simple one-step immunoassay has the merit of potentially reducing time and cost and has an improved dynamic range.

Acknowledgments

One of the authors (Sang Il Jeon) thanks Kangnung National University for partial financial support of this work. This work was partially supported by NIH Grant RR17329. We thank the University of Utah ChemChip group and especially Rupert Davies, Daniel Bartholomew, and Dr. Jarmila Janatova for helpful discussions;

we also thank Dr. Rueyming Luor, Microgenics for helpful discussions.

References

- [1] R.F. Wiegand, K.L. Klette, P.R. Stout, J.M. Gehlhausen, Comparison of EMIT® II, CEDIA, and DPC® RIA assays for the detection of lysergic acid diethylamide in forensic urine samples, *J. Anal. Toxicol.* 26 (2002) 519–523.
- [2] S.H. Jenkins, Homogeneous enzyme immunoassay, *J. Immunol. Methods* 150 (1–2) (1992) 91–97.
- [3] D.R. Henderson, S.B. Friedman, J.D. Harris, W.B. Manning, M.A. Zoccoll, CEDIA™, a new homogeneous immunoassay system, *Clin. Chem.* 32 (1986) 1637–1641.
- [4] D. Wild, *The Immunoassay Handbook*, Nature Pub., NY, 2001.
- [5] B.A. Way, K.G. Walton, J.W. Koenig, B.J. Eveland, M.G. Scott, Comparison between CEDIA and EMIT II immunoassays for the determination of benzodiazepines, *Clin. Chim. Acta* 271 (1998) 1–9.
- [6] R. Davies, D.A. Bartholomeusz, J.D. Andrade, Personal sensors for the diagnosis and management of metabolic disorders, *IEEE Eng. Med. Biol. Mag.* 22 (2003) 32–42.
- [7] D.R. Henderson, Methods for protein binding enzyme complementation assays, US Patent, 4708929, (1987).
- [8] V. Hanin, O. Dery, D. Boquet, M.-A. Sagot, C. Creminon, J.-Y. Couraud, J. Grassi, Importance of hydropathic complementarity for the binding of the neuropeptide substance P to a monoclonal antibody: equilibrium and kinetic studies, *Mol. Immunol.* 34 (1997) 829–838.
- [9] P.R. Edwards, C.H. Maule, R.J. Leatherbarrow, D.J. Winzor, Second-order kinetic analysis of IAsys biosensor data: its use and applicability, *Anal. Biochem.* 263 (1998) 1–12.
- [10] N.N. Gorgani, C.R. Parish, S.B.E. Smith, J.G. Altin, Histidine-rich glycoprotein binds to human IgG and Clq and inhibits the formation of insoluble immune complexes, *Biochemistry* 36 (1997) 6653–6662.
- [11] D.R. Hall, D.J. Winzor, Use of a resonant mirror biosensor to characterize the interaction of carboxypeptidase A with an elicited monoclonal antibody, *Anal. Biochem.* 244 (1997) 152–160.
- [12] L. Nieba, A. Krebber, A. Pluckthun, Competition BIAcore for measuring true affinities: large differences from values determined from binding kinetics, *Anal. Biochem.* 234 (1996) 155–165.
- [13] D.R. Hall, J.R. Cann, D.J. Winzor, Demonstration of an upper limit to the range of association rate constants amenable to study by biosensor technology based on surface plasmon resonance, *Anal. Biochem.* 235 (1996) 175–184.
- [14] D.R. Hall, N.N. Gorgani, J.G. Altin, D.J. Winzor, Theoretical and experimental considerations of the pseudo-first-order approximation in conventional kinetic analysis of IAsys biosensor data, *Anal. Biochem.* 253 (1997) 145–155.
- [15] E.P. Diamandis, T.K. Christopoulos, *Immunoassay*, Academic Press, NY, 1996.
- [16] A. Nichtl, J. Buchner, R. Jaenicke, R. Rudolph, T. Scheibel, Folding and association of β -galactosidase, *J. Mol. Biol.* 282 (1998) 1083–1091.
- [17] C.K. Mathews, K.E. van Holde, K.G. Ahern, *Biochemistry*, third ed., Addison Wesley Longman Inc., NY, 1999.
- [18] T. Yamazaki, K. Kojima, K. Sode, Extended-range glucose sensor employing engineered glucose dehydrogenases, *Anal. Chem.* 72 (2000) 4689–4693.
- [19] A. Bromberg, R.A. Mathies, Homogeneous immunoassay for detection of TNT and its analogues on a microfabricated capillary electrophoresis chip, *Anal. Chem.* 75 (2003) 1188–1195.
- [20] S. Brolin, G. Wettermark, *Bioluminescence Analysis*, VCH, N.Y., 1992.

lost p.

Water and Hydrogels

MU SHIK JHON* and J. D. ANDRADE, *Division of Materials Science and Engineering, College of Engineering, University of Utah, Salt Lake City, Utah 84112*

Summary

The apparent biocompatibility of many synthetic and natural aqueous gel materials has encouraged their study and testing for a wide variety of biomedical device applications. Many of the physical and in particular the interfacial properties of such gels are highly dependent on the organization of water within and on the surface of the hydrogel. Water is an important component of such gels, varying from about 30 to nearly 100 wt-%, yet the role of water in the gels has been virtually ignored. This paper briefly reviews the nature of water structure in pure bulk water, in solutions, and at interfaces. Polywater or anomalous water is also briefly reviewed. Evidence is presented that the water in many hydrogel systems can exist in at least three different, structurally distinct forms. A hypothesis is presented which can be used to evaluate and study the nature of water in bulk hydrogels. Consideration is also given to the role of organized water at the hydrogel surface on the interfacial properties of such systems.

INTRODUCTION

Water is the most common liquid on Earth and is the very medium of life, yet its peculiar properties are often overlooked or ignored. Water exhibits a variety of unusual properties. It shows a maximum density at 4°C. Compared with the other Group VI hydrides (H_2S , H_2Se , H_2Te), it has a melting point, boiling point, heat of fusion, and heat of vaporization much higher than expected. The viscosity of water shows a peculiar decrease with increasing pressure above one atmosphere. A number of apparent thermal anomalies or "kinks" have been reported and may play a role in biological processes at interfaces.¹

* On leave from the Korea Advanced Institute of Science, Seoul, Korea.

20. N. N. Fedyakin, *Kolloid Zh.*, **24**, 497 (1962).
21. B. V. Derjaguin, I. G. Ershova, B. V. Shedezyuyi, and N. V. Churayer, *Doklady Acad. Nauk SSSR*, **170**, 876 (1966).
22. D. H. Everett, J. M. Haynes, and P. J. McElroy, *Sci. Prog. Oxf.*, **59**, 279 (1971).
23. W. Drost-Hansen, *Chem. Phys. Letters.*, **2**, 647 (1968).
24. W. Drost-Hansen, *Ind. Eng. Chem.*, **61**, 10 (1969).
25. J. Timmermans and H. Bodson, *Compt. Rend.*, **204**, 1804 (1937).
26. R. C. Weasti, Ed., *Handbook of Chemistry and Physics*, Chemical Rubber Co., 52nd ed., 1971, p. E 203.
27. M. S. Jhon, E. R. Van Artsdalen, J. Grosh, and H. Eyring, *J. Chem. Phys.*, **47**, 2231 (1967).
28. O. Wichterle and D. Lim, *Nature*, **185**, 117 (1960).
29. S. D. Bruck, *Trans. Amer. Soc. Artif. Intern. Organs.*, **18**, 1 (1972).
30. J. D. Andrade, *Med. Instrumentation*, **7**, 110 (1973).
31. H. B. Lee, H. S. Shim, and J. D. Andrade, *Polym. Prepr.*, **13**, 729 (1972).
32. A. S. Hoffman, W. G. Kroft, and C. Harris, *Polym. Prepr.*, **13**, 723, 740 (1972).
33. J. D. Andrade, Ph.D. dissertation, Univ. Denver, Denver, Colorado, 1969.
34. M. Aizawa and S. Suzuki, *Bull. Chem. Soc. Japan*, **44**, 2963 (1971).
35. J. Mizuguchi, M. Takahashi, and M. Aizawa, *Nippon Kagaku Zasshi*, **91**, 723 (1970).
36. J. R. Hansen and W. Yellin, in *Water Structure at the Water-Polymer Interface*, H. H. G. Jellinek, Ed., Plenum, 1972, p. 19.
37. C. F. Hazelwood, B. L. Nichols and N. F. Chamberlain, *Nature*, **222**, 747 (1969).
38. M. F. Refojo, *J. Appl. Polymer Sci.*, **5A-1**, 3103 (1967).
39. M. Ilavsky and W. Prins, *Macromolecules*, **3**, 425 (1970).
40. D. H. Rasmussen and A. P. Mackenzie, in *Water Structure at the Water-Polymer Interface*, H. H. G. Jellinek, Ed., Plenum, 1972, p. 126.
41. H. B. Lee, M. S. Jhon, and J. D. Andrade, manuscript submitted.
42. J. D. Andrade, H. B. Lee, M. S. Jhon, S. W. Kim, and J. B. Hibbs, Jr., *Trans. Amer. Soc. Artif. Internal Organs*, **19**, 1 (1973).
43. K. Johansson and J. C. Erickson, *J. Coll. Interface Sci.*, **40**, 398 (1972).
44. W. Drost-Hansen, *J. Geophys. Res.*, **77**, 5132 (1972).
45. R. A. Horne, A. F. Day, R. P. Young, and N. T. Yu, *Electrochim. Acta*, **13**, 397 (1968).
46. S. D. Bruck, *J. Biomed. Res.*, **7**, 387 (1973).

Received December 18, 1972

A number of theories have been proposed to explain the structural nature of water and to account for its anomalous behavior. Several extensive reviews are available.² Unfortunately, none of the theories available is satisfactory.

Water exhibits different properties in different situations.^{1,2} Dilute aqueous solutions exhibit significant changes from normal water structure and properties. As the solution becomes more concentrated, the modifications become more extensive and may even change in kind. More concentrated solutions, such as hydrogels or physiological fluids, exhibit more extensive changes.

In order to make some progress towards understanding the nature of water in biological systems, and more immediately in biomedical hydrogels, we must characterize the structure and properties of pure water and of simple aqueous solutions.

PURE WATER

The available models for the structure of water can be classified into two categories: 1) mixture models, which assume the presence of two or more species; and 2) uniformist models, which assume that each water molecule is subject to the same intermolecular force interactions as any other water molecule.

Mixture Models

One of the most popular mixture models is the flickering cluster model (Fig. 1) proposed by Frank and Wen.³ According to them clusters of hydrogen-bonded water molecules swim in a medium of unbonded or monomer water; the cluster life time is believed to be of the order of 10^{-11} sec. Thus water molecules are believed to interact to form transitory liaisons and structures with life times of the order of 100–1000 times longer than molecular vibrations. This model does not include any details as to the nature of the clusters.

Nemethy and Scheraga⁴ modified the flickering cluster concept by assuming the water molecules to be linked by four, three, two, one, and no hydrogen bonds. This model has been rather successful in explaining a number of the properties of water but is not completely adequate. Recently Vand and Senior⁵ have shown that the Nemethy-Scheraga model can be improved by using nine energetically distinct types of water molecules instead of five.

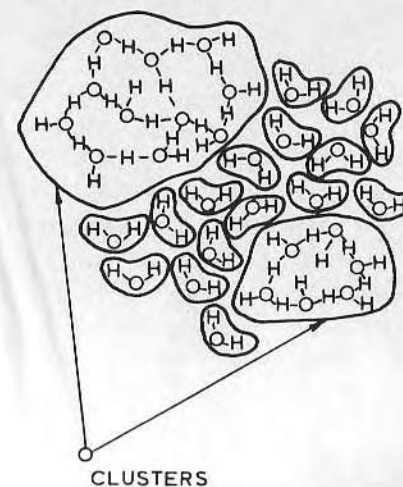


Fig. 1. Schematic representation of the Frank and Wen flickering cluster model of liquid water (redrawn after ref. 4).

A number of interstitial models are also available. These models assume the presence of a structured water lattice, such as ice-I or a distorted tetrahedron hydrogen-bonded lattice with the unbonded or monomer water occupying the so-called interstitial spaces. The Samoilov interstitial model⁶ explains the high density of liquid water compared to ice as due to the incorporation of free water molecules into the ice-like structure.

Pauling's clathrate cage model⁷ can also be considered an interstitial model. He proposed a model for liquid water analogous to that for the structure of gas hydrates, such as $\text{Cl}_2 \cdot 8\text{H}_2\text{O}$ and $\text{CH}_4 \cdot 6\text{H}_2\text{O}$, wherein the water molecules are hydrogen-bonded in large cage-like structures containing methane, chlorine, etc. The Pauling model for water consists of dodecahedral cages containing 46 molecules in the hydrogen-bonded cage with 8 nonhydrogen bonded molecules. This model predicts the density but cannot predict the dielectric constant of water.

The significant structure theory of liquids⁸ was applied to water by Marchi and Eyring.⁹ This early model did not lead to a maximum in the density. Later Jhon et al.¹⁰ developed a new significant structure model of water to explain the properties of water. The model is visualized¹¹ as containing at least two solid-like clusters in equi-

librium with each other and with the gaslike molecules (monomer water). One of these structures is a cluster of about 46 molecules with a structure and density similar to ice-I.¹¹ These clusters are dispersed in an ice-III-like structure which is 20% more dense than ice-I, but is still hydrogen bonded. The ice-III structure arises from compression and bending of the hydrogen bonds. When a cluster of ice-I-like molecules disappear, they change their structure cooperatively to a cluster of about 46 ice-III-like molecules. When ice melts, most of the ice-I-like structure deforms into a denser ice-III-like structure. At the same time, fluidized vacancies are introduced, but the net result of melting is a contraction in the volume. The volume decrease continues until 4°C where most of the ice-I-like structure which remained on melting is now destroyed. Above 4°C, water begins to behave as a normal liquid. According to the model the cluster size does not change appreciably with temperature but the cluster concentration changes. This model has explained most of the thermodynamic, dielectric, surface and transport properties of water.¹⁰

Uniformist Models

These models attempt to explain water in terms of distorted hydrogen bonds, rather than broken hydrogen bonds as in the mixture models. These models satisfactorily explain the x-ray radial distribution curves and dielectric properties of water.

Bernal and Fowler¹² envisaged the structure of water to be entirely due to tetrahedral hydrogen bonds. Pople¹³ suggested a model where in melting is a result of the bending of hydrogen bonds, thus destroying the regular ice lattice, and producing a liquid state consisting of an irregular arrangement of water molecules with many bent hydrogen bonds.

Concluding Remarks Regarding Water Structure

There are no methods available to study the instantaneous structure of water.^{2d} A method with a time resolution of 10^{-13} to 10^{-14} sec (the vibration time) or less would be required. Only a few methods are available for the study of vibrationally averaged structures, here the resolution time is greater than 10^{-13} sec but must be less than 10^{-10} sec (the diffusion time); infrared and Raman spectroscopy,

copy, neutron inelastic scattering, and dielectric relaxation are suitable.

Many common experimental methods, such as x-ray diffraction, thermodynamic data, and NMR, provide information on the diffusion-averaged structures, i.e., observation times are greater than 10^{-10} sec.

Considering all the evidence, water probably consists of a mixture of different clusters, whose cluster life time is less than 10^{-10} sec^{3-5,9} and whose probable cluster size is about 46 molecules.¹⁰

Absorption spectroscopic studies indicate that the concentration of monomer is very low.^{14,15} Cooperative phase changes probably occur.¹⁰

STRUCTURE OF AQUEOUS SOLUTIONS

Because of the incomplete knowledge of the structure of water, our understanding of aqueous solutions is not satisfactory; an acceptable model of water would help us understand the behavior of aqueous solutions. A number of excellent reviews are available.^{2,6,14} The classic paper of Frank and Wen³ provided the basis for understanding the effect of solutes on water structure.

Aqueous solutions containing ions of high charge density, such as LiF and MgCl_2 , have a positive hydration effect which increases the local ordered structure of water by immobilizing the water around the ions. Aqueous solutions containing ions with a lower charge density, such as KBr and CsI, show a negative hydration effect which decreases the ordered structure of water beyond the electrostricted layer by creating a zone of water more disorganized than bulk water.

Nonpolar solutes like hydrocarbon or R_4^+N salt clearly increase the stabilized or ordered structures in aqueous solution by forming certain kind of icebergs or cages of water molecules around the solute molecules. Solute which show positive hydration effects are called *structure makers*. These solutes increase the viscosity of water, and give rise to positive excess partial molar heat capacities. Solute which show negative hydration effects are called *structure breakers* and act in the opposite direction to structure makers. The nature of hydrated water around solutes can be visualized as a cage-like structure with dielectric constant, $\epsilon = 2$ (normal bulk water has a dielectric constant of about 80). Samoilov et al.⁶ developed their theory of

aqueous solutions in terms of the molecular-kinetic close hydration configuration. Nemethy et al.^{4,16} have made theoretical attempts to explain the effects of nonpolar solutes and of alcohols on the structure of water. Their calculated thermodynamic properties, such as free energy, enthalpy, entropy and heat capacity, of aqueous solutions of hydrocarbons, as well as for the transfer of alcohols from dilute hydrocarbon solutions to dilute aqueous solutions, are in good agreement with those observed experimentally. Jhon et al.^{8,17} extended the significant structure theory of water to ionic solutions. The partition function which is being considered consists of mainly five terms; the partition function of the ion, of both pure water and hydrated water, a mixing term, and electrostatic terms derived from Debye-Huckel theory. The calculated results are quite satisfactory. Recently Herman¹⁸ and Sung et al.¹⁹ applied the significant structure theory of liquids to aqueous hydrocarbon solutions.

In summary, a number of models for dilute aqueous solutions of electrolytes and apolar solutes are available. Several of these models produce results which are in satisfactory agreement with many properties of these solutions. Dilute salt solutions, including physiologic saline, may be treated by the significant structure approach.

POLYWATER

A polymer of pure water with properties somewhat more like those of a real polymer than those of ordinary water was discovered in the Soviet Union by Fedyakin²⁰ and extensively investigated by Derjaguin et al.²¹ Polywater (or anomalous water) is prepared by the condensation of water vapor in fused quartz or glass capillaries 2 to 50 μ in diameter at relative pressures somewhat less than unity. Some of the reported properties of this water are: 1) lower vapor pressure than the normal form; 2) greater density and stability to temperatures to 500°C; 3) higher viscosity (up to 15 times normal); 4) different thermal expansion behavior; 5) solidification at -40°C to a glass-like state; and 6) oxygen-oxygen distance is 2.3 Å (compared with 2.8 Å for water). However, it can only be produced in very small quantities, by a process of evaporation and condensation into fine capillaries.

Some interesting speculations about the structure of polywater have appeared; a recent review is available.²² Through many diffi-

cult experiments such as infrared and laser-Raman spectra, ESR, and NMR, which shed light on molecular structure, it is now widely believed that anomalous water is not pure water but may be a boracious, silicacious or carbonaceous hydrate.

WATER AT INTERFACES

There is substantial evidence for the existence of ordered water structures near certain aqueous/solid interfaces.^{1,23,24} Particular importance has been attached to the existence of thermal anomalies in the properties of interfacial water,¹ although no obvious evidence for anomalous behavior has been observed for bulk water. It has been suggested that these anomalies are evidence of higher order phase transitions, such transitions only occurring in partially ordered, structure units of a certain minimum size. Figure 2 shows the surface tension of water as determined by Timmermans and Bodson.²⁵ The surface tension appears to have an inflection point in the vicinity of around 12–14°C.²³ The dielectric constant of water decreases with the thinness of the film from more than 20 for films about 5 μ in thickness to less than 10 for films about 2 μ in thickness; also the density maximum temperature varies with the thinness of the film.²⁴

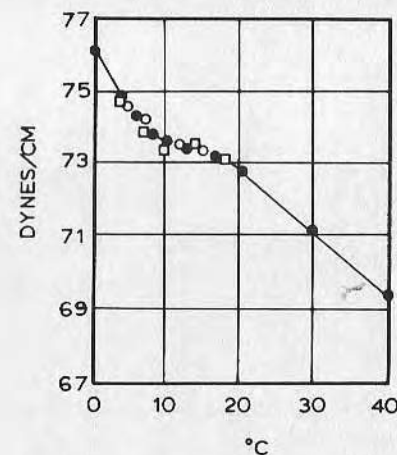


Fig. 2. Surface tension of water as a function of temperature (redrawn after refs. 24 and 25).

If one merely plots handbook refractive index data for water²⁶ as a function of temperature, thermal kinks can be observed (Fig. 3).

There is no doubt that structure differences must exist between bulk water and interfacial water. The nature and extent of the ordering of the interfacial water molecules will depend upon the solid surface. Evidence for more "orderliness" is seen from the surface tension paper by Jhon et al.²⁷ in which they assumed that the molecules in the top layer are in an asymmetric field and tend to orient in the direction of the field. There is substantial evidence that water

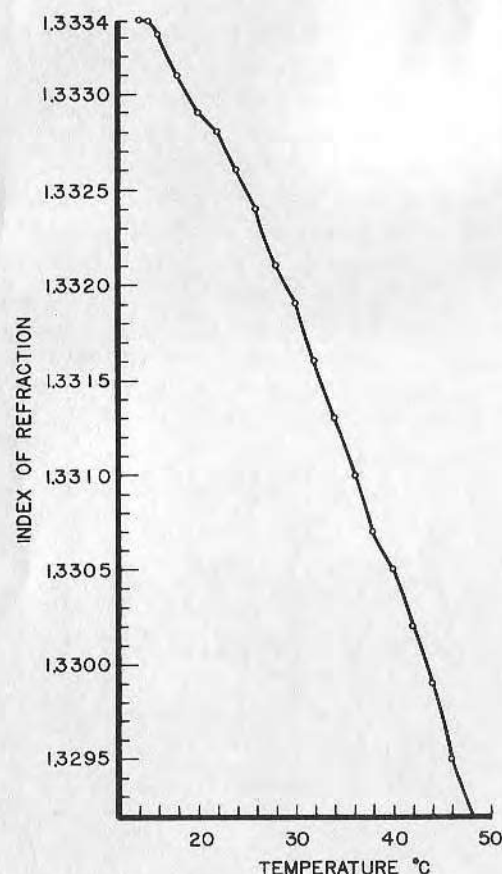


Fig. 3. Refractive index data for liquid water as a function of temperature (data from ref. 26).

may exist in a highly polarized or structured form in the vicinity of polar substrates or solutes. Water in the vicinity of apolar solutes or substrates is believed to consist of cage-like structures.^{1,2d}

We can safely conclude that the nature of interfacial water is not well understood.

WATER IN HYDROGELS

There is substantial interest in the biomaterials community in the development of synthetic hydrogels. These materials have been extensively discussed in the literature.²⁸⁻³⁰ A number of investigators have produced hydrogel surfaces on conventional polymer substrates by surface grafting.^{31,32} Andrade has discussed the possible role of water in biocompatibility by an interfacial free energy analysis.^{30,33} There has been much speculation and little reported work on the possible correlation between the water content of a hydrogel and its biotolerability.²⁹ To develop optimum synthetic biomedical hydrogels, a basic problem is to understand the nature of water in such gels.

We hypothesize that there are at least three kinds of water in hydrogels: hydrated water (hereafter called Z water); interfacial water, having a certain ordered arrangement, probably not cage-like (hereafter called Y water), and finally "normal" or bulk water (hereafter called X water).

The following arguments support our hypothesis. Aizawa et al.³⁴ measured the thermal expansion of Sephadex (Fig. 4); high water content gels were found to show an extremely sharp volume change at 0°C, as observed for bulk (X) water; on the contrary, low water content gels exhibited no anomalous changes in the specific volume in the range from -30 to 0°C—such behavior is expected from water of hydration or Z water. For medium water content gels, a gradual decrease in the specific volume was observed from -20° to 0°C. This may be mainly due to Y water (Fig. 4). Mizukuchi et al.³⁵ measured the specific conductivity (and also the activation energy) as a function of water content for agarose gels (Figs. 5 and 6). We can see the presence of three activation energies: one corresponds to X water, the second corresponds to Z water, the last one is between X water and Z water. NMR and infrared spectroscopic studies also demonstrate the existence of X, Y, and Z water. In Figure 7, infrared studies of stratum corneum by Hansen et al.³⁶ shows the appearance of three bands. According to high resolution NMR

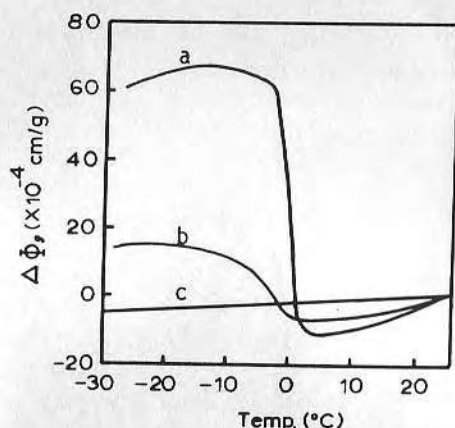


Fig. 4. Thermal expansion of Sephadex G-50 gels; $a = 83\%$, $b = 50\%$, $c = 29\%$ wt-% water (redrawn after ref. 34).

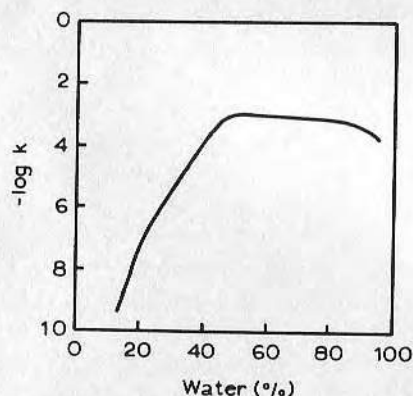


Fig. 5. Agarose gel at 25°C: relation between % water and specific conductivity (redrawn after ref. 35).

studies of muscle water by Hazlewood et al.,³⁷ the water exists in at least two ordered phases, which can be distinguished by the widths of their NMR signals (Fig. 8), by deuterium exchange, and by vacuum drying. This may indicate the existence of Z water and probably Y water.

Synthetic hydrogels proposed as biomaterials may also exhibit significant water ordering. For example, the popular polyhydroxy-

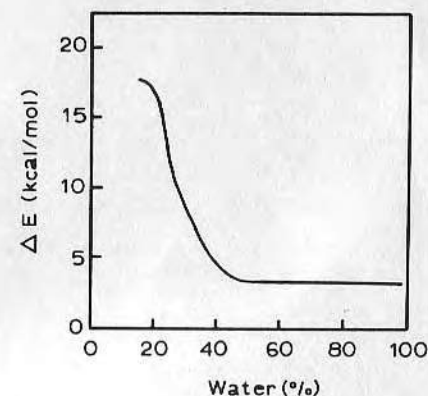


Fig. 6. Agarose gel: Activation energy for ion conduction as a function of water content (redrawn from ref. 35).

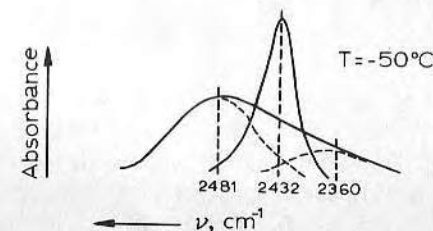


Fig. 7. Schematic infrared spectra of the O-D oscillators for H-O-D in stratum cornea at -50°C (redrawn from ref. 36).

ethyl methacrylate gel²⁸ is known to be extensively crosslinked by a noncovalent mode, probably by hydrophobic bond interactions^{38,39} as a result of water organization around the nonpolar portions of the polymer.

The interfacial or Y water hypothesized here may represent a range of possible interfacial structures, depending on the local environment; at the present stage in the development of models for bulk and interfacial water structures, and with the experimental tools available, it would be extremely difficult to separate out the various components of interfacial water. We have, therefore, chosen for the present to lump all interfacial or transition structures into the Y water category.

There is thus substantial evidence that a fraction of water in hydrogels (including biological tissues) may be significantly different

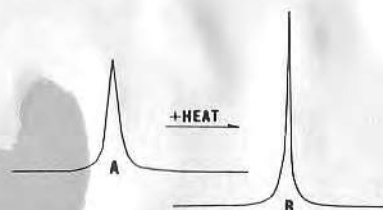


Fig. 8. High resolution NMR of rat muscle before (A) and after (B) heat denaturation of proteins (redrawn from ref. 37).

from normal or bulk water and different from water of hydration.^{41,42} Such water structuring must be expected to play a role in the interfacial properties of such gels, including the internal surface of the cardiovascular system and the surfaces of biomaterials.⁴² The interfacial free energy at the interface between a highly water structured surface and an aqueous solution may be substantial.³⁰ For example, the interfacial energy at the ice-water interface is of the order of 25 erg/cm².⁴⁰ Thus, if one accepts the interfacial free energy hypothesis of biotolerability,³⁰ various hydrogels may differ significantly in their interfacial free energies—and probably in their biocompatibility—due to differences in water content and water organization at the gel—water interface.⁴² This may be the reason for some of the present confusion regarding the biocompatibility or incompatibility of hydrogel systems.^{29,42}

Much more work is needed before we can begin to understand the nature of water in natural and synthetic hydrogels.⁴¹ Then we may begin to consider the role of water near the surface of a hydrogel or intima on the bio- and blood compatibility of such interfaces. The study of water in well-controlled synthetic hydrogels may prove useful as model systems for understanding the nature and role of water in biological tissues.⁴²

Note added in proof: The question of thermal anomalies in the surface tension of water has been considered in some very recent and very precise studies.⁴³ Drost-Hansen⁴⁴ has attempted to correlate the various studies and conflicting results. It appears that surface tension studies in fine capillaries may exhibit anomalies, which are not seen with a Wilhelmy plate or related technique.⁴⁴

The X, Y, Z hypothesis for water in gels is somewhat similar to the α , β , bulk suggestion made by Horne et al. in 1968.⁴⁵

The question of water properties in hydrogels in relation to blood compatibility was briefly discussed by Bruck recently in this journal.⁴⁶

The evidence for water structuring in at least one common hydrogel, polyhydroxyethyl methacrylate, is now substantial.^{38,39,41,42} Whether or not such structuring is important in the interfacial properties of such gels remains to be determined.

The authors gratefully acknowledge many exciting and stimulating discussions with their colleagues and students in the Colleges of Medicine and Engineering, in particular Dr. John Hibbs and Dr. Sung Kim. Mr. Van Wagenen provided Figure 3. We thank Mr. Manuel Arevalo for the art work and Mr. David Malm for library services. This work is being supported by the U. S. Atomic Energy Commission, Division of Applied Technology, under Contract AT(11-1)-2147.

References

1. W. Drost-Hansen, H. D. Brown, ed., in *Chemistry of the Cell Interface, Part B*, Academic Press, 1971.
2. a) *Water and Aqueous Solutions*, R. Horne, Ed., Wiley, New York, 1972.
b) *Water—A Comprehensive Treatise*, Vol. I, F. Franks, Ed., Plenum, New York, 1972.
c) J. L. Kavanau, *Water & Solute-Water Interactions*, Holden-Day, 1964.
d) S. N. Vinogradov and R. H. Linnell, *Hydrogen Bonding*, Van Nostrand-Reinhold, 1971.
e) D. Eisenberg and W. Kauzmann, *The Structure & Properties of Water*, Oxford University Press, 1969.
3. H. S. Frank and W. Y. Wen, *Disc. Faraday Soc.*, **24**, 133 (1957).
4. G. Nemethy and H. Scheraga, *J. Chem. Phys.*, **36**, 3382, 3401 (1962); **41**, 68 (1964).
5. V. Vand and W. A. Senior, *J. Chem. Phys.*, **43**, 1869, 1873, 1878 (1965).
6. O. Ya. Samoilov, *Structure of Aqueous Electrolyte Solutions and the Hydration of Ions*, Consultants Bureau, New York, 1965.
7. L. Pauling, in *Hydrogen Bonding*, L. Hadzi, Ed., Pergamon, 1959, p. 1.
8. H. Eyring and M. S. Jhon, *Significant Liquid Structures*, Wiley, New York, 1969.
9. R. P. Marchi and H. Eyring, *J. Phys. Chem.*, **68**, 221 (1964).
10. M. S. Jhon, J. Grosh, T. Ree, and H. Eyring, *J. Chem. Phys.*, **44**, 1465 (1966).
11. H. Eyring and M. S. Jhon, *Chemistry*, **39**, 8 (1966).
12. J. D. Bernal and R. H. Fowler, *J. Chem. Phys.*, **1**, 515 (1933).
13. J. A. Pople, *Proc. Roy. Soc., A*, **205**, 163 (1951).
14. M. C. R. Symons, *Nature*, **239**, 257 (1972).
15. D. P. Stevenson, *J. Phys. Chem.*, **69**, 2145 (1965).
16. N. Laiken and G. Nemethy, *J. Phys. Chem.*, **74**, 3501 (1970).
17. Y. K. Sung and M. S. Jhon, *J. Korean Chem. Soc.*, **14**, 185 (1970).
18. R. B. Herman, *J. Phys. Chem.*, **75**, 363 (1971).
19. Y. K. Sung, U. S. Kim, and M. S. Jhon, *J. Korean Chem. Soc.*, in press.

Swelling and Osmotic Pressure

According to Flory (8), the network structure may have several roles. In a solvent the network dissolves and takes the role of a solute. In a solution it permits the passage of solvent molecules and keeps out other dissolved materials and, hence, acts as a membrane. As the network swells the polymer chains are elongated and exert a force in opposition to the swelling. In this case, the network acts as a pressure generating device. His theory of swelling is based on the balancing of the osmotic pressure by the mechanical contraction. To obtain his formal expression, Flory utilizes the Flory-Huggins polymer solution theory assuming random mixing between solute and solvent and a rigid lattice. The expression includes two terms, an entropy term (combinational) and a heat term due to intermolecular forces (non-combinational). Later, Prigogine et al. (9) developed a corresponding state theory for polymer solutions with a more rigorous expression for the non-combinational contribution than the Flory-Huggins approach. However, the combinational term is still used in its original form.

In the swelling of hydrogels, the random mixing assumption between high polymer and water is not generally valid, because of the high degree of structuring of water in some gel networks. The Prigogine theory, which is limited to non-polar and moderately polar systems with no hydrogen bonding, is also not generally applicable.

In this paper, a new semi-empirical interaction parameter, Δ_2 , is introduced and used in an equation of swelling based on a "Solubility Model" (10) to avoid the above-mentioned difficulties. The equilibrium condition for isotropic swelling (9) classically requires that

$$\left(\frac{\partial \Delta F_m}{\partial N_1}\right)_{T,P} + \left(\frac{\partial \Delta F_{el}}{\partial N_1}\right)_{T,P} = 0, \quad [1]$$

where ΔF_m and ΔF_{el} are the free energy of mixing and elastic behavior, respectively, and N_1 is the mole fraction of solvent. The "Solubility Model" (10) still carries the same elastic term, but the first term is modified. The process of transferring one mole of water from bulk to gel network involves three steps (Figure 1):

4

The Role of Water in the Osmotic and Viscoelastic Behavior of Gel Networks

MU SHIK JHON,* SHAO MU MA, SACHIKO HATTORI, DONALD E. GREGONIS, and JOSEPH D. ANDRADE

Department of Materials Science and Engineering, University of Utah, Salt Lake City, Utah 84112

The existence of an ordered structure at water/solid interfaces has been generally accepted. A structured molecule possess certain preferred orientations and cannot move independent of its neighboring molecules. In the case of water the word "structured" should not be misinterpreted; we do not mean that water possess long range orderness. By "structure" we mean the orderness relative to the bulk water. In a strict sense, even the molecules in bulk water are structured because of hydrogen bonding and other near neighbor interactions.

Drost-Hansen (1) has discussed a three-layer model for the structure of water near certain water/solid interfaces. According to this model, water molecules near the solid surface are structured; those sufficiently far away from the surface have bulk water structure and those in between have decreasing orderness as a function of distance from the interface. Others (2,3) have indicated the existence of three states of water in natural macromolecular gels (2) or in membranes of cellulose acetate (3). Jhon and Andrade (4) proposed a three-state model of water in hydrogel systems. They suggested that three classes of water exist in hydrogels, namely X water (bulk water), Z water (bound water); and Y water (intermediate forms or interfacial water). Following this, Lee, Jhon and Andrade (5,6) tested the model by thermal expansion, specific conductivity, differential scanning calorimetry, and proton spin-lattice nuclear magnetic relaxation studies for poly(hydroxyethyl methacrylate) (PHEMA gels). Very recently, Choi, Jhon and Andrade (7) again extended the model by means of thermal expansion, specific conductivity, and dielectric relaxation studies for (2,3-dihydroxypropyl methacrylate) gels (DHPMA gels).

In this paper theories for the osmotic and viscoelastic behavior of hydrogels are developed in terms of water structure. Some experimental results on the viscoelastic behavior of hydrogels are presented.

*On leave from Korea Advanced Institute of Science, Seoul, Korea; to whom correspondence should be addressed.

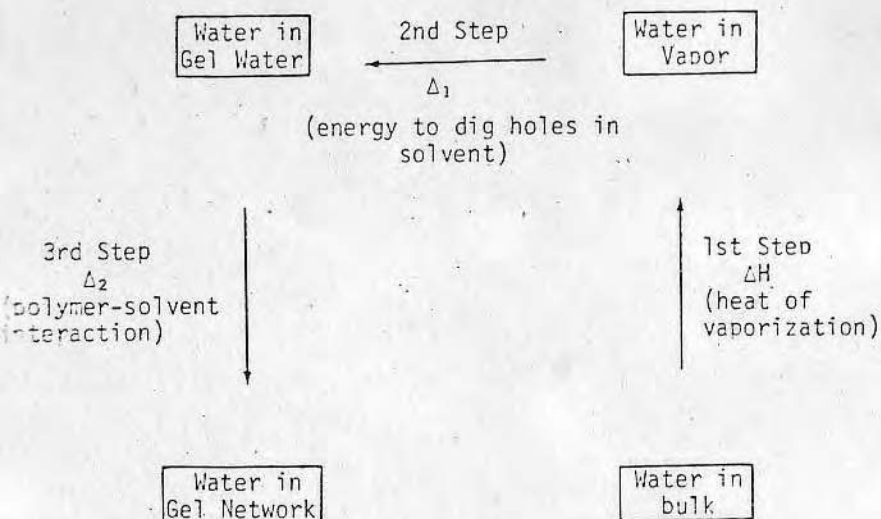


Figure 1. A schematic of the process of transferring one mole of water from bulk to gel network

First Step. To bring a mole of water from the bulk phase to the vapor phase: This requires an energy which equals the heat of vaporization of water, ΔH_V :

$$\Delta H_V = \Delta H_V^0 + \int_0^T C_p dT, \quad [2]$$

where ΔH_V^0 is the heat of vaporization at some reference temperature, T , and C_p is the specific heat. **Second step.** To bring water molecules from the vapor phase to the existing gel water: At or near equilibrium the gel network is expanded with water, which consists of X, Y and Z types, filling the empty spaces. The energy, Δ_1 , required in this step is for creating a mole of cavity of the size of the solute molecule (water in vapor) against the solvent (gel water) surface tension:

$$\Delta_1 = 4\pi r^2 (\gamma_Z Z + \gamma_Y Y + \gamma_X X) / (1 + K), \quad [3]$$

where $4\pi r^2$ is the surface area of the water molecule; γ_X , γ_Y , γ_Z , are the surface tensions and X, Y, Z are the weight fractions of the three types of water, X, Y, Z respectively.

The term $1/(1 + K)$ needs a little more explanation. Jhon, Grosh, Ree and Eyring [11] proposed a model in which (bulk)

water is visualized as containing at least two solid-like structures, the ice-I-like open structure and the ice-III-like closed structure, in equilibrium with each other and with the gas-like molecules (A gas-like molecule refers to a molecule which is surrounded by holes). A term $1/(1 + K)$ is introduced in equation [3] on the assumption that the energy of cavity formation is negligible in the ice-I-like part of the liquid structure, and K is the equilibrium constant between ice-I-like and ice-III-like domains. **Third step.** To bring water molecules in gel water to gel network: This step requires an energy of interaction between the polymer molecules and the surrounding water molecules, Δ_2 [12]:

$$\Delta_2 = f n \int_{AB}^{\infty} U(R) <S_{A+R+B}>_{AV} dR, \quad [4]$$

where A and B denote water and high polymer, respectively; n is the number density of solvent molecules; f is the quantity which takes account of the fact that the distribution of solvent molecules of the potential minimum is denser than the average density; $U(R)$ is the intermolecular potential of A and B molecules at a separation distance, R; and $<S_{A+R+B}>_{AV}$ is the average value of the surface area. To evaluate $U(R)$ and $<S_{A+R+B}>_{AV}$, the reader should consult the cited references [10, 12]. Although the new interaction parameter Δ_2 is difficult to evaluate directly, it can be obtained for available systems in the input data in Equation [2], Equation [3] and second terms in Equation [1] are provided.

Experiments to support this semi-empirical solubility theory would be first, to determine the interaction parameter, Δ_2 , for various gel-water systems. These can be obtained by measuring swelling degrees as the only input data, the rest being available in the literature. Swelling experiments on PHEMA networks made of controlled purity are underway. The obtained Δ_2 will be compared to the Flory interaction parameter χ (8). Other solvent systems such as alcohols should also be studied. Second, a phase diagram may be constructed for the water-polymer system. Perfect symmetry at the consolute temperature will support the hypothesis of random mixing of water and polymer molecules. Deviations from it would indicate support of the solubility theory.

The three-state model of water structure can also be applied to osmotic pressure of polymer solutions. The usual expression for osmotic pressure can be used except that the volume should be replaced by $V(X f_x)$, where f_x is the ratio between the solubility of solute in X or bulk water to that in gel water. We believe that only the portion of water available for osmotic pressure should be included in the osmotic pressure equation. Tying both swelling and osmotic pressure experiments together with the three-state theory, one may

perform a swelling and/or osmotic pressure experiment of pure water as a function of temperature. As water is heated from -30°C to 100°C, any change in swelling and/or osmotic pressure would be partly due to melting of ice-I-like clusters (11).

Viscoelastic Properties

The effect of solvent on the viscoelastic behavior of hydrogels has been widely reported in the literature (13,14,15). In creep and stress relaxation measurements, the retardation time and relaxation time are functions of solvent. In dynamic studies the solvent reduces the γ relaxation process and shifts the β process to lower temperatures. Furthermore, the concentration and the nature of low molecular weight compounds affect the size and shape of the secondary loss maximum as well as the apparent activation energy. In equilibrium studies, C_2 in the Mooney-Rivlin equation is affected by the solvent.

Hydrogels, in the rubbery region, behave much like rubber. Therefore, in this study, a theory for the stress-strain relation in hydrogels was developed by modifying the theory of rubber elasticity. Consider a freely orienting chain which contains n segments. The force F needed to maintain the chain at an average elongation \bar{L} is given by the expression:

$$F = \frac{kT}{\ell_0} L^* \left(\frac{\bar{L}}{n\ell_0} \right) \text{ or } \bar{L} = n\ell_0 L \left(\frac{\ell_0 F}{kT} \right). \quad [5]$$

The stress σ needed to maintain a rubber network at high elongation is given by (16)

$$\sigma/\nu kT = \frac{1}{3} n^{\frac{1}{2}} L^*(\alpha/n^{\frac{1}{2}}) - \alpha^{-2}, \quad [6]$$

where ν , α , ℓ_0 , k and T are, respectively, the number of chains per unit volume, the extension ratio, the segment length, Boltzmann's constant, and the absolute temperature. L and L^* are the Langevin function and inverse Langevin function, respectively which are defined by $x = L(y) = \coth y - 1/y$ and $y = L^*(x)$, respectively. For a hydrogel with mainly X water, it is reasonable to assume that the polymer chains can rotate freely and Equations [5] and [6] apply. However, for hydrogels with mostly Z water, due to the constrained state, only two limited conformations can occur, i.e., internal isomerization between two conformers keeping the position of each chain end fixed.

In magnetic theory, it is known that the magnetic field shifts the relative amount of two orientations. For M magnetic dipoles each of which can exist either in the direction of the magnetic field, H , or against the field, the relation between the magnetization, I , and the magnetic field takes

the form [17] $I/mM = \tanh \left(\frac{mH}{kT} \right)$, where m is the magnetic moment. In polymer elasticity the force plays a corresponding role. The equivalent expression for polymer elasticity can be written as:

$$Z \left(\frac{\ell_0 F}{kT} \right) = \frac{e^{\ell_0 F/kT} - e^{-\ell_0 F/kT}}{e^{\ell_0 F/kT} + e^{-\ell_0 F/kT}} = \tanh (\ell_0 F/kT). \quad [7]$$

We shall refer to $Z \left(\frac{\ell_0 F}{kT} \right)$ as the Z function.

For hydrogels with mostly Y water structure, we expect that both the L function and the Z function should fail to apply and a Y function should govern:

$$Y(\ell_0 F/kT) = \int_0^\pi \sin\theta \cos\theta \tanh (\ell_0 F \cos\theta/kT) d\theta. \quad [8]$$

In this case, not only two orientations (conformer) are permitted, but the position of each chain end is not fixed. With the same argument the numerical value of a Y function lies between the corresponding X function and Z function. Hence, equation [6] can be modified as follows:

$$\alpha/\nu kT = \frac{1}{3} n^{\frac{1}{2}} [XL^*(\alpha/n^{\frac{1}{2}}) + YY^*(\alpha/n^{\frac{1}{2}}) + ZZ^*(\alpha/n^{\frac{1}{2}}) - \alpha^{-2}], \quad [9]$$

where Y^* , Z^* are the inverse Y function and inverse Z function, respectively.

To test our hypothesis, the stress-elongation curves for three poly(hydroxyethyl methacrylate) gels with different water contents were obtained from stress-strain measurements at room temperature (23°C) (Figure 2). The observed data are given by the solid lines in the figure. The values of X , Y and Z are taken from Lee (5,6). Choosing $n = 100$ (we found that results obtained for $n = 100$ and $n = 1000$ do not differ significantly), the values of σ can be calculated as a function of α . The constants, νkT , needed for fitting the experimental curves are 1.09×10^7 dynes/cm² (Gel I, 45% water); 6.03×10^7 dynes/cm² (Gel II, 31% water); and 2.59×10^7 dynes/cm² (Gel III, 29.9% water). The calculated points are indicated in the figure. Gels I and II were prepared with the indicated amount of water in the polymerization mix while Gel III was prepared with 100% hydroxyethyl methacrylate monomer and then swelled to 29.9% water content. Although the water content in Gel II and Gel III are about the same, the former is considerably tougher than the latter.

It is possible that, at 23°C, the behavior of Gel II is not within its rubbery region, since the agreement between the calculated and measured σ values for this gel is less

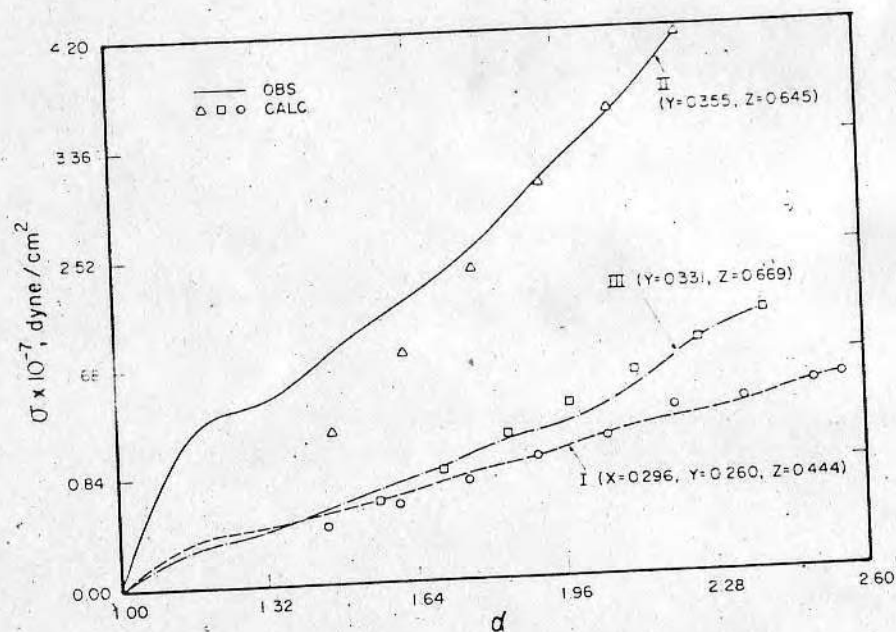


Figure 2. Stress-elongation curve

satisfactory than those for the other two gels.

Summary

A theory is developed to interpret the osmotic, swelling and viscoelastic behavior of hydrogel networks in terms of a three-state model of water structure. For isotropic swelling under equilibrium conditions, Flory assumed random mixing between the solvent molecules and the polymer molecules. Since water molecules in hydrogels possess higher degrees of order than those in the bulk, it is believed that the solubility theory (10) should be used instead of the classical Flory theory. This is because solubility theory considers the free energy of mixing of water with the gel network, which includes the heat of vaporization of water, the energy required to create holes in the gel water and the energy of interaction between water and polymer. In our theory only the portion of water available for osmotic pressure was included in the osmotic pressure equation. For the viscoelastic behavior of hydrogels, the theory of rubber elasticity was modified to accommodate the effect of three types of water on their stress-strain relationship. Polymer chains with mainly X water can rotate freely, those with mainly Z water can only have two restricted conformations and those with mainly Y water can have intermediate behavior. In actual cases, the contributions from all three types of water should be considered since they are coexisting in any polymer-water system. A few experiments are proposed. According to some experimental results, the theory provides good agreement.

Acknowledgement

We gratefully acknowledge support of this work by NIH Grant HL1692101 and NSF Grant GH33996X.

Abstract

A three-state model of water structure in hydrogels has been extended to describe the osmotic, swelling and viscoelastic behavior of gel networks. The solubility theory modification of the classical Flory theory is proposed to explain the osmotic and swelling behavior of gel networks. In describing the viscoelastic behavior of hydrogels, three functions, governed by the three types of water, are used to explain the stress-strain relations in the rubbery region.

Literature Cited

1. Drost-Hansen, W., *Indust. Eng. Chem.* (1969) 61, 10.
2. Aizawa, M., and Suzuki, S., *Bull. Chem. Soc. Japan* (1971) 44, 2907.
3. Krishnamurthy, S., McIntyre, D., and Santee, E. R., Jr., *J. Polym. Sci.* (1973) 11, 427.
4. Jhon, M. S., and Andrade, J. D., *J. Biomed. Mater. Res.* (1973) 7, 509.
5. Lee, H. B., Andrade, J. D., and Jhon, M. S., *Polymer Preprints* (1974) 15, 706.
6. Lee, H. B., Jhon, M. S., and Andrade, J. D., *J. Colloid and Interface Sci.* (1974) 51, 225.
7. Choi, S. H., Jhon, M. S., and Andrade, J. D., Submitted for publication.
8. Flory, P. J., "Principles of Polymer Chemistry," Cornell University Press, Ithaca, New York (1953).
9. Prigogine, I., Belleman, A., and Endert-Chowles, A., *J. Chem. Phys.* (1956) 24, 518.
10. Jhon, M. S., Eyring, H., and Sung, Y. K., *Chem. Phys. Letters* (1972) 13, 36.
11. Jhon, M. S., Grosh, J., Ree, T., and Eyring, H., *J. Chem. Phys* (1966) 44, 1465.
12. Kihara, T., and Jhon, M. S., *Chem. Phys. Letters* (1970) 7, 559.
13. Janacek, S., and Kolarik, J., *Coll. Czech. Chem. Comm.* (1965) 30, 1597.
14. Janacek, J., and Ferry, J. D., *J. Poly. Sci.* (1969) Part A-2, 7, 1681.
15. Ilavsky, M., and Prins, W., *Macromolecules* (1970) 3, 415.
16. Bueche, F., *J. Appl. Poly. Sci.* (1960) 4, 107.
17. Hill, T. L., "An Introduction to Statistical Thermodynamics," Addison-Wesley Publishing Company, Inc., Reading and London (1960).

반투막을 통한 수화된 이온의 투과속도 탈수화율 및 완화시간에 관한 연구

全武植* · 李海邦** · 金城完 · Joseph D. Andrade

미국 유타대학교 재료공학과

(1976. 7. 13 접수)

Ion Permeability, Dehydration and Relaxation Times of Hydrated Ions Through Membranes

Mu Shik Jhon*, Hai Bang Lee**, Sung Wan Kim and Joseph D. Andrade

Department of Materials Science and Engineering, University of Utah

Salt Lake City, Utah 84112

(Received July 13, 1976)

요 약. 간단한 통계역학적 방법을 사용 수화된 이온의 완화시간, 탈수화시의 활성화 에너지, 탈수화율 등을 계산하였다. 구상한 model에 의하면 수화된 물과 탈수화된 물 간의 평형상수, 물-이온간 에너지 항, 각종 species 간의 혼합 factor들이 들어있다.

이론과 실험은 잘 맞는 결과를 보이고 있다.

또한 이온이 탈수화시의 압력의 영향도 아울러 논의하였다.

ABSTRACT. A simplified statistical mechanical method was developed for the calculation of the dehydration fraction, activation free energy of dehydration, and the relaxation times of hydrated ions.

The model used includes the equilibrium constant between hydrated and dehydrated water, a water-ion interaction potential energy term, and a mixing factor for the species present. The agreement between theory and experiment is good.

The pressure dependence of ion dehydration is also discussed.

INTRODUCTION

There have been a number of papers which indicate that the dehydration of hydrated ions

plays a significant role in ionic diffusion through biological membranes, porous networks, and the specific adsorption of ions at the metal-solution surface¹⁻³. Recently Kim and Rubin⁴ evaluated the theoretical free energy of activation for dehydration of hydrated ions using an early partition function similar to that of Eley and

*To whom correspondence should be addressed: Korea Advanced Institute of Science, Seoul, Korea.

**Present address: Dental Research Center, University of North Carolina, Chapel Hill, North Carolina 27510

Evans⁵.

In our study, a simplified method is used for the calculation of the dehydration of hydrated ions in terms of the equilibrium constant between hydrated water and free water (i. e., dehydrated water), since liquid partition functions for ionic solutions are not well developed^{6,7}.

We also discuss the correlations between the activation energy for ion dehydration and the relaxation times of hydrated ions ranging from several seconds to 10^{-11} seconds. The pressure dependence on the dehydration of hydrated ions is explicitly included in this paper and evaluated for certain systems.

THEORY

Assuming that the partial dehydration of ions at the membrane/solution interface is the rate determining step in ion diffusion through membranes, the partition function of the initial state, f , which consists of N_i ions with N_{bw} hydrated water molecules, is written as follows:

$$f = (f_{bw})^{N_{bw}} (f_{ion})^{N_i} \frac{N!}{N_i! N_{bw}!}, \quad (1)$$

where f_{bw} and f_{ion} are the partition functions of hydrated or bound water and that of ion, respectively, and $N = N_i + N_{bw}$. Similarly, the partition function of the activation state for dehydration f^* , which consists of N_i ions, N_{bw}^* hydrated water molecules and N_{fw}^* free water molecules is given by

$$f^* = (f_{bw})^{N_{bw}^*} (f_{fw})^{N_{fw}^*} (f_{ion})^{N_i} \frac{N!}{N_i! N_{bw}^*! N_{fw}^*!} \quad (2)$$

where f_{fw} is the partition function of free water. Since the total number of water molecules for the initial and activated states are the same, $N_{bw} = N_{bw}^* + N_{fw}^*$. Therefore, the equilibrium constant K^* between initial and activated state is given by

$$K^* = (f^*/f) (e^{-V_0/kT})^N, \quad (3)$$

where V_0 is the activation energy barrier for the hydration, k is the Boltzmann constant, and T the absolute temperature. With the use of Equations (1) and (2), Equation (3) can be rearranged as:

$$K^* = \frac{N_{bw}!}{N_{bw}^*! N_{fw}^*!} \frac{(f_{bw})^{N_{bw}^*} (f_{fw})^{N_{fw}^*}}{(f_{bw})^{N_{bw}}} \cdot (e^{-V_0/kT})^N. \quad (4)$$

To simplify Equation (4) by eliminating the explicit expression for partition functions, the following procedures were considered. Let x_b and x_f be the probability of water molecule bound to water molecules and onto the ions at the interface. Then, $N_{bw}^* = x_b N_{bw}$, $N_{fw}^* = x_f N_{bw}$, and $x_f + x_b = 1$. The equilibrium constant K between the free water state and the hydrated state is:

$$K = x_f/x_b = f_{fw}/f_{bw} \quad (5a)$$

and

$$x_b = 1/1+K, \quad x_f = K/1+K. \quad (5b)$$

Combining (5a), (5b), and (4), one obtains

$$K^* = \frac{N_{bw}!}{N_{bw}^*! N_{fw}^*!} \frac{(f_{bw})^{1/1+K} (f_{fw}K)^{K/1+K} N_{bw}}{(f_{bw})^{N_{bw}}} (e^{-V_0/kT})^N. \quad (6)$$

Rearranging Equation (6), K^* is given by:

$$K^* = \frac{N_{bw}!}{N_{bw}^*! N_{fw}^*!} (K^{K/1+K})^{N_{bw}} (e^{-V_0/kT})^N \quad (7)$$

The standard free energy of activation for having N_{fw}^* free water from hydrated ions is

$$\Delta G^* = -kT \ln K^*. \quad (8)$$

The relaxation lifetime, τ , of a hydrated water molecule for ions is also written as (4)

$$\tau = \frac{h}{kT} e^{\Delta G^*/kT} \quad (9)$$

ΔG^* and τ can be obtained if the values of K ,

V_0 and the mixing factors in Equation (7) are known.

We take N as Avogadro's number; N is given by:

$$N = N_{\text{ion}} + N_{bw} = N_{\text{ion}} + (N_{\text{ion}} \times n_{bw}). \quad (10)$$

Here, n_{bw} is the hydration number of ions in the bulk solution and can be obtained from experiment, literature or theory⁸⁻¹⁰. The mixing factor in Equation (7) can be obtained; i.e., N_{bw} from Equation (10) and N_{bw}^* and N_{fw}^* from Equation (5).

Since experimental values for K are not available, best fit values are used, i.e., 0.155 for K^+ , 0.084 for Na^+ , 0.047 for Li^+ , 0.014 for Ca^{2+} , 0.010 for Mg^{2+} , and 0.017 for Al^{3+} at 25 °C. The potential energy barrier V_0 can be obtained from the following relationship:

$$V_0 = n_{bw}^* U_0 - n_{bw} U_0, \quad \text{where} \quad n_{bw}^* = \frac{1}{1+K} n_{bw}. \quad (11)$$

Equation (11) indicates the total potential energy difference of the hydrated ion cluster in the activated and initial states. In the activated state, the potential energy of interaction of free water with hydrated ion clusters is assumed to be zero. The same potential energy of interaction, U_0 , between water-ion pair is assumed for both the initial and activated states.

Then, the total potential energy of interaction, U_0 , between the ion and one water molecule about the Z axis is:

$$U_0 = -\frac{Ze\mu\cos\theta}{r^2} + \frac{Ze\theta_z(3\cos^2\theta-1)}{2r^3} - \frac{(Ze)^2\alpha_w}{2r^4} - \frac{3}{2} \frac{\alpha_i\alpha_w}{r^6} \frac{I_i I_w}{I_i + I_w} + Ar^{-12}. \quad (12)$$

Here, Z, r, θ, e and I are the sign of the ion, the equilibrium distance between center of the ion and that of water, the angle between Ze and r axis, the electronic charge and ionization

potential, respectively; μ, θ_z and α are the dipole moment of water, quadrupole moment of water, and isotropic polarizability, respectively. The subscripts i and w denote ion and water, respectively. The repulsive constant A can be obtained using the condition $\left(\frac{\partial U_0}{\partial r}\right)_{r=r_i+r_w} = 0$, which is given as

$$\frac{2Ze\mu\cos\theta}{r^3} - \frac{3Ze\theta_z(3\cos^2\theta-1)}{2r^4} + \frac{2(Ze)^2\alpha_w}{r^5} - 9 \frac{\alpha_i\alpha_w}{r^7} \frac{I_i I_w}{I_i + I_w} - 12Ar^{-13} = 0. \quad (13)$$

To relate the pressure dependence of hydrated ions on dehydration, one must know the expression for K from Equation (11). The equilibrium constant can be written as

$$K = e^{-\Delta H/RT} e^{\Delta S/R} e^{-P\Delta V/RT} = K_0 e^{-P\Delta V/RT}, \quad (14)$$

where $\Delta H, \Delta S$ and ΔV are the molar enthalpy change, the molar entropy change and the molar volume difference between hydrated and bulk water, respectively. If $P=1$ atm, the effect in the last term in Equation (14) is neglected.

RESULTS AND DISCUSSION

Using the equations presented, the activation free energy for the dehydration of hydrated ions, the dehydration fraction, the relaxation lifetime, and the pressure dependence of the dehydration of the hydrated ion were calculated at the membrane interface. Table 1 lists the input physical data for the calculations.

In this paper, we discussed the dehydration processes using data for ionic diffusion through a biological membrane such as the squid axon membrane, which is assumed to form a restricted opening to the primary hydrated ions. The present treatment can be extended to other ions in water, and porous networks which involve dehydration effects.

Table 1. Input physical data used in the calculation.

	K ⁺	Na ⁺	Li ⁺	Ca ²⁺	Mg ²⁺	Al ³⁺	H ₂ O
$r, \text{\AA}^a$	1.38	0.95	0.60	0.99	0.65	0.50	1.38
$\alpha \times 10^{24} \text{cm}^{-3b}$	1.39	0.156	0.0288	0.918	0.0859	0.0557	1.44
I, eV^c	31.81	47.29	75.62	51.21	80.14	119.96	8.65
n_{bw}^d	3	4	5	10	13	6 ^(e)	

^a R. M. Noyes, *J. Amer. Chem. Soc.*, **84**, 513 (1962).^b E. Paschalis and W. Weiss, *Theoret. Chim. Acta(Berl.)* **13**, 381(1969).^c Handbook of Chemistry and Physics, 51st Ed., The Chemical Rubber Co., 1970.^d See reference (8).^e See reference (9).Table 2. Calculated values of ΔG^* , Δn and U_0 .

	K ⁺	Na ⁺	Li ⁺	Ca ²⁺	Mg ³⁺	Al ³⁺
$\Delta G^*, \text{Kcal/mole}$	7.08	7.45	7.93	8.16	11.12	19.77
Δn	0.4	0.31	0.23	0.14	0.13	0.1
$-U_0, \text{Kcal/mole}$	17.50	24.15	35.43	58.32	85.62	197.8

A. The Activation Free Energy of the Dehydration of Hydrated Ions, ΔG^* . Applying Equations (7) and (8), and also using Equations (10) through (13), one can evaluate ΔG^* and $\Delta n = n_{bw} - n_{iw}$. The results are summarized in Table 2.

It is of interest in Table 2 that the values of ΔG^* are in the order $\text{Al}^{3+} > \text{Mg}^{2+} > \text{Ca}^{2+} > \text{Li}^+ > \text{Na}^+ > \text{K}^+$. Some available experimental values of Li^+ , Na^+ and K^+ ions for the squid axon in the resting state are in the order $P_K > P_{Na} > P_{Li}$ (11), and Δn values are in the order of $\text{K}^+ > \text{Na}^+ > \text{Li}^+ > \text{Ca}^{2+} > \text{Mg}^{2+} > \text{Al}^{3+}$. It is quite likely that the degree of dehydration is related with the order of magnitude of ΔG^* for ions. It is a little discouraging to see that the theory and experimental data are in qualitative agreement.

B. Relaxation Time of Dehydration of Hydrated Ions, τ . There are several papers on the relaxation lifetime of hydrated ions¹²⁻¹⁶. The observed values are in the range of 10^{-9} seconds to several seconds. However, very few experimental data are available for the relaxa-

tion time of hydrated water at an interface^{17,18}. Using Equation (9), the relaxation time of a hydrated ion, τ , at the interface is obtained and compared with experimental values of τ in bulk liquid in Table 3.

Our results for alkali ions are about 10^{-8} sec, which is in the range of upper limit values observed at the mercury/electrolyte solution interface^{17,18} and is comparable with 10^{-9} sec of bulk solution. Again, one sees that our simplified procedures provide a good prediction of the wide range of τ values.

C. Pressure Dependence of the Dehydration of Hydrated Ions. Since we have an explicit functional expression for pressure dependence on equilibrium constant, K , and the hydration number of an ion at an interface, n_{bw} , one can evaluate these values at different pressures. Table 4 list the calculated values of n_{bw} and K values for K^+ ion with change in pressure up to the 10^5 atm. For these calculations, the ΔV value was assumed to be -2cc .¹⁹

In Table 4, one sees that dehydration of hydrated ions is quite slow up to 10^3 atm, but

Table 3. Relaxation times of hydrated water.

	K ⁺	Na ⁺	Li ⁺	Ca ²⁺	Mg ²⁺	Al ³⁺
τ sec (calc.)	1.3×10^{-8}	2.4×10^{-8}	5.3×10^{-8}	7.8×10^{-8}	1.1×10^{-5}	25
τ sec ^a	10^{-9}	10^{-9}	10^{-9}	10^{-9}	10^{-6}	7.5

^a I. M. Klotz, "Membrane and Ion Transport", Vol. I, P. 106, Ed. E. Edward Bitter, Wiley Interscience, New York 1970.

Table 4. Calculated values of K at 25 °C and n_{bw} for K⁺ ions vs. pressure.

P_{atm}	K	n_{bw}
10 ²	0.156	2.60
10 ³	0.168	2.56
10 ⁴	0.350	1.32
10 ⁵	547	0.005

above this pressure, increases rapidly and finally at 10⁵ atm, very few water molecules exist in the hydrated state.

ACKNOWLEDGEMENT

This work was supported by NIH Grant HL 16921-01 from the National Institutes of Health and NSF Grant GH 38996X and Euisok Research Foundation.

REFERENCES

1. B. Hille, *Proc. Nat. Acad. Sci., (U.S.)*, **68**, 645, (1971).
2. P. Mueller and D. O. Rudin, "Current Topics in Bioenergetics", Vol. 3, Ed. by D. R. Sandi, Academic Press, New York, 1969.
3. J. O'm Bockris and A. K. N. Reddy, "Modern Electrochemistry", Vol. 2, Chap. 7, Plenum Press, New York, 1970.
4. S. H. Kim and B. T. Rubin, *J. Phys. Chem.*, **77**, 1245 (1973).
5. D. D. Eley and M. G. Evans, *Trans. Faraday Soc.*, **34**, 1093, (1938).
6. H. Eyring and M. S. Jhon, "Significant Liquid Structures", John Wiley, New York, 1969.
7. J. H. Hildebrand and R. L. Scott, "The Solubility of Non-Electrolytes", 3rd Ed., Reinhold Publishing Corp., New York, 1950.
8. J. O'm Bockris and A. K. N. Reddy, "Modern Electrochemistry", Vol. 1, p. 125, Plenum Press, New York, 1970.
9. J. W. Akitt, *J. Chem. Soc., (A)*, **18**, 2865 (1971).
10. Y. K. Sung and M. S. Jhon, *J. Korean Chem. Soc.*, **14**, 185 (1970).
11. J. W. Woodbury, S. H. White, M. C. Mackey, W. I. Hardy and D. B. Chang, "Physical Chemistry An Advanced Treatise", Vol. 9B, Chap. 11, Ed. by H. Eyring, Academic Press, New York, 1970.
12. R. E. Connick and R. E. Poulson, *J. Chem. Phys.*, **30**, 759 (1959).
13. H. H. Baldwin and H. Tauba, *J. Chem. Phys.*, **33**, 206, (1960).
14. M. Eigen, *Pure Appl. Chem.*, **6**, 97 (1963).
15. E. Wicke, *Angew. Chem. Intern. Ed., Engl.*, **5**, 107 (1966).
16. D. Fiat and R. E. Connick, *J. Amer. Chem. Soc.*, **90**, 608 (1958).
17. Y. I. Melik-Gackazyan, *Zh. Fiz. Khim.*, **26**, 560 (1952).
18. T. N. Anderson, J. L. Anderson, D. D. Bode, Jr., and H. Eyring, *J. Res. Inst. Catal, Hokkaido Univ.*, **16**, 449 (1968).
19. M. S. Jhon, J. Grosh, T. Ree and H. Eyring, *J. Chem. Phys.*, **46**, 1465, (1966).